Vibration Suppression and Safety Seat Motion Design of a Hyper-Active Seat

A Thesis
Presented to
The Academic Faculty

by

Samuel J. Klooster

In Partial Fulfillment
of the Requirements for the Degree
Master of Science in Mechanical Engineering

School of Mechanical Engineering
Georgia Institute of Technology
March 2004

Vibration Suppression and Safety Seat Motion Design of a Hyper-Active Seat

Approved by:

Dr. William Singhose, Advisor

Dr. Wayne Book

Dr. Nader Sadegh

Date Approved: 24 March 2004

To my wife,

Jennith K. Klooster,

for putting up with Atlanta traffic.

ACKNOWLEDGEMENTS

I would like to thank my advisor Dr. William Singhose for the guidance and advice given about my research. Your insights help me gain the understanding I needed to complete this thesis.

I would like to thank my committee Dr. Wayne Book and Dr. Nader Sadegh for their comments and suggestions.

I would also like to thank Dr. Kris Kozak for his help and determination in designing and building the Hyper-Active seat.

Finally I would like to thank the companies of the Fluid Power Group for providing funding and supplies to complete my research.

TABLE OF CONTENTS

LIST OF TABLES

LIST OF FIGURES

SUMMARY

Whole-body vibration is an important problem facing operators of off-road vehicles. Research has shown that operators exposed to low-frequency whole-body vibration can experience temporary and even permanent injuries. One solution to this problem is to develop an active seat capable of canceling the vibrations felt by the operator. Several passive, semi-active, active, and fully active seats have been designed and built to address this problem. Furthermore, controllers have been developed to optimize the seat performance. Vibration cancellation seating systems seem to be a promising and practical way to reduce the effects of whole-body vibration.

To extend developments in this area, a Hyper-Active seat has been designed and built at the Georgia Institute of Technology. The seat utilizes a 3 Revolute-Prismatic-Revolute (R$\underline{\text{P}}$R) parallel manipulator design which allows for the independent control of the vertical, horizontal and pitch angle directions. The seat is powered using three hydraulic actuators which are controlled using MATLAB's Simulink, xPC Target, and Real-Time Workshop. Controllers were developed to control the position of the seat, as well as cancel unwanted vibration. To test the performance of the Hyper-Active seat, the system identification of the seat was undertaken using open-loop forcing functions. The seat was evaluated in each degree of freedom to understand the potential of the seat to cancel harmful vibration.

In addition to reducing harmful vibrations, the seat can double as a safety seat to reduce injuries during a frontal collision. If the front edge of the seat bottom can be raised very quickly, then the forward motion of the passenger can be reduced during a crash. An optimal method for performing this motion is developed.

CHAPTER I

INTRODUCTION

1.1 Seated Injuries

Terrain-induced, low-frequency vibrations pose a problem to operators of off-road vehicles and heavy machinery. The vibration they experience is known as whole-body vibration, which occurs when the body is supported on a vibrating surface (e.g., sitting on a seat which vibrates, standing on a vibrating floor or lying on a vibrating surface). Whole-body vibration occurs in transportation (e.g., road, off-road, rail, air, and marine transport) and when near heavy machinery [42]. The vibrations cause the operator's whole body to vibrate, as opposed to just one part of their body, say their hand or foot. Harmful effects of whole-body vibration are experienced when the exposure time is longer than the recommended standard set by ISO 2631 [3]. Some of the harmful effects can include permanent damage to the spine, as well as increasing fatigue, which may decrease the performance of the operator.

Whole-body vibration can occur in any of the six degrees of freedom of the body (vertical, fore-aft, side-to-side, pitch angle, roll angle, and yaw angle). Research by Prasad *et al.* shows that the vertical direction is predominantly more harsh on the operator than any other direction [39]. These results seem natural because a tractor driving over a bump in the road will experience more whole-body vibration in the vertical direction, than in any other direction.

The second most harmful direction for whole-body vibration depends on the type of vehicle being operated. Tractors tend to have a pitching motion when pulling a trailer, plough, or another heavy piece of equipment. The extra weight behind the tractor amplifies the pitching motion, causing an increase in whole-body vibration. Other vehicles, such as a construction vehicle produce more whole-body vibration in the side-to-side motion. This is due to driving over uneven surfaces.

Along with the importance of protecting the operator from whole-body vibration, it is

also important to protect them during a front-end collision. During a collision, operators tend to slide off the front of the seat and slip under the steering wheel. This action is know as submarining. During such action, the operator tends to acquire injuries that are very painful and may even result in death. One method to solve such a problem is to install a safety seat. A safety seat is designed to cradle the operator during a collision, thereby potentially reducing their injuries [22, 18, 7].

To potentially cradle an operator and reduce injuries, the safety seat must reduce the kinetic energy of the occupant. One possible motion of the safety seat is to elevate the front edge of the seat bottom [2]. This motion slows the relative motion of the operator with respect to the seat, and reduces the kinetic energy of the occupant.

The Hyper-Active seat developed at the Georgia Institute of Technology has the capability to solve these two major problems. Figure 1 shows the Hyper-Active seat positioned on the excitation base. First, the Hyper-Active seat is a fully active seat, which has the capability of suppressing vibrations and reducing fatigue or permanent injuries to the operator. Second, the Hyper-Active seat has the ability to perform as a safety seat during a collision, possibly reducing injuries to the operator. These two abilities make it an excellent solution to these problems.

1.1.1 Harmful Frequency Range

Whole-body vibration is harmful to humans because it excites the natural frequency of the body. The dynamics of the human body has been researched to determine which frequencies are most harmful. Gniady and Bauman from Aura Systems determined the natural frequencies of the human body in the sitting position. The human body usually has a natural frequency between 4 and 5 Hz and a low tolerance for amplitudes between 0.5 and 1.5 g's (r.m.s.) [20]. Table 1 shows a number of vital body parts, and the corresponding natural frequencies. Most of the vital organs of the body, such as the stomach, spine, and heart have a natural frequency around the 4 to 5 Hz range, as suggested by Gniady's research. Knowledge of the most harmful frequency range of the sitting human body dictates the necessary frequency range of a vibration cancellation device.

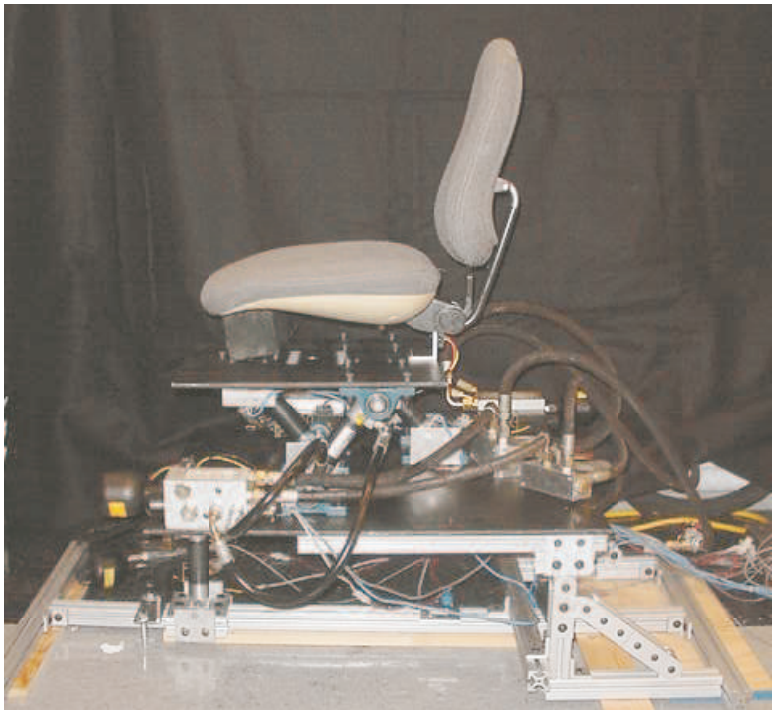

Figure 1: Hyper-Active Seat Developed at the Georgia Institute of Technology

1.1.2 Effects of Whole-Body Vibration

Whole-body vibration has many ill effects on the operators. Health effects can range from fatigue to permanent damage to the spine of the operator. Many studies have been conducted to link the exposure of whole-body vibration to common health problems experienced by operators of vibrating machinery. These studies show the effects of whole-body vibration, and some debate whether the ISO standard is strict enough [43, 31, 20].

Table 1: Natural Frequencies of the Human Body

Body Part	Natural Frequency	Units
Trunk	3-6	Hz
Eyeball	20-25	Hz
Chest	4-6	Hz
Thorax	3	Hz
Spine	3-5	Hz
Heart	4-5	Hz
Shoulders	2-6	Hz
Head	30	Hz
Stomach	4-7	Hz
Colon	20-25	Hz

The severity of whole-body vibration caused by certain types of machinery and the sensitivity of humans to those vibrations led ISO to develop standards for exposure to whole-body vibration. ISO standard 2631 [3] recommends a maximum of 8 hours of exposure time for operators who are exposed to vibrations in the 4 to 8 Hz range with an amplitude greater than 0.064 g's (r.m.s.). Although exposure levels are recommended by ISO, Mehta, *et al.* researched the vibration level of tractors in India to determine if the standards were too lax. Their studies determined that the tractor exceeded the 4 and 8 hour vibration levels specified by ISO 2631 under most operating conditions [31]. Furthermore, when the operator is ploughing or harrowing a field, the exposure time for the operator should not exceed 2.5 hours [31]. Mehta's research shows that the guidelines set by ISO may not be strict enough to protect operators from whole-body vibration under certain circumstances.

Other fields of work, such as operators of mining, agricultural, and construction vehicles often work up to 12 hours per day and are exposed to vibration frequencies of 0 to 20 Hz at amplitudes of 0.2 to 1.2 g's (r.m.s.) [20]. These working conditions greatly exceed the suggested limits set by ISO. The exposure over time could have a permanent effect on the health of the operator. The combination of high-amplitude and low-frequency vibrations of the vehicle and the low tolerance of the human body causes serious health risks for operators who are subjected to prolonged exposure.

Rehn studied a number of different drivers of forest machines, snowmobiles, and snow groomers in Sweden. The survey revealed the prevalence of the symptoms were largely in the neck, shoulders, and thoracic regions, but not much in the lower back. The drivers also reported that driving an all-terrain vehicle negatively influenced their health. Between 35 and 48% of the driving groups reported episodes of illness and disorders that were related to driving an all-terrain vehicle [40]. This research showed both the short term, and long term effects of whole-body vibration.

Schwarze, *et al.* looked at the relationship between the occupational exposure to whole-body vibration and degenerative processes in the lumbar spine. The study looked at the possibility that the acceleration guideline of 0.8 m/s^2 was to high. The study was conducted on 388 subjects from Germany, of who, 165 were operators of heavy machinery. The

participants were between the ages of 30 and 40 and had 10 years of vibration exposure. The data was collected by survey method, and participants were then divided into 4 groups, based on their level of vibration exposure. The group was examined by doctors, and then reevaluated 4 years later. It was reported that operators of earth moving machinery in construction sites frequently had the highest intensities of vibration. After looking at all the data, they determined that the current acceptable acceleration level of 0.8 m/s^2 was too high, and needed to be reduced to 0.6 m/s^2. The study also found that a considerable number of cases of lower back pain, or lumbar syndrome, (about 27 to 35%) can be attributed to whole-body vibration [43].

Rehn and Schwarze's research show the extreme effects of whole-body vibration; however, even limited amounts of vibration can cause problems for operators of off-road vehicles. Salvendy's research showed exposure to whole-body vibration will first affect the sight and ability to properly control the hand and foot [42]. This could cause operators to be less responsive, possibly leading to poor workmanship, or even accidents. The notion of driver fatigue was also a common factor in research conducted by Prasad [39]. Although driver fatigue is not a primary effect of whole-body vibration, an operator who is fatigued will not operate the machinery at its full potential.

Along with the negative health effects of whole-body vibration, there are also financial effects. Excessive vibration forces operators to retire earlier than necessary because of spinal ailments and other vibration injuries. This early retirement forces employers to find other inexperienced drivers who lack "road sense" and increases the possibility of accidents [34]. This leads to an increase in insurance rates for the employer, increasing the cost of their work. A fatigued worker will cost an employer extra time and money to complete a job. Also, employers will have to pay extra for health insurance premiums and disability pay for employees who are experiencing the negative effects of whole-body vibration.

A vibration cancellation system would have the ability to reduce the effects of whole-body vibration on the operator. This would lead to a decrease in health related problems experienced by the operator. Along with the health benefits, investing in a vibration cancellation system could help reduce the increasing costs to employers due to whole-body

vibration.

1.2 Solutions for Vibration Suppression

The best method for reducing whole-body vibration is to solve the problem at its source. If the engine is creating the whole-body vibration, it should be redesigned to eliminate the vibrations. In the case of some vehicles, simply fixing holes in the roads could greatly reduce the levels of vibration. However, some sources of whole-body vibration cannot be redesigned or fixed. For off-road vehicles, the source of most of the whole-body vibration comes from driving areas where there are no roads. The whole-body vibration caused in this manor needs to be attenuated with a vibration cancellation system.

There are three main areas where vibration cancellation systems are placed on vehicles. The most common place is to put a suspension system between the tire and the rest of the vehicle. Most off-road vehicles have this type of vibration cancellation system, as do all automobiles. Although the tire suspension system works great for most vehicles, some vehicles are restricted by it, and therefore cannot use a tire suspension for vibration cancellation. Tire suspension systems are not practical for tractors and other agricultural equipment due to the draught height. When a tractor is pulling agricultural equipment, it is important that the height of the tractor above the ground is kept constant. This is the case for plowing or planting a field. A tire suspension system would vary the height of the tractor causing uneven planting to occur.

Another place to put a vibration cancellation system is on the cab of the vehicle. Semi-trucks usually have a tire suspension system, along with a cab suspension. The advantage of having two systems is to further reduce the amount of whole-body vibration which the tire suspension could not attenuate. Most vehicles do not have a cab suspension due to the high costs associated with putting a vibration cancellation system on the whole cab. A more common solution, and the third area where vibration cancellation systems are placed on the vehicle, is on the seat.

Placing a seat suspension on a vehicle protects the operator from whole-body vibration. It also does not restrict the ability of the vehicle, such as planting a field in the case of

a tractor. A seat suspension system also costs less than a cab or tire suspension due to the heavy duty springs and dampers required on a tire suspension to support the weight of the whole vehicle. A seat suspension only has to support the weight of the operator and therefore can use less costly components. Due to these reasons, a seat suspension may be the best way to attenuate whole-body vibrations on an off-road vehicle.

1.2.1 Types of Seat Suspension Systems

There are four main types of seat suspension system: passive, semi-active, active, and fully active. Passive seat systems are the most common because they are cheap and effective for most vibration. Passive systems include springs and passive dampers which reduce the vibration of the operator's seat. Passive systems cannot realistically attenuate the entire frequency range of whole-body vibration, specifically in the 1 to 7 Hz range. This is due to the amount of travel of the system necessary to cancel the vibration.

Figure 2 shows a model of a passive system. The transfer function for this model is:

$$\frac{X}{Z} = \frac{Cs^2}{s^2 + 2\zeta\omega_n s + \omega_n^2}, \tag{1}$$

where ζ is the damping ratio and ω_n is the natural frequency. For good vibration attenuation, Y would be approximately equal to minus Z, ω_n must be 1/4 to 1/5 of the lowest input. Therefore to cancel vibrations at 4 Hz requires a seat natural frequency of 1 Hz, which translates to a large displacement. Furthermore, to suppress a vibration of 2 Hz requires a seat natural frequency of 0.5 Hz and the ability of the seat to travel very large distances. It is obvious from this example of a passive seat suspension, that it is impractical to have a passive seat suspension with a travel of more than a few inches. Other means of attenuating vibrations are necessary.

Semi-active seat suspension systems are somewhat common, and they give better results with damping vibrations than passive systems. The defining trait of semi-active systems is that they can only dissipate energy and not create energy. Semi-active systems can use springs and active dampers which generally use electro-rheological (ER) or magneto-rheological (MR) fluid to actively damp vibrations. These suspension systems work the following way. A sensor detects the vehicle's vibration, and a controller controls the flow

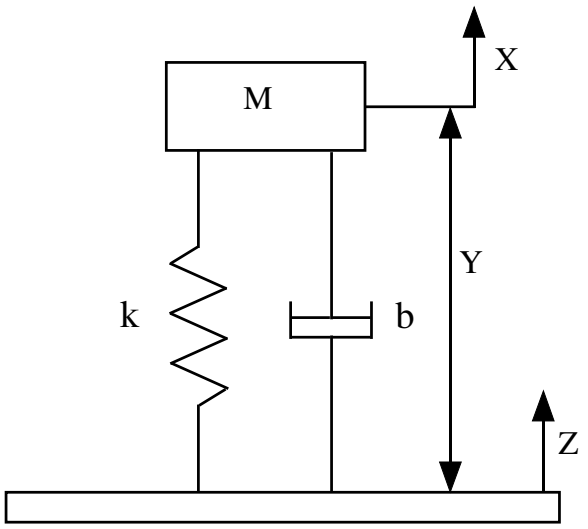

Figure 2: Model of Passive Seating System

and timing of fluid through the active damper to attenuate the vibration of the seat. This method is slightly more advanced than a passive seat, however it does not fully attenuate vibrations in the 1 to 7 Hz frequency range.

Active seat suspension systems are fairly uncommon due to the cost and power requirements of the seating system. However, active suspension systems suppress vibrations better than passive and semi-active suspension systems. Active systems are capable of suppressing vibrations in the 1 to 7 Hz range, which make them ideal for whole-body vibration cancellation. These seat suspension systems generally have springs and dampers, but their defining characteristic is that the active actuators can dissipate energy, as well as create energy. The ability to dissipate and create energy allows for greater vibration attenuation in the low-frequency range.

Fully active seat suspension systems are the most uncommon; however, they perform the best for attenuating vibrations in the harmful frequency ranges. Fully active systems contain only active components, and do not include any springs or dampers, which allows them to react faster and more effectively. Fully active suspension systems cost about the same as active suspension systems; however, they have a much higher power requirement. This is due to the fact that fully active suspension systems are required to use the active actuators to continuously support the weight of the seat and the operator, while active

suspension system usually have a spring which supports most of the load.

The Hyper-Active seat constructed at the Georgia Institute of Technology is a fully active seat suspension system. Three hydraulic actuators support the load of the seat and the operator. Although the seat will have a higher power requirement, the seat will be able to attenuate vibrations better than an active seat suspension system. Furthermore, it is designed to be retrofitted with supporting springs so that it can operate in an active, rather than a fully active, mode.

1.2.2 One Degree of Freedom Seat Suspension Systems

Many types of seat suspension systems have been developed over the years. Most seats have one degree of freedom, namely the vertical direction, but some have more than one degree of freedom. Not only do active seat suspensions have different configurations, but they use very different actuators. Some common types of actuators have been hydraulic, pneumatic, and electric. Each type of actuator has its advantage, however, one must also consider for which type of vehicle the seat suspension system is being designed.

Electromechanical actuators are the most popular actuators, because most vehicles have access to electricity. Gniady and Bauman from Aura Systems have developed an active seat using 4 magnetic actuators, which supply 450 lb_f, and a coil spring under the seat. The acceleration of the seat is measured by a single accelerometer located on the seat. The seat has only one degree of freedom, the vertical direction, due to cost benefit analysis, but more degrees of freedom could be added. The seat is capable of suppressing vibrations up to 20 Hz with an acceleration up to 1.5 g's [20]. Perisse and Jezequel used an electromagnetic actuator which can be used as a motor (actuator) or a generator (electromagnetic brake) [38]. This gives the ability to provide or dissipate energy from the system. Kawana and Shimogo developed a one degree of freedom active seat with an electric servo-motor and ball-screw mechanism [25]. Ryba, used an electromagnetic force generator with an electromagnetic clutch [41]. Liu and Wagner developed an active seat suspension system using an elector-mechanical actuator [28]. Electromechanical actuators have remained most popular due to the ease of accessing electricity, and also their fast reaction time.

Table 2: Operating Pressure of Construction Vehicles

Vehicle	Operating Pressure (psi)
Bulldozer	6,000
Loader Backhoe	2,900 - 3,000
Grader	2,500
Forklift	2,250
Tractor	3,000

Pneumatic power is also a popular option for active seats. Stein analyzed a fully active system, which used an electropneumatic cylinder to connect the seat and the chassis. The main concern with modeling the seat this way is the system will consume more power than an active system, just to keep the mass at equilibrium [46]. Stein has written many papers analyzing the design of active seat suspension systems using pneumatics. One reason that pneumatic power is very popular is that it has some of the advantages of hydraulics, without the extra equipment. Along with being used on active seats, Hurwitz developed a passive seat where the operator sits on a cushion of air [23]. Although not as popular as electromechanical actuators, pneumatic actuators are still a viable option.

Hydraulic power is very popular on certain types of vehicles. The idea of a hydraulic active seat suspension systems on off-road vehicles such as construction or agricultural vehicles can be realized, because hydraulic power is readily available on these types of vehicles. Table 2 shows the typical operating pressure of different construction vehicles. Each vehicle has more than enough power to operate an active seat. Grimm *et al.* developed a hydraulic active seat to attenuate vibrations in the vertical direction. The seat was designed to suppress vibrations up to 10 Hz [21]. Suggs and Stikeleather experimented with a fully active hydraulically powered seat. The seat attenuated vibrations in the vertical direction and was field tested on a tractor [51, 52]. Along with active seats, hydraulic power is also used on semi-active seats. Choi, uses an ER fluid actuator to supply power to the semi-active seat [12]. The Hyper-Active seat developed at the Georgia Institute of Technology uses hydraulic power, because the main intended application is agricultural.

1.2.3 Multiple Degrees of Freedom Seat Suspension Systems

Most active seats have one degree of freedom and control the vertical position of the seat. However, an active seat with two or more degrees of freedom would be able to react better to the variety of disturbances that occur in off-road vehicles. Although the vertical direction contains the most intense vibrations felt by operators, they are subjected to vibration in other directions as well. Nevala, *et al.* have developed an active seat that controls the vertical and horizontal directions [35]. Research has also been done on an active seat that controls the roll and pitch angles [59].

After the vertical direction, there does not seem to be any agreement on the order of most important degrees of freedom. For example, Leo, *et al.* developed a three degree of freedom active seat for a hybrid-electric vehicle. The three degrees of freedom were the vertical, pitch angle, and roll angle directions. The seat was designed to attenuate vibrations between 4 and 14 Hz. Nevala, *et al.* developed a two degree of freedom hydraulically powered active seat which controls the vertical and horizontal directions [35]. The seat utilizes a scissor mechanism to magnify the stroke of the actuator. Young and Suggs built an active suspension seat that isolated the roll and pitch of off-road vehicles [59, 60].

There has been a variety of multi-degree of freedom active seats developed. The ultimate active seat would suppress vibrations in all six possible degrees of freedom, however this seat has never been developed due to the cost and power requirements to actuate all six degrees of freedom. Leo, *et al.* were the only group to research more than two degrees of freedom, however these degrees of freedom are not ideal for attenuating vibration on most agricultural equipment.

Vibration suppression in the fore-aft and pitch angle direction are generally neglected. Agricultural equipment operated with heavy mounted implements, such as a plow or trailer, tend to oscillate in these directions [30, 31, 39]. To combat this problem, Marsili, *et al.* developed a two degree of freedom passive seat which combined with a tire suspension on the tractor attenuated vibrations felt by the operator [30]. This tractor was unique, in that it had a limited tire suspension that aided vibration suppression. The Hyper-Active seat attenuates vibration in the vertical, fore-aft, and pitch angle directions, making it an ideal

seat for agricultural applications.

1.2.4 Vibration Suppression Control Algorithms

Once an active, fully active, or even semi-active seat suspension system has been designed and built, there needs to be a way to control the seat to attenuate the vibrations. Many control algorithms have been used on the seat suspension systems mentioned above. Some things to consider when designing a control algorithm are the states available for feedback, the frequency range of vibrations to attenuate, and the actuator limits. Another thing to consider is the cost and complexity of designing the controller.

One of the first tasks to be completed when designing a controller is to develop a model of the seat suspension system. The complexity of the model depends on how accurate the model needs to be to design a good controller. There are three main parts of a model to consider: the vehicle, seat, and occupant. Liu and Wagner developed a complete model using a 7 degree of freedom quarter car model, a complicated seating model, and a 4 degree of freedom human model [28]. Kim *et al.* used a three degree of freedom model of a human [26]. Other researchers, such as Perisse, added a model of the foam pad of the seat [38]. Although some researchers developed very complicated models, others developed their controllers from very simple models. The complexity of the model is highly dependent on the needs and performance of the controller.

Once the model has been developed, a controller can be designed. Many types of controllers have been applied to semi-active, active, and fully active seat suspension systems. Grimm *et al.* used two control loops on their active seat. One loop controlled the vibration attenuation and a second loop controlled the drift of the seat away from the center of the workspace. The drift controller was sampled at a much slower sampling rate as to not conflict with the vibration attenuation controller [21]. Kawana and Shimogo used optimal control to attenuate vibrations [25]. Oshinoya *et al.* developed a one degree of freedom active seat which they equipped with sliding mode control. They compared the results to a passive seat and an optimal controller, which showed that the sliding mode controlled seat suppressed the vibration the best, even when noise was introduced into the system [36].

Cheok, implemented a discrete-time frequency-shaping parametric LQ control [11]. Choi, used sliding mode control to control the semi-active ER fluid actuated seat [12]. Liu and Wagner applied many controllers to a semi-active and active seat suspension system. The seating systems were controlled using relative, Proportional-Integral (PI), variable structure system, and optimal control. The relative and optimal controllers worked best for the semi-active and active actuators respectively [29]. Each controller has its advantages and disadvantages when applied to the seating system.

One controller which is used far more than any other controller is the "skyhook" controller. The "skyhook" controller is a simple and effective controller which uses no information about the actual system. The simplicity and effectiveness makes it a very popular choice for researchers. Ryba used a "skyhook" controller on an active seat to attenuate the vibration [41]. The control law can be written as:

$$\text{IF} \quad \dot{x}(\dot{x} - \dot{y}) > 0 \quad \text{THEN} \quad F_D = k\dot{x} \quad \text{ELSE} \quad F_D = 0, \tag{2}$$

where $\dot{x}$ is the velocity of the seat, $\dot{y}$, is the velocity of the vehicle floor, F_D is the force to cancel the vibration, and k is the control constant [41]. The force is proportional to the velocity of the seat. Choi *et al.* used a "skyhook" controller on a MR fluid damper to suppress vibrations. They use the acceleration on the seat and the displacement between the seat and the frame as feedback [13]. Stein, *et al.* used two controllers on their active vibration control system. The inner loop controlled the over-all position of the seat and kept the seat from drifting to one extreme of the actuator or the other. The outer loop provided the vibration control and was based on the "skyhook" principle [50]. Perisse and Jezequel use "skyhook" semi-active control and cascade regulator active control to suppress the vibration of the operator [38].

Pantelelis and Kanarachos developed a hybrid "skyhook" controller [37]. The equations are:

$$F_{control} = c * velo + d * disp \tag{3}$$

and

$$F_{control} = \frac{A}{B + |velo + accel * \triangle t|} * velo, \tag{4}$$

where A depends on the actuator's saturation limit and B is introduced to avoid instabilities when the denominator approaches zero and is set to 0.05. The hybrid "skyhook" controller takes into account the displacement between the vehicle and the seat, as well as the velocity of the seat.

Optimization is also a popular tool to find the best parameters for all types of seat suspension systems. Baumal used Genetic Algorithms (GA) to optimize a passive and active controller [5]. Demic used the Hook-Jeeves method due to the nonlinearities of the system, to optimize the parameters of a hydraulically powered active seat [14]. Deprez *et al.* used a global optimization technique to determine the controller parameters for a passive and semi-active seat [15]. As the power of computers has increased, optimization has become a viable option, and will continue to be used in the future.

Another ingenious way to address the problem of vibration attenuation is to reformulate the problem into a form that was a well known solution. Zhang and Alleyne reformulated the problem of vibration suppression and turned it into a tracking control problem. They then used an optimal controller to track the negative of the input [62]. Changing the problem into a tracking control problem allows for a number of tracking control algorithms which can be used.

Once a controller is developed for the seat suspension system, it may be a good idea to analyze the power requirements of the seat. Understanding the power requirements will give a better understanding of the amount of power the seat suspension system will drain from the main vehicle.

1.2.5 Power Requirements

One important piece of information that is often overlooked, is the power requirements of the seat. Most researchers do not consider this, because their research is concentrated on attenuating vibrations, and they are not worried about how the seat suspension system will interact with the rest of the vehicle. A fully active and active seat suspension system may have a significant drain on the resources of the vehicle. It is important to know exactly how much power is required by the seat suspension system, to make sure that the operation of

the seat is not interfering with other operations on the vehicle.

Junker and Seewald developed an equation for finding the power requirements for a tractor. The equation is:

$$P_p = \frac{1}{\eta p} * P * A_k * V_k, \tag{5}$$

where ηp is the pump efficiency, P is the operating oil pressure, A_k is the piston area, and V_k is the piston speed [24]. This method could be easily used for finding the average power requirement by simply knowing the average piston speed. One problem with using this method, is that it really does not apply to fully active seat suspensions. A fully active seat suspension is using power, even though it is just holding the seat at equilibrium. Although the seat is not moving, a constant pressure in the hydraulic cylinders is required. Due to leakage and other factors which lowers the pressure, the pump uses power to increase the pressure to the equilibrium pressure. This equations does not take that into account. A fully active seat at equilibrium would have a piston velocity of zero, and therefore a calculated power use of zero, this however would not be accurate.

Ballo, determined that he could calculate the power consumption of an electro-hydraulic powered active seat in a manor similar to Junker and Seewald [4]. After calculating the power consumption of a fully active seat suspension system, he placed a spring on his active seat to reduce the power requirements.

One way to calculate the power requirements of a fully active seat would be to measure the power requirement of the seat at equilibrium. One could assume a linear relationship between the velocity of the cylinder and the power requirement. After calculating the power requirements for a few velocities, interpolation could be used to obtain the power requirement at zero velocity. This would give the power requirement at the equilibrium position. Now that the power requirement of the seat can be calculated, there needs to be a reliable method for testing the seat.

1.2.6 Test Stand

Once an active seating system is developed, there needs to be a way to test the seat for different vibrational inputs. One way is, of course, to attach the seat to an off-road vehicle

to see the performance of the seat over actual terrain. Although this method seems the most accurate for testing an active seat, there can be many difficulties using this method if the prototype hardware has not been tested for different environments.

These reasons lead to the need for a test stand on which the active seat can be tested without transferring hardware around. Test stands give the added advantage of knowing the exact input which goes into the seat. This way, results can be reproduced, and controllers tuned for optimal performance. The development of the test stand can be as simple as a single actuator, producing vibrations in the vertical direction, or as complicated as a four post shaker, which is capable of simulating vibrations in more than one degree of freedom.

Stein and Ballo, developed a test stand for their active seat powered by one hydraulic cylinder. The chassis of the vehicle was simulated by a rigid arm fixed at one end by a pivot and driven by a hydraulic cylinder at the other end [49]. This produces a vertical and pitch motion which are coupled together. The coupling between the vertical and pitch angle is small if the arm length is long. Therefore most of the motion is in the vertical direction. The shaker is capable of inducing vibrations which are known and reliable; this way the controller can be tuned for the best performance for any vibration.

1.3 Safety Seats

A safety seat is designed to move in some way during a vehicle collision to decrease occupant injuries. One important motion of a safety seat is to increase the angle of the seat bottom, effectively increasing the normal and frictional forces on the occupant and preventing them from "submarining" under the steering wheel [7, 33, 44]. Figure 3 shows one possible motion of a safety seat and the response of the occupant. Another possible movement of a safety seat is to elevate the side of the seat during a side impact[58]. These two different configurations potentially decrease the chance that the occupant will be injured during a collision.

During the initial stages of a collision, two major forces are felt by the operator assuming the force of a seat belt or airbag is neglected. The friction force between the seat and the occupant is felt as the occupant begins to slide off the seat, along with the normal force,

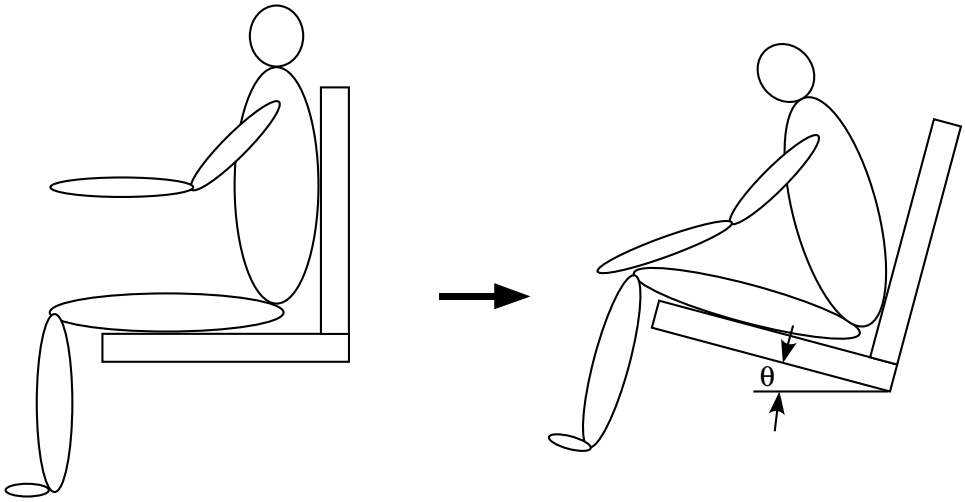

Figure 3: Diagram of Possible Safety Seat Motion

which is related to the friction force through the kinetic friction coefficient. These two forces are used to decrease the relative velocity of the operator. Increasing either of these forces will slow the relative velocity of the occupant. However, safety seat designers must be careful in designing the motion of the safety seat, because these two forces can inadvertently injure the occupant.

1.3.1 Crash Pulse

The normal force between the seat bottom and the occupant depends on the safety seat configuration, as well as the crash-pulse signature or acceleration. A crash-pulse acceleration can be constructed from experimental data by crashing the vehicle travelling 35 mph into a concrete barrier or theoretically predicted. The pulse for an average vehicle is on the order of 100 to 120 ms in duration, and reaches a maximum deceleration of 25 to 35 g's [19, 53, 27]. Figure 4 shows the crash-pulse signature for the 2000 Isuzu Rodeo [19]. Figure 5 shows the crash-pulse for the 2000 Volkswagen Jetta [19]. The acceleration levels and duration are similar for Figures 4 and 5, therefore designing the optimal trajectory for a safety seat for either of these two vehicles, would be somewhat similar.

Some work has been done in order to reshape the crash-pulse signature. Researchers have attempted to alter the crash-pulse by rearranging engine components along with changing materials to soften the shock of a collision. However, the magnitude and duration of the

crash-pulse signature is similar for most vehicles. The extreme deceleration of the vehicle poses a threat to the occupant and a safety seat has the potential to soften the blow.

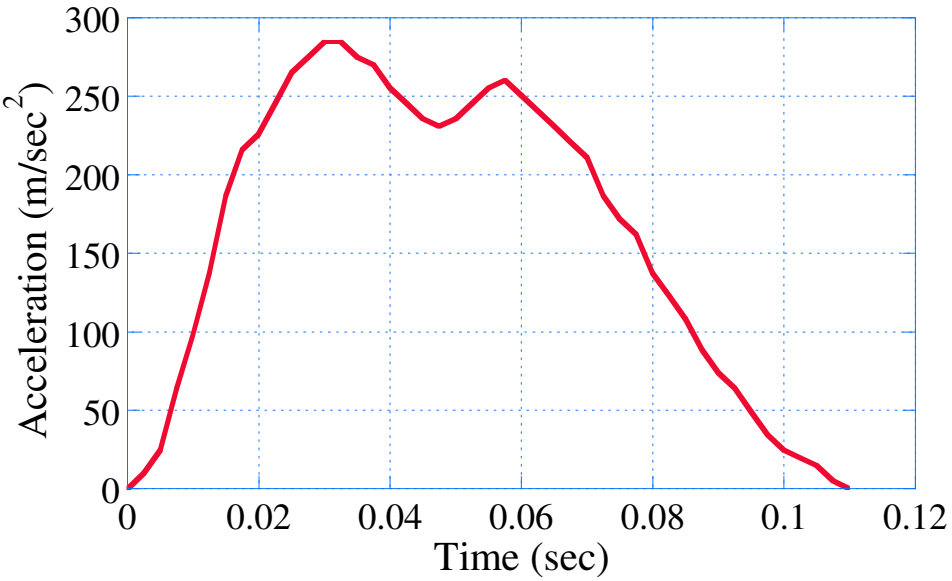

Figure 4: Crash Pulse Signature - 2000 Isuzu Rodeo

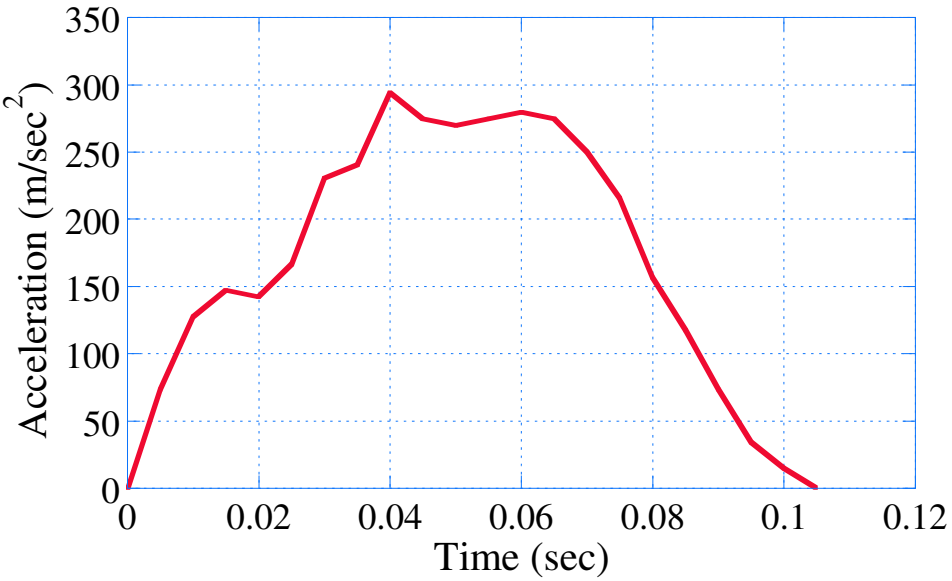

Figure 5: Crash Pulse Signature - 2000 Volkswagen Jetta

Table 3: Airbag Deployment Times (ms)

Make/Model	Test 1	Test 2
1997 Dodge Neon	40	42
1997 Hyundai Elantra	34	22
1995 Ford Taurus	26	26
1997 Pontiac Trans Sport	25	27
1996 Nissan Quest	20	18
1997 Infiniti Q45	52	56

1.3.2 Time Required to Reposition a Safety Seat

In order for the safety seat to be effective, it must be able to move very quickly. To get an idea of the necessary quickness of the safety seat, one can look at the time required to deploy an airbag. Meyerson, *et al.* recorded that the airbag deployment time for cars varied between vehicles [32]. Table 3 shows the results. The tests were conducted with a high speed camera, and the results were timed from the beginning of the collision, to the time the airbag was fully deployed. The time varies from vehicle to vehicle, however, it is clear that the deployment time is generally between 20 and 55 ms.

Research has shown that for frontal collisions of 50 km/hr, it takes the occupant about 50 ms to collide with the steering wheel. The airbag requires about 15 ms to inflate, therefore the sensor has to ignite the airbag in 20 to 40 ms after the crash. For a side airbag, the time that it takes the occupant to hit the car door after a crash is about 20 ms. It takes a side airbag 10 ms to inflate because of the decreased volume, therefore the sensor must ignite the side airbag in about 5 ms [17]. Some common crash sensor used are the Twin Reed Switch Type Safing Sensor TMSD-H**51D and NRS-603W. These sensors generally take about 10 ms from the time the collision is sensed, to the time the airbag is triggered. This leaves roughly 40 ms to deploy the airbag, or in our case, to move the safety seat. It is important to note that the crash sensors are developed for speeds of 50 mph. An agricultural vehicle will travel at slower velocities, therefore the Hyper-Active seat will have longer to configure to a safety seat position.

1.3.3 Limits on Humans

An increase in the seat bottom angle leads to a greater force between the occupant and seat. A possible negative side effect of this approach is an increase in the relative velocity in the vertical direction, even though the overall relative velocity is decreased. This could result in the occupant's head impacting the vehicle ceiling. Another effect which is generally forgotten, is that it is possible to increase the normal force too much, which could crush the occupants spine.

The human body has a limit on the acceleration which it can handle in the vertical direction. Normal forces exerted on the occupant by a safety seat during a crash can very similar to the forces seen from an ejection seat. Accelerative forces of approximately 20 g's are considered to be the safe upper limit for seat-ejection experiments, since fracture of the lumbar vertebrae has been reported beyond 20 g's [10, 1]. This limit is different than the acceleration limit in the horizontal direction. Research has concluded that a human can withstand more than 29 g's, and stop from a velocity of 50 mph within 6 inches without injury with the use of seat belts and airbags [34]. However, a safety seat is designed to protect occupants without the use of seat belts and airbags.

1.3.4 Current Safety Seats

Safety seats have not been widely researched in universities. Mercedes-Benz is the only company to have commercially introduced a safety seat. Their seating system will automatically increase the seat cushion inclination of the occupant's seat. This prevents the occupants from submarining [2]. Other than this seat, there has not been a commercially available safety seat on the market.

The idea of a safety seat is not a new concept. Their has been many patents granted on the design of a safety seat. The patents have been generally granted to large companies, such as Deere and Company, Ford, and GM, however, some have also been granted to private inventors. The patents tend to fit into three main categories:

1. Safety seats that elevate the front of the seat [22, 18, 7, 45]

2. Safety seats that lower the back of the seat [55, 54]

3. Safety seats that move the whole seat to a different position [8, 61, 9].

One reason more active safety seats are not found in commercial vehicles, is the power requirement to activate the seat. The seat needs to be moved very quickly which means fast, expensive actuators. This adds to the cost of the vehicle, which most consumers are not willing to pay. Safety seats have been powered by active and passive means. The active power ranges from springs, to pyrotechnics, as found in airbags, while passive means use the vehicles inertia. Along with the power requirements, extra space is needed to provide for the motion of each seat.

1.4 Thesis Organization

This thesis is organized into five chapters. This first chapter has identified the problem of whole-body vibration on humans. It outlined the harmful range of vibrations and looked at a number of solutions to this problem. One of the best solutions was developing a seating system which reduces the amount of vibration to which the occupant was exposed. A number of seating systems were discussed, as well as the controllers that were developed to control the seats. The concept of a safety seat was introduced, as well as research that has been conducted in this field.

Chapter two discusses the design and building of the Hyper-Active seat. The seat design, which uses a 3R<u>P</u>R configuration, will be introduced, as well as the components used to construct the seat. The design and components of the excitation base, which induces vibrations into the Hyper-Active seat is described. The software and controller design of the seat is outlined. The position and vibration cancellation controllers are discussed, as well as the excitation base controller.

Chapter three discusses experimental system identification of the Hyper-Active seat. A model of the seat is developed in multiple degrees of freedom using the step and frequency response. The position controller is evaluated in each of the degrees of freedom. The performance of the vibration cancellation controller is evaluated against an uncontrolled Hyper-Active seat. The two systems are compared using a sine wave at various frequencies to

represent a bump at different speeds. The Root-Mean-Squared (RMS) average acceleration and the displacement amplitude are recorded for the various inputs. The performance of the vibration cancellation controller is evaluated on these two criteria.

Chapter four discusses safety seat optimization and design. A fixed-seat model is developed to show how the seat bottom angle, coefficient of kinetic friction, and slide distance affect the relative kinetic energy of an occupant during a front-end collision. A moving-seat model is used to collect data about the relative velocity and maximum normal force of the occupant while varying four parameters; the X and Y end position, the ending angle θ, and the duration of the move. An arced path is constructed, and the degrees in the circle are varied to understand the effect of changing the path. These parameters will be used to design the optimal path for a safety seat.

Finally, chapter five gives conclusions about the design and building of the Hyper-Active seat, as well as the experimental results. Methods for designing safety seats are discussed, as well as the optimal path of the seat. The future work of the research is also discussed.

CHAPTER II

HYPER-ACTIVE SEAT CONSTRUCTION

2.1 Designing the Hyper-Active Seat

A number of details need to be considered when designing a Hyper-Active seat for vibration suppression and safety seat motion. There is a balance between fulfilling the design requirements and making sure the seat is kept at a reasonable cost. The concern for this project is mostly on meeting the requirements and secondly on the cost of the seat. It is important that the Hyper-Active seat will cancel the unwanted vibration, but also be able to be used as a tool for furthering education. Figure 6 shows a sketch of the Hyper-Active seat. The design and building of the Hyper-Active seat was largely accomplished with the participation of Dr. Kris Kozak and the support of the companies of the Fluid Power and Motion Control Center at the Georgia Institute of Technology.

Figure 6: Sketch of the Hyper-Active Seat

2.1.1 Design Specifications for the Hyper-Active Seat

The main design requirement of the Hyper-Active seat was that it would be able to cancel low-frequency vibrations which are harmful to the operators of off-road vehicles. As mentioned in Section 1.1.1, frequencies in the 1 to 7 Hz range are harmful to humans. This is the target range of frequencies which the Hyper-Active seat must attenuate. Deere and Company currently has a one-degree-of-freedom Active Seat™ which has been designed to attenuate vibrations only in the vertical direction [16]. The goal of the Hyper-Active seat is to attenuate vibrations in more than just the vertical direction.

Deere and Company was consulted to determine what the most important degrees of freedom were in their target markets. It was determined that the most important degree of freedom was the vertical direction, and the second and third most important degrees of freedom were the fore-aft motion, along with the pitch motion. As mentioned in Section 1.2.3, tractors tend to have a lot of vibration when they are pulling a trailer or other heavy farm implements. Therefore, it was decided to construct a 3 degree-of-freedom Hyper-Active seat prototype, which will suppress vibrations in the vertical, fore-aft, and pitch angle directions. Figure 7 shows a picture of the Hyper-Active seat developed at the Georgia Institute of Technology. To provide the best vibration cancellation performance, the Hyper-Active seat will be a fully active seat, meaning, that it will not have additional springs or dampers along with the actuators. Even though the Hyper-Active seat will be able to suppress vibrations better than an active seat, it will require a lot of power.

The Hyper-Active seat needs to have a power source which is readily available on most off-road vehicles. Hydraulic power is commonly used on tractors and other farming vehicles. Table 2 shows that tractors generally have high pressure hydraulics available for a number of farming tasks. The John Deere 8020 and the 8020T tractors which include the Active Seat™ as an option currently have 2,900 psi of hydraulic pressure. The hydraulic pump on these tractors have a flow rate of 33.5 gal/min which would be more than enough to move the seat fast enough to cancel unwanted vibration in the low-frequency range. Hydraulic power is the best power source available on tractors due to its abundant supply and ability to move the seat with enough velocity and force to cancel the unwanted vibrations.

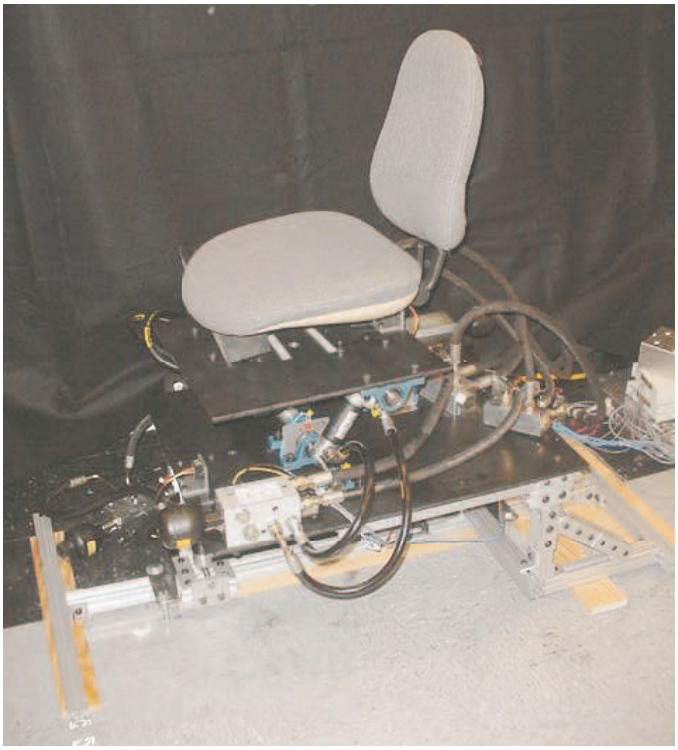

Figure 7: Hyper-Active Seat Developed at the Georgia Institute of Technology

Another goal of the design was to incorporate a number of components from the current Deere and Company Active Seat™. Deere and Company donated a number of hydraulic cylinders, manifolds, valve drivers, and accelerometers to be utilized in the design process. Most of these components require hydraulic power, which enforces the decision to use hydraulic power. Taking all these requirements into consideration, a Hyper-Active seat was developed to cancel vibrations felt by the operator.

2.1.2 3RPR Configuration of the Hyper-Active Seat

A 3 Revolute-Prismatic-Revolute (RPR) parallel manipulator was selected for its ability to accomplish the tasks at hand. The design utilizes a parallel kinematical architecture in a variable geometry truss configuration. This architecture and configuration provides the desired three degrees of freedom while balancing the competing issues of actuator force transmission and workspace size. This configuration has the added benefit of containing no kinematic platform singularities within the workspace. Figure 8 shows the 3 RPR parallel manipulator.

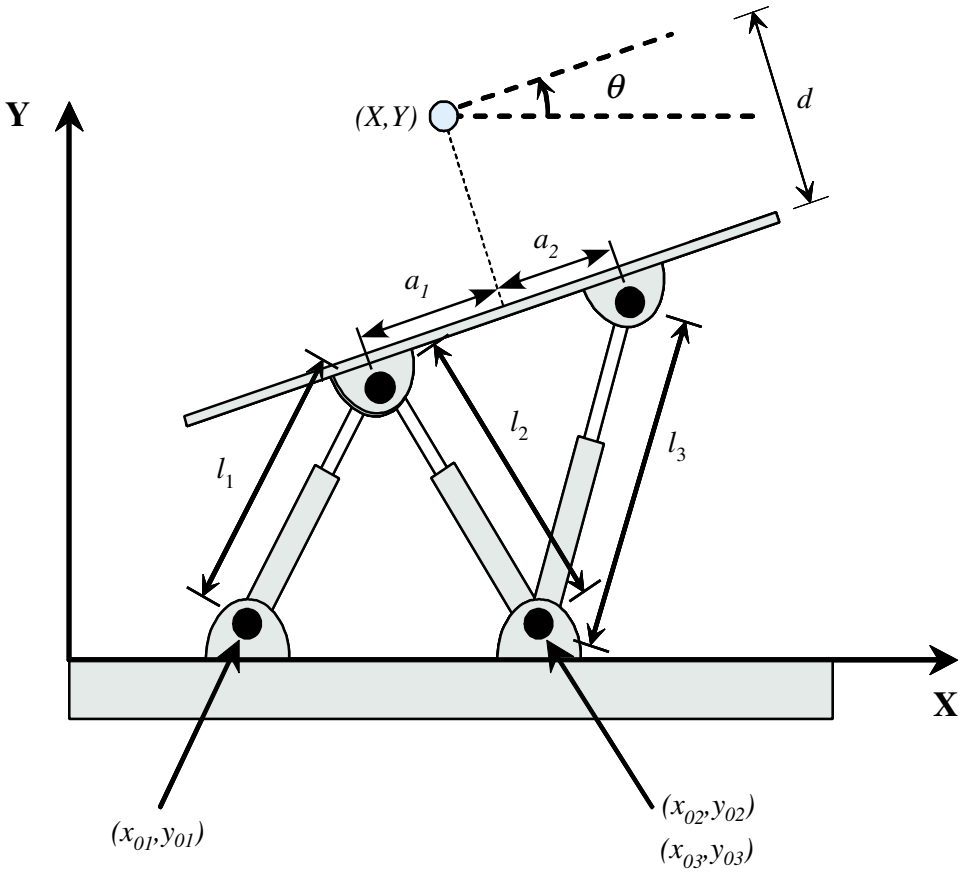

Figure 8: Diagram of 3RPR Mechanism

One important thing to consider is that the Hyper-Active seat is not a two dimensional seat, as Figure 8 seems to portray. The seat is a three dimensional seat, and therefore, the actuators need to be placed very carefully to balance the weight of the operator. The seat must also be able to account for any unexpected torque in the roll angle direction. Along with being able to balance the load of the seat and the operator, the configuration must have a workspace which is large enough to allow for the vibration cancellation.

2.1.2.1 Inverse Kinematics of the Hyper-Active Seat

Movement control of the Hyper-Active seat in the vertical, Y, fore-aft, X, and pitch angle, θ, requires the knowledge of the leg lengths. To obtain these lengths, encoders are used to measure the angles between the actuators and the top and bottom plates of the seat. The angle measurements are then used to estimate the leg lengths of the seat. Figure 9 shows the four angles that are measured by encoders. Using these four angle measurements, the

three leg lengths can be calculated using these relationships:

$$l_1 = \frac{b\sin(\theta_2)}{(\cos\theta_1)(\sin\theta_2) - (\sin\theta_1)(\cos\theta_2)} \tag{6}$$

$$l_2 = \frac{b\tan(\theta_1)}{(\sin\theta_2) - (\tan\theta_1)(\cos\theta_2)} \tag{7}$$

$$l_3 = \frac{b\sin(\phi_2)}{(\sin\phi_3)(\cos\phi_2) - (\sin\phi_2)(\cos\phi_3)}, \tag{8}$$

where the four angles are labelled in Figure 9. The measurement of the leg lengths are a necessary part of the jacobian calculation, and therefore needed for the control of the Hyper-Active seat.

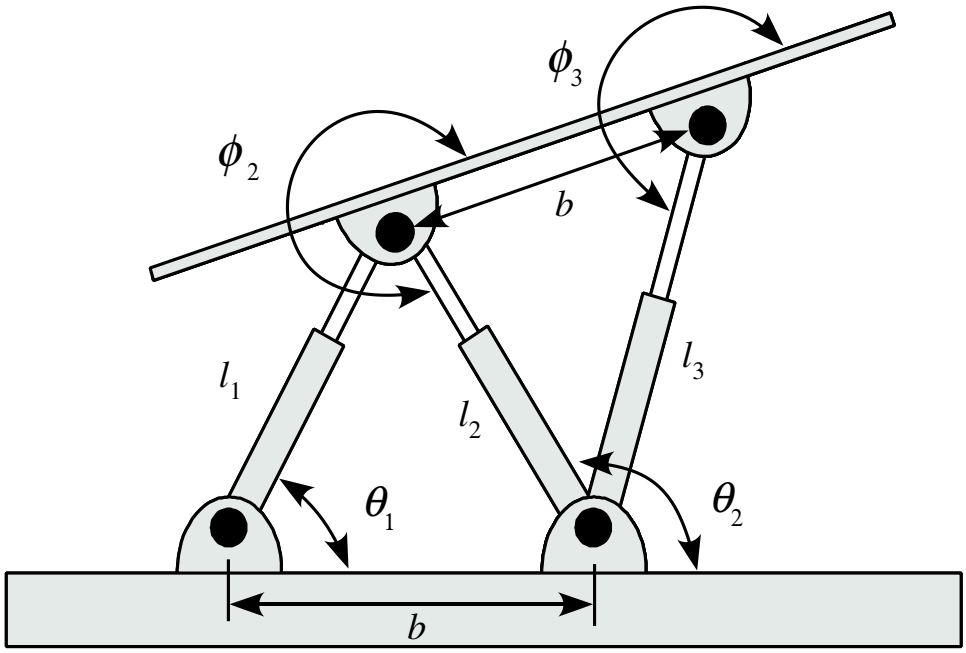

Figure 9: Measured Angles of the Hyper-Active Seat

To move the Hyper-Active seat in the three directions, the inverse kinematics are needed. The inverse kinematics transfer the desired X, Y, θ coordinates into leg lengths. The inverse kinematics are calculated using the following equations:

$$l_1 = [(X + d\sin\theta - a_1\cos\theta - x_{01})^2 + (Y - d\cos\theta - a_1\sin\theta - y_{01})^2]^{1/2} \tag{9}$$

$$l_2 = [(X + d\sin\theta - a_1\cos\theta - x_{02})^2 + (Y - d\cos\theta - a_1\sin\theta - y_{02})^2]^{1/2} \tag{10}$$

$$l_3 = [(X + d\sin\theta + a_2\cos\theta - x_{03})^2 + (Y - d\cos\theta + a_2\sin\theta - y_{03})^2]^{1/2}, \tag{11}$$

where the coordinates and kinematic parameters are shown in Figure 8. The inverse kinematics and the measurement of the leg lengths make it possible to control the Hyper-Active seat. However, this method wastes time with the transferring of coordinates, and is not the ideal way. The Hyper-Active seat is controlled using the jacobian relationship.

2.1.2.2 Jacobian of the Hyper-Active Seat

The jacobian relationship transfers the desired coordinates into leg lengths. This may seem similar to the inverse kinematics, however, in this method the X, Y, and θ coordinates are used as feedback, instead of the leg lengths. This way, the actual coordinates are compared to the desired coordinates. This method of controlling the seat in the coordinate space rather than controlling the seat in the leg length space, is a more suitable method of controlling the seat.

To control a 3R$\underline{\text{P}}$R parallel manipulator, certain relationships must be known. It is vital to understand the relationship between the leg lengths and the X, Y, θ coordinate space. This relationship is found using the jacobian relationship. The jacobian of a 3R$\underline{\text{P}}$R relates the velocity of the leg lengths, to the velocity in the coordinate space. The equation for this relationship is shown below:

$$\dot{\bar{l}} = J\dot{\bar{x}}, \tag{12}$$

where J is the jacobian, $\dot{\bar{l}}$ is the velocity of the leg lengths and $\dot{\bar{x}}$ is the velocity of the coordinate space. $\dot{\bar{l}}$ is more precisely defined as:

$$\dot{\bar{l}} = \begin{bmatrix} \dot{l}_1 \\ \dot{l}_2 \\ \dot{l}_3 \end{bmatrix}, \tag{13}$$

where $\dot{l}_1$ is the velocity of cylinder #1, $\dot{l}_2$ is the velocity of cylinder #2, and $\dot{l}_3$ is the velocity of cylinder #3. The definition of $\dot{\bar{x}}$ is better described as:

$$\dot{\bar{x}} = \begin{bmatrix} \dot{X} \\ \dot{Y} \\ \dot{\theta} \end{bmatrix}, \tag{14}$$

where $\dot{X}$ is the velocity of the Hyper-Active seat in the horizontal direction, $\dot{Y}$ is the velocity of the seat in the vertical direction, and $\dot{\theta}$ is the velocity of the seat in the pitch angle direction.

The jacobian also relates the change in position of the leg lengths to the change in the position in the coordinate space. Equations (15) - (18) show how this result is derived:

$$\dot{\bar{l}} = J\dot{\bar{x}} \tag{15}$$

$$\frac{d\bar{l}}{dt} = J\frac{d\bar{x}}{dt} \tag{16}$$

$$\frac{d\bar{l}}{dt}dt = J\frac{d\bar{x}}{dt}dt \tag{17}$$

$$\Delta\bar{l} = J\Delta\bar{x}, \tag{18}$$

where $\Delta\bar{l}$ is the change in position of the leg lengths, and $\Delta\bar{x}$ is the change in position of the coordinate space. This relationship provides a means to the control of the Hyper-Active seat in the coordinate space.

The jacobian matrix J shown in (15) can be calculated by differentiating (9) - (11) and then collecting the terms. The jacobian matrix, J, for the 3RPR is:

$$J = \begin{bmatrix} -\frac{x_{01}-d\sin\theta-X+a_1\cos\theta}{l_1} & -\frac{y_{01}+a_1\sin\theta-Y+d\cos\theta}{l_1} & \cdots \\ -\frac{x_{02}-d\sin\theta-X+a_1\cos\theta}{l_2} & -\frac{y_{02}+a_1\sin\theta-Y+d\cos\theta}{l_2} & \cdots \\ \frac{X+a_1\cos\theta+d\sin\theta-x_{03}}{l_3} & \frac{Y+a_1\sin\theta-d\cos\theta-y_{03}}{l_3} & \cdots \end{bmatrix}$$

$$\begin{bmatrix} -\frac{-Xa_1\sin\theta-Xd\cos\theta+Ya_1\cos\theta+x_{01}a_1\sin\theta+x_{01}d\cos\theta-Yd\sin\theta+y_{01}d\sin\theta-y_{01}a_1\cos\theta}{l_1} \\ -\frac{-Xa_1\sin\theta-Xd\cos\theta+Ya_1\cos\theta+x_{02}a_1\sin\theta+x_{02}d\cos\theta-Yd\sin\theta+y_{02}d\sin\theta-y_{02}a_1\cos\theta}{l_2} \\ \frac{-Xa_1\sin\theta+Xd\cos\theta+Ya_1\cos\theta+x_{03}a_1\sin\theta-x_{03}d\cos\theta+Yd\sin\theta-y_{03}d\sin\theta-y_{03}a_1\cos\theta}{l_3} \end{bmatrix}, \tag{19}$$

where the variables are defined in Figures 8 and 9. The jacobian has the advantage of relating the velocities of the leg lengths and the coordinate directions, as well as, the change in leg length and the change in coordinate direction. This allows for both the control of position and velocity as will be shown in Section 2.5.2.

Table 4: Workspace of 3RPR

Direction	Center	Calculated Range	Calculated Total Travel	Experimental Range	Experimental Total Travel
Vertical	7.55 in	6.09 - 8.99 in	2.90 in	6.04 - 9.16 in	3.12 in
Horizontal	8.75 in	6.56 - 10.94 in	4.38 in	6.42 - 11.11 in	4.69 in
Pitch Angle	0.00 rad	-0.37 - 0.37 rad	0.74 rad	-0.31 - 0.35 rad	0.66 rad

2.1.2.3 Forward Kinematics of the Hyper-Active Seat

In order to know the exact position of the Hyper-Active seat in the workspace, the forward kinematics are used. The forward kinematical equations, which give X, Y, and θ in terms of the leg lengths, can be obtained using (9) - (11):

$$\theta = \pi + \theta_2 - \phi_2 \tag{20}$$

$$X = \frac{l_1 \cos\theta_1 + 2a_1 \cos\theta + b + l_2 \cos\theta_2}{2} \tag{21}$$

$$Y = \frac{l_1 \sin\theta_1 + 2a_1 \sin\theta + l_2 \sin\theta_2}{2}. \tag{22}$$

The X, Y, and θ values are used in the jacobian relationship and are very useful to feedback the position of the Hyper-Active seat.

2.1.3 Workspace of the Hyper-Active Seat

The Hyper-Active seat was designed to have a significant amount of travel in each direction; noting the restriction of the cylinders donated from Deere and Company. Table 4 shows the theoretical and experimental range of travel of the seat, as well as the coordinates for the center of the workspace. Their is no need to calculate the workspace around any other point other than the center because the Hyper-Active seat will have a position centering control loop. This additional control loop will bring the seat back to the center position in the chance that it would drift from the center position during vibration cancellation.

The workspace calculations for the vertical, horizontal, and pitch angle directions can be seen in Section B.1. Now that the calculations have been made, the Hyper-Active seat can be tested to find the exact workspace. Figure 10 shows the vertical movement of the Hyper-Active seat from the center of the workspace. The seat has about 3.12 inches of travel, slightly more than predicted by the calculations. The small amounts of residual vibration

shown at the beginning of Figures 10 - 12 are due to the Hyper-Active seat moving to the center of the workspace. Figure 11 shows the horizontal travel of the seat. The seat has 4.69 inches of travel in the horizontal direction. The seat has more horizontal than vertical movement due to the placement of the actuators. It was felt that it was better to place the actuators in the current configuration to maximize force and speed in the vertical direction. Figure 12 shows the experimental range of the Hyper-Active seat in the pitch angle direction. The experimental results of 0.66 rad, are slightly less than the calculated values. One reason that the experimental values are different than the predicted values is due to the extra height of the seat from the bearings. The bearings give the seat extra height, which was not taken into account for the calculations.

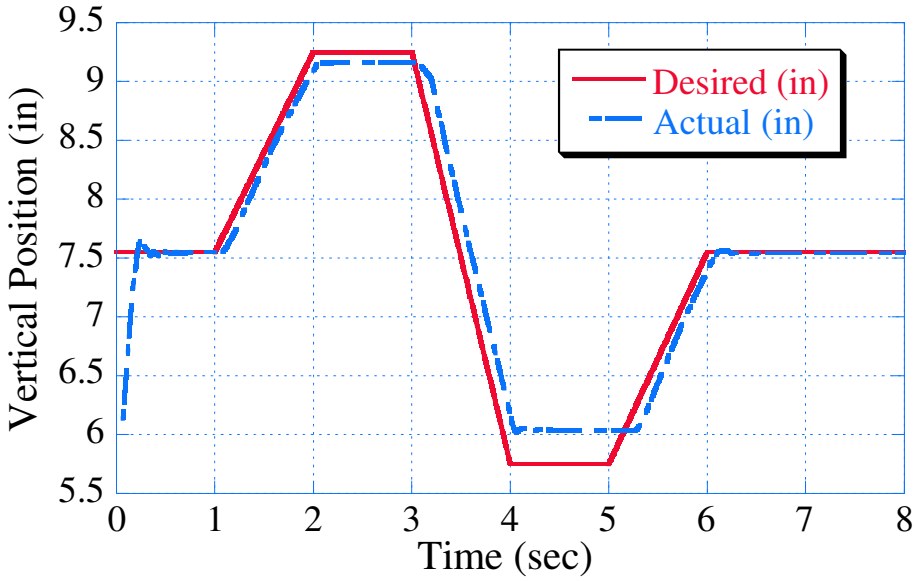

Figure 10: Vertical Workspace Range of the Hyper-Active Seat

2.1.4 Hyper-Active Seat Pump Parameters

The Hyper-Active seat is powered by a 30 gpm variable displacement pump operating at 3,000 psi. This is very similar to what is available on the John Deere 8020 and 8020T tractors. However, the three cylinders powering the seat run on a maximum of 7 gpm at 500 psi. One can see that the current pump will have more than enough flow rate and pressure to meet the demand of the Hyper-Active seat. The variable-displacement pump

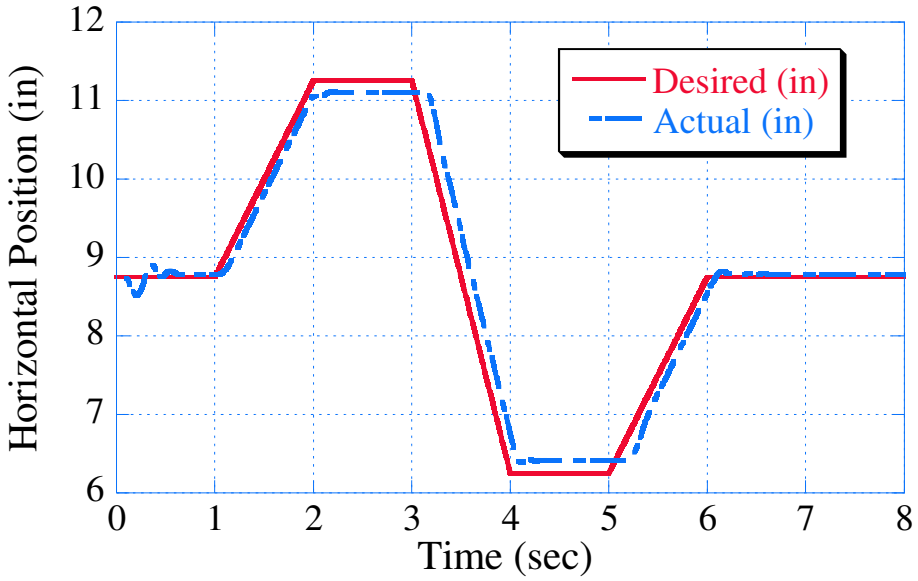

Figure 11: Horizontal Workspace Range of the Hyper-Active Seat

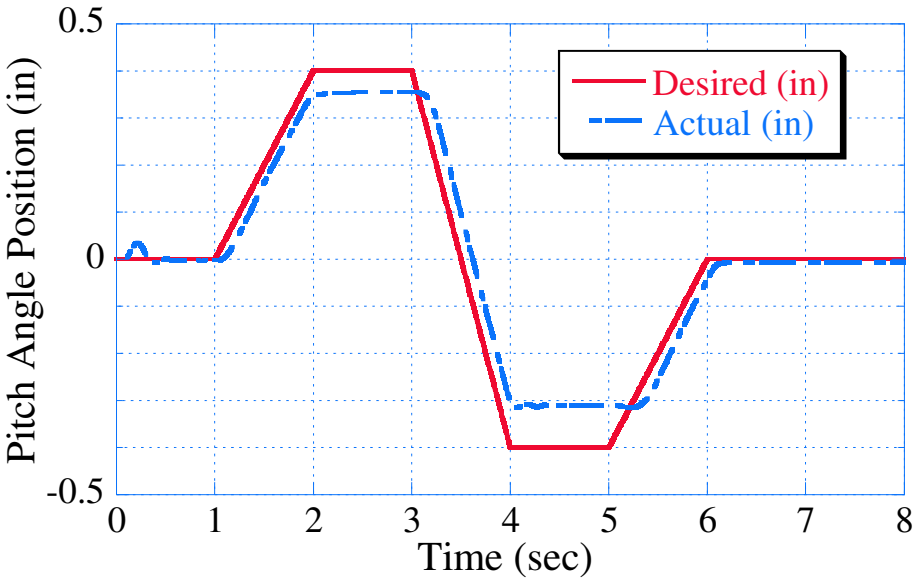

Figure 12: Pitch Angle Workspace Range of the Hyper-Active Seat

allows for different flow rates through the hydraulic lines. The cylinders and manifolds that Deere and Company donated were designed for a fix-displacement pump. One issue this brings forth is there is a small amount of pulsing that occurs in the hydraulic lines. This does not deter from the performance of the Hyper-Active seat. However, it is important that the hydraulic hoses are clamped down to reduce wear of the hoses.

2.1.5 Hyper-Active Seat Force Calculations

Figure 13 shows the inside of one of the hydraulic cylinders. Since the piston of the cylinder has the rod attached to one side, there will be a difference in the amount of force the cylinder can supply in each direction. The equation for the force of the piston is:

$$Force = Pressure * Area. \tag{23}$$

The cylinder will have more force extending than contracting due to more surface area in the extension direction. Figure 14 shows the six directions that the force was calculated. Table 5 shows the forces in each of the directions. Note that the pitch angle calculations are torques, instead of force. The forces were calculated at the center of the workspace, so they will be slightly larger or smaller when the seat moves away from the center of the workspace. The Hyper-Active seat has more than enough force in all directions to safely cancel the vibrations for any size load and configure the seat into a safety seat.

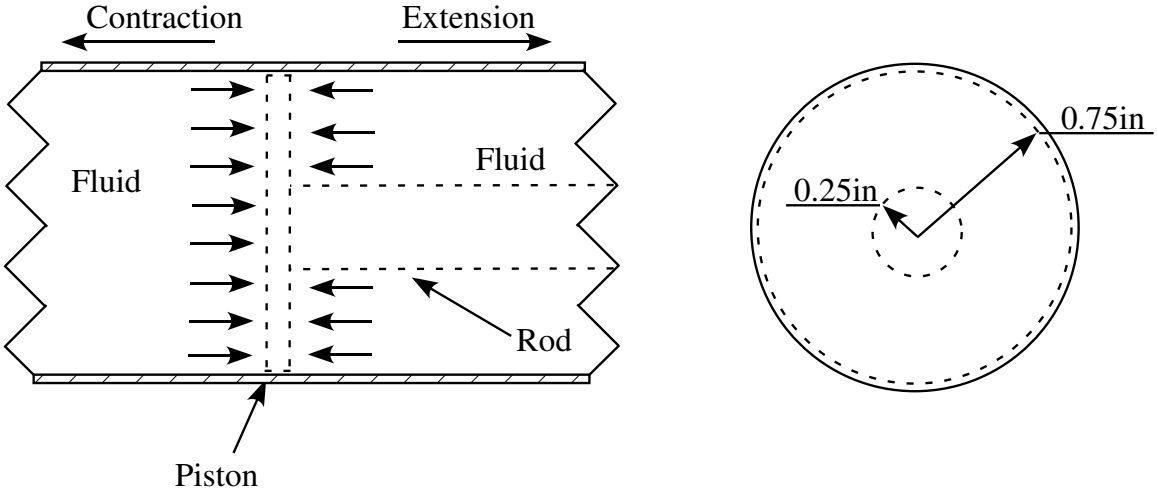

Figure 13: Hydraulic Cylinder Sketch

2.1.6 Hyper-Active Seat Speed Calculations

The velocity of the cylinders is important to know because it limits the range of vibrational frequencies that can be eliminated. It is also important if the Hyper-Active seat was going to be used as a safety seat. A safety seat is discussed in detail in Section 1.3. One main movement of a safety seat is to raise the front of the seat by some angle in the time of a

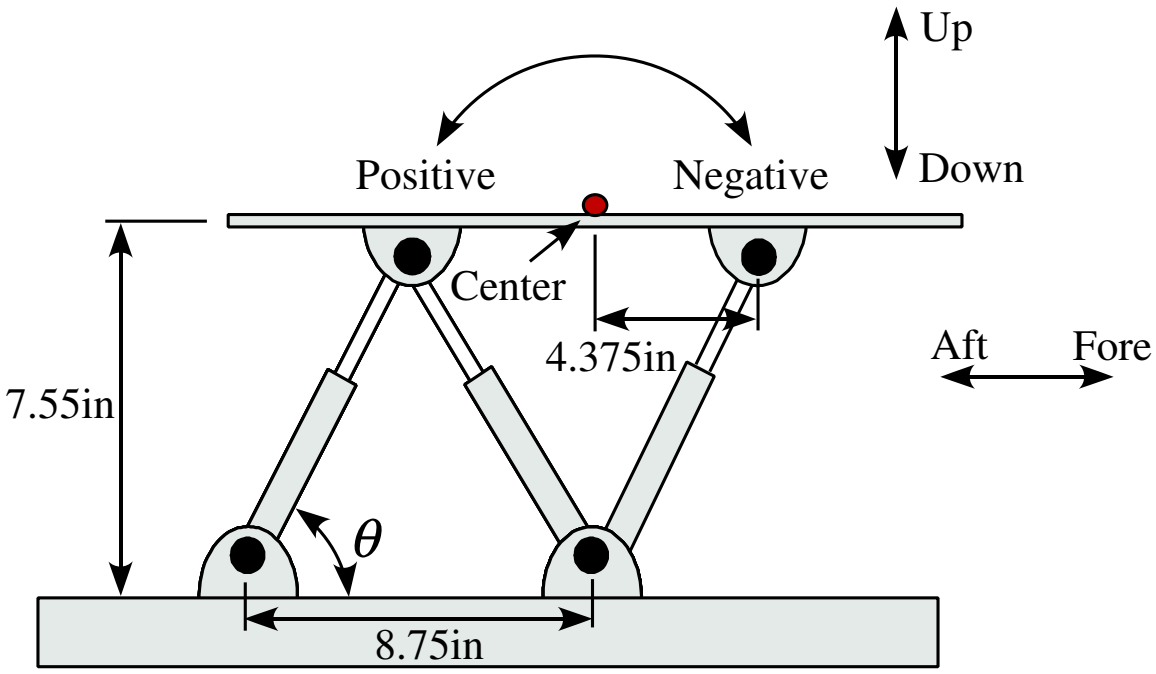

Figure 14: Hyper-Active Seat Force Calculation Directions

Table 5: Force of the Hyper-Active Seat

	Direction	Force
Vertical	Up	2293.5 lbf
	Down	2038.6 lbf
Horizontal	Fore	1279.8 lbf
	Aft	1230.6 lbf
Pitch Angle	Positive	9290.8 in-lbf
	Negative	9662.5 in-lbf

crash. This rotation must occur very quickly to reposition the seat before the occupant slides to far in response to the crash-pulse. The equation for the velocity of a hydraulic cylinder is:

$$Velocity(in/\sec) = \frac{77 * Flow}{20 * Area}, \tag{24}$$

where the $Flow$ is in gallons per minute, and the $Area$ is the area of the piston in inches squared. The maximum theoretical speed of the cylinders is 15.25 in/sec. The calculation is given in Section B.3. The time it would take the Hyper-Active seat to rotate 10 degrees, or raise the front of the seat 1.28 in, is 84 ms. This is longer than the time recommended to configure a safety seat mentioned in Section 1.3.2, however it would be possible to replace

the current front cylinder of the Hyper-Active seat with a faster actuator. This would allow the seat to move into a safety seat in the recommended 50 ms.

2.2 Hyper-Active Seat Components

The Hyper-Active seat was built with only a few main components. The top and bottom of the seat are made of 3/8" steel to provide the support needed for the occupant. The cylinders for the seat, which are currently used on the John Deere Active Seat™, were donated by Deere and Company. Along with the cylinders, Deere and Company also donated the valves, valve drivers, and manifolds. The cylinders are connected to the two steel plates using ball bearing connections. These allow the seat to move smoothly into different configurations. Rotary encoders are used as feedback on the bearings to calculate the exact position of the seat. Finally, the electronic inputs and outputs of the seat are input into MATLAB's xPC Target through computer boards for data acquisition and control.

2.2.1 Hyper-Active Seat Bottom and Top Plates

As mentioned above, the top and bottom of the Hyper-Active seat are made out of 3/8" steel. Holes were drilled in the two plates for mounting the ball bearings and for bolting the encoder brackets. The use of such a sturdy base will provide the support needed for a cushion seat and operator.

2.2.2 Hydraulic Cylinders, Valve Drivers, and Manifolds of the Hyper-Active Seat

Three proportional flow control valves are used to control the cylinder lengths. Table 6 shows the parameters of the cylinders and valves. One important thing to note is, even though the tractor pump may have an operating pressure 3,000 psi with a flow rate of 30 gpm, the valves which supply the cylinders have a maximum pressure of 500 psi with a flow rate of 7 gpm.

The valves are proportional valves, which are controlled using current. To close the valve, one must supply a null current to the valve. If a current greater than the null current is applied, the cylinder extends, and likewise, if a current less than the null current is applied,

Table 6: Cylinder and Valve Parameters

Parameter	Value
Cylinder Length	7.50 in
Cylinder Stroke	2.50 in
Cylinder Piston Radius	0.75 in
Valve Pressure	500 psi
Valve Flow Rate	7 gpm

Table 7: Experimental Results for Finding the Null Current

Parameter	Cylinder #1	Cylinder #2	Cylinder #3	Excitation Base
Extension Voltage	3.27	3.40	3.53	5.90
Contraction Voltage	2.42	3.10	3.23	5.60
Voltage Associated with the Null Current	2.85	3.25	3.38	5.75

the cylinder contracts. Each valve has the null current written on the valve. However, the controller, MATLAB xPC Target allows the user to apply a voltage as an output, not a current. Therefore, the null current was found through experimental means. The voltage supplied to each valve was slowly increased and decreased until the cylinders no longer extended or contracted. Once these values were found, the average was taken and used as the voltage associated with null current. Table 7 shows the results of the null current experiments. The voltage associated with the null current was found without any weight on the seat. This should not be a problem when weight is added, because the controller will minimize the error between the actual location and the desired location.

One important thing noted by Deere and Company, is the piston of the cylinders and manifolds have small holes incorporated in their design. These holes allow for a small amount of leakage in the system which adds damping to the system. However, with the addition of these holes, comes the possibility that the cylinders will experience a dead band. This may provide some difficulty in controlling the Hyper-Active seat.

2.2.3 Hyper-Active Seat Rotary Encoders

Four channel quadrature rotary encoders were selected as a means to measure the angles of the Hyper-Active seat. Three encoders are all that are needed to supply the feedback necessary to calculate the three leg lengths, however, to provide more accurate measurements,

a fourth was added. Rotary encoders are used as an indirect way to measure the leg lengths because it was felt that linear potentiometers or other measuring equipment would take up too much space under the seat. Rotary encoders are small enough to fit compactly under the seat, while allowing the cylinders to move the seat throughout the workspace.

The HEDS-9000-U00 encoders from US Digital Corporation are four channel encoders that have 2048 counts per revolution. They provide ample angle accuracy. Combined with the software in MATLAB xPC Target, the encoders will have an accuracy of 0.044 degrees. The encoders run on +5 volts, which can easily be supplied by the output of one of the National Instrument cards which is used to control the valve drivers. The rotary encoders are mounted on the 5/8" steel shafts which will be discussed in Section 2.2.5.

2.2.4 Hyper-Active Seat Accelerometers

Figure 15 shows the location of the accelerometers on the Hyper-Active seat. An excitation base was built below the Hyper-Active seat to input vibrations into the seat. The base of the Hyper-Active seat is attached to the excitation base by a fixed pivot point at one end, and a hydraulic cylinder at the other. The extension and contraction of the cylinder moves the seat in an arced motion about the pivot point. One will notice that in the current configuration, the seat will experience a coupling between the vertical motion and the pitch angle motion. Due to the availability of two accelerometers, they are currently only placed to sense vibrations in the vertical direction. The accelerometer on the base of the seat will sense the incoming vibration, while the accelerometer on the top of the seat will measure the amount of vibration the occupant feels in the vertical direction. With the addition of more accelerometers, or by repositioning the current accelerometers, the acceleration in other directions can be sensed.

The accelerometers were designed to sense low amounts of acceleration. They have a range of $\pm 2.0 g's$ which translates to a signal between 0 and 5 volts. Table 8 shows the relationship between the output voltage and the sensed acceleration. Since the accelerometer readings are fairly linear, an accelerometer gain can be calculated which gives the acceleration at any voltage.

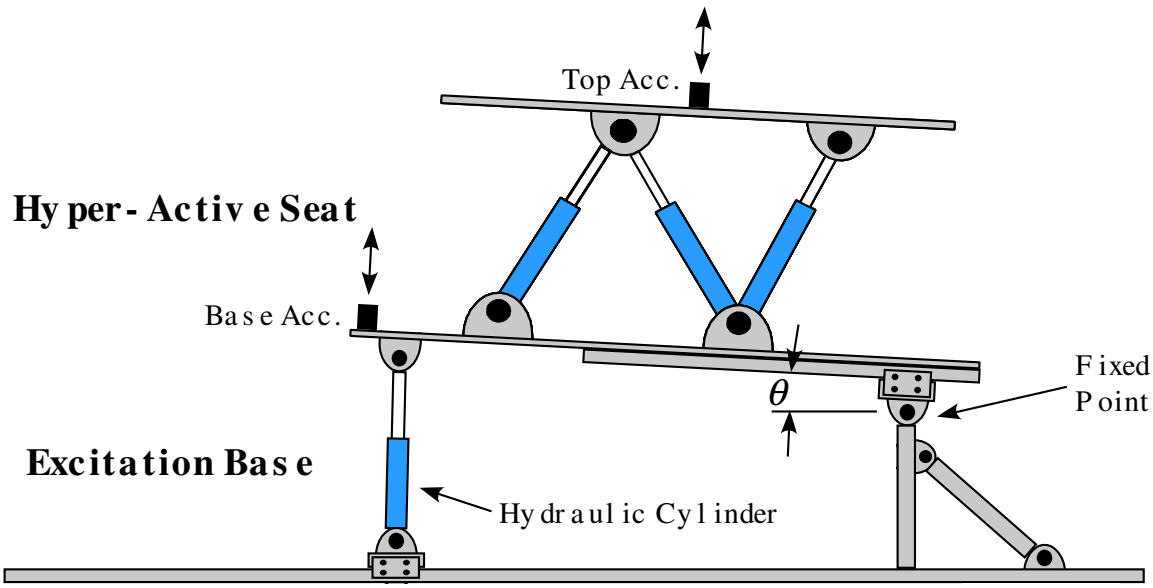

Figure 15: Accelerometer Placement on the Hyper-Active Seat

Table 8: Accelerometer Voltage Verses Acceleration

Acceleration	Seat Top Accelerometer	Seat Base Accelerometer
1.0 g	3.78 v	3.79 v
0.0 g	2.56 v	2.56 v
-1.0 g	1.19 v	1.22 v

2.2.5 Hyper-Active Seat Bearings and Shafts

The Hyper-Active seat has twelve ball bearings to ensure smooth movement of the seat. The SKF SY 5/8" TF ball bearings were selected due to the ease of use. The bearings are self-aligning which allows for small discrepancies in the placement of the bearings. This is a necessary feature when one is trying to align a 3RPR parallel manipulator. It is very difficult to align twelve different bearings, which are all perpendicular to one plane.

Along with the twelve ball bearings, six 5/8" steel shafts are used to connect the ball bearings to the cylinders. Figure 16 shows a diagram of how one of the hydraulic cylinders is connected to a shaft, ball bearings, and then to the seat bottom or top plate. The cylinder is pinned to the steel shaft, and then each side of the steel shaft is connected to a bearing. This configuration allows for smooth movement of the seat. The cylinders are pinned to the

shafts to ensure there is no slipping between the cylinder movement and the shafts. This is very important because the rotary encoders measure the rotation of the cylinders on the shafts.

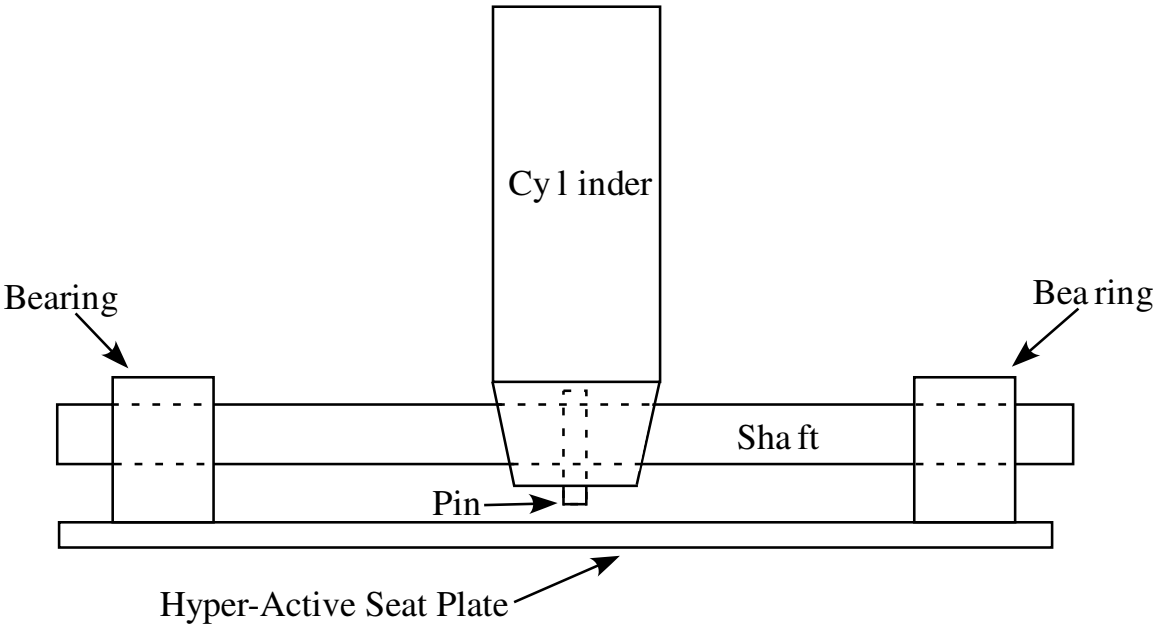

Figure 16: Diagram of Hyper-Active Seat Bearings and Shaft Configuration

2.3 Excitation Base

The Hyper-Active seat is capable of canceling vibrations in the X, Y, and θ directions. To test the ability of the Hyper-Active seat, vibrations need to be input into the base of the seat. An excitation base was built, to produce the vibrations for the seat to cancel.

2.3.1 Design of Excitation Base

Figure 17 shows the Hyper-Active seat sitting on the excitation base in a configuration which will input a coupled vertical and pitch angle vibration. However, the vibration is mostly in the vertical direction. The excitation base also has the ability to slide the position of the seat, using the sliding plates, so the center of the Hyper-Active seat is centered directly over the pivot point. Figure 18 shows the excitation base in the pitch angle configuration. When the center of the seat is directly over the center point, the excitation base will input only pitch angle vibrations into the seat. The amount of coupling between the vertical and

pitch angle direction, is directly related to the position of the Hyper-Active seat over the pivot point.

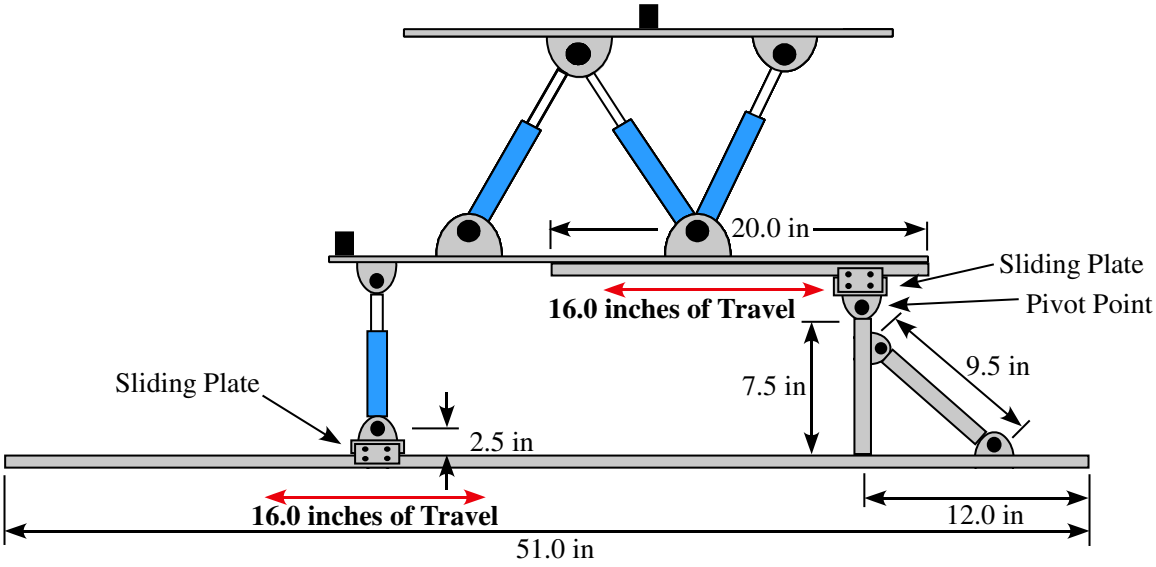

Figure 17: Excitation Base and Hyper-Active Seat in Vertical Configuration

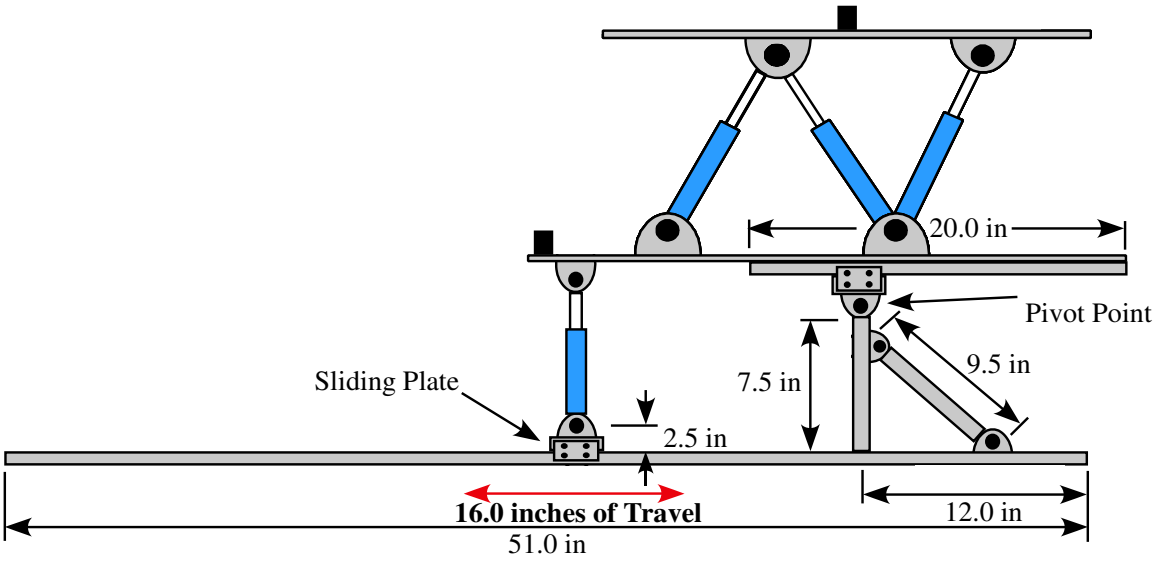

Figure 18: Excitation Base and Hyper-Active Seat in Pitch Angle Configuration

The excitation base is constructed of 80/20 extruded aluminum. This allows for a sturdy design and quick assembly. The pivot point of the excitation base is reinforced with

an angled piece of 80/20 for extra strength, as shown in Figures 17 and 18. The excitation base is designed allowing for 16 inches of travel for the Hyper-Active seat. This ranges from having the pivot point in the center of the Hyper-Active seat, to having the pivot point on the end of the seat.

The two sliding plates shown in Figures 17 and 18 are designed to allow easy changes in testing configuration. Once two of the four bolts are loosened, the Hyper-Active seat can be reconfigured into any position along the 20" track. The excitation base only gives 16" of travel and not 20", because the sliding plates are 4" in length. Repositioning the seat allows for the testing of the Hyper-Active seat with a number of different degrees of coupling between the vertical and pitch angle directions.

2.3.2 Components of the Excitation Base

The excitation base was designed with one hydraulic cylinder. The cylinder has enough force to create the needed vibrations for the Hyper-Active seat, as shown in Section 2.1.5. As before, the voltage associated with the null current needed to be found experimentally. Table 7 shows the experimental results of finding the voltage associated with the null current. This voltage is higher for the excitation base cylinder due to the extra weight on the cylinder. The voltage associated with the null current is directly related to the amount of weight on the cylinder.

The excitation base was controlled using position feedback. A LX-PA Series String Potentiometer from UniMeasure was used to measure the excitation base position. This potentiometer has a linear relationship between the distance the string is extended to the corresponding voltage it outputs. This relationship was found by plotting the string length verses the output voltage. Figure 19 shows the resulting linear equation that was found experimentally. This equation was then used in MATLAB to control the output of the excitation base.

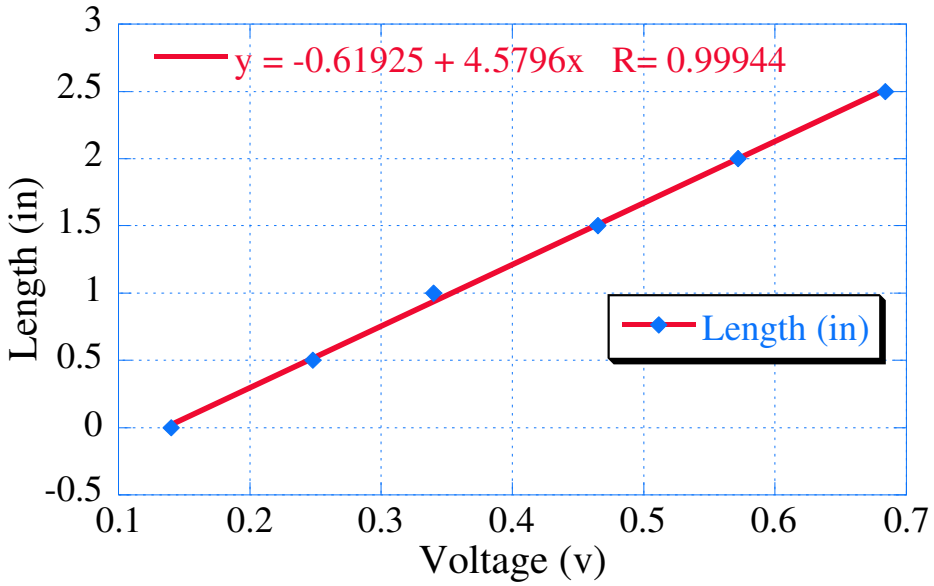

Figure 19: String Distance Verses Output Voltage of the String Potentiometer

2.4 Software Design Using Simulink for the Hyper-Active Seat

The Hyper-Active seat is controlled using MATLAB's xPC Target and Simulink. The control scheme is created using Simulink and xPC Target blocks. The Simulink diagram is then converted into C code using MATLAB's Real Time Workshop (RTW). This allows for the control of the Hyper-Active seat in real-time. Some of the advantages of using Simulink for the controller design is that control systems can be tested very quickly. A new type of controller can be designed and implemented very quickly, without waiting to reprogram C code. One drawback of using MATLAB's xPC Target, is that it only supports certain data acquisition cards. This made it difficult to find cards that would work with the current hardware setup.

2.4.1 Data Acquisition Computer Boards used for the Hyper-Active Seat

The Hyper-Active seat has analog and digital inputs and analog outputs that need to be controlled. The four rotary encoders are digital inputs and they require a special encoder card. The string potentiometer on the excitation base, along with the two accelerometers are analog devices. They require an analog to digital conversion. Finally, the four valve

drivers which control the cylinder position all require an analog output. These require a digital to analog conversion.

The main data acquisition card is a National Instrument 6052E. This card has more than enough inputs, however, it only has two digital to analog conversion outputs. Therefore, another National Instrument 6052E data acquisition card is used to handle the remainder of the digital to analog conversion outputs. A PCI-QUAD04 encoder card was purchased from Measurement Computing. The encoder card keeps track of the encoder counts so the sampling rate can be set as desired. These three cards handle the inputs and outputs of the Hyper-Active seat.

2.4.2 Hyper-Active Seat Voltage/Velocity Cylinder Relationship

The control of the Hyper-Active seat turned out to be very challenging. The hydraulic valves seemed to have large dead bands, which occurred when a voltage was being output to the valve driver, yet the cylinders would not move. It was discovered that this phenomena, mentioned in Section 2.2.2, was a result of the small holes drilled in the cylinder pistons and manifolds to add damping to the system. It was noticed that increasing the weight on the seat decreased the dead band, however adding weight to the system was not an acceptable design solution.

The solution to this problem involved mapping the voltage/velocity relationship of each cylinder. As noted in Section 2.1.2.2, the 3R<u>P</u>R jacobian is a relationship between the velocity of the leg lengths and the velocity in the coordinate space. Since the output of the jacobian is the velocity of each leg, or cylinder length, velocity can be compared to the voltage/velocity to get the corresponding voltage to send to the valve driver. This eliminates the dead band.

The velocity of each cylinder was recorded at incremental changes of the voltage from the voltage associated with the null current. The velocity was calculated by recording the slope while the cylinder moved from one position to another. Figure 20 shows the voltage/velocity relationship between each of the Hyper-Active seat legs. Cylinder #1 has a large dead band which affected the position of the Hyper-Active seat. The dead band

is mostly evident in Cylinder #1 due to the geometry of the 3RPR structure. Cylinders #2 and #3 are supporting the majority of the weight from the top plate. The added weight decreased the dead band in these cylinders. This was evident when the seat was disassembled and the individual cylinders were tested. Without the weight of the top plate, each cylinder had the same size dead band.

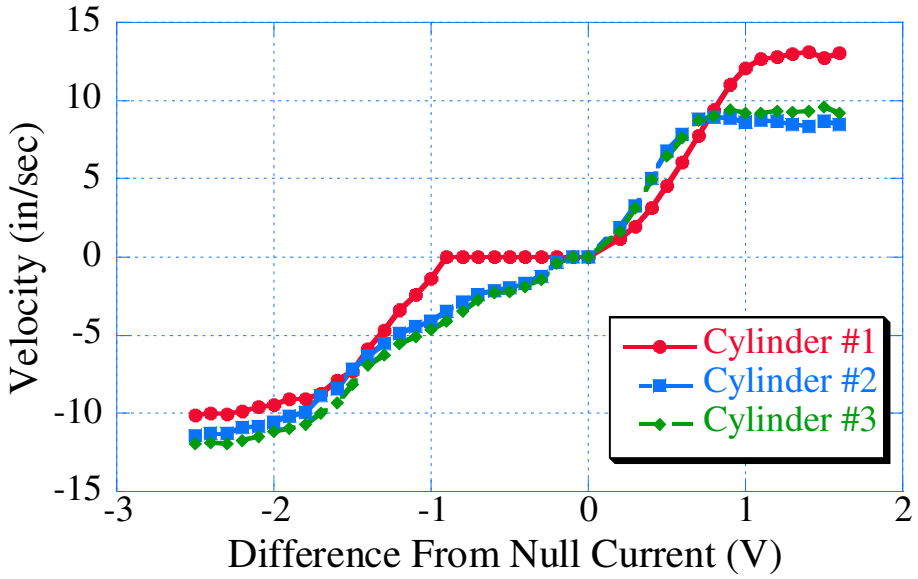

Figure 20: Hyper-Active Seat Cylinder Voltage/Velocity Relationship

Now that the cylinder voltage/velocity relationship is understood, the inverse relationship can be used to control the seat. Figure 21 shows the inverse relationship of the cylinder extension (positive) velocity verses voltage greater that the voltage associated with the null current. Fourth order polynomial equations were fit to the data to minimize the effect of the dead band. The equations for the voltage greater than the voltage associated with the null current are:

$$Cylinder_1 = -25.363x^4 + 34.74x^3 - 3.5029x^2 + 5.2798x + 0.0036, R = 0.9999 \quad (25)$$

$$Cylinder_2 = 1.4786x^4 - 37.4580x^3 + 39.685x^2 + 2.6109x + 0.0052, R = 0.9998 \quad (26)$$

$$Cylinder_3 = 35.450x^4 - 89.047x^3 + 64.868x^2 - 1.6482x + 0.0029, R = 0.9998. \quad (27)$$

The same inverse relationship can be found for the cylinder contraction (negative) velocity verses voltage less that the voltage associated with the null current. Figure 22 shows the

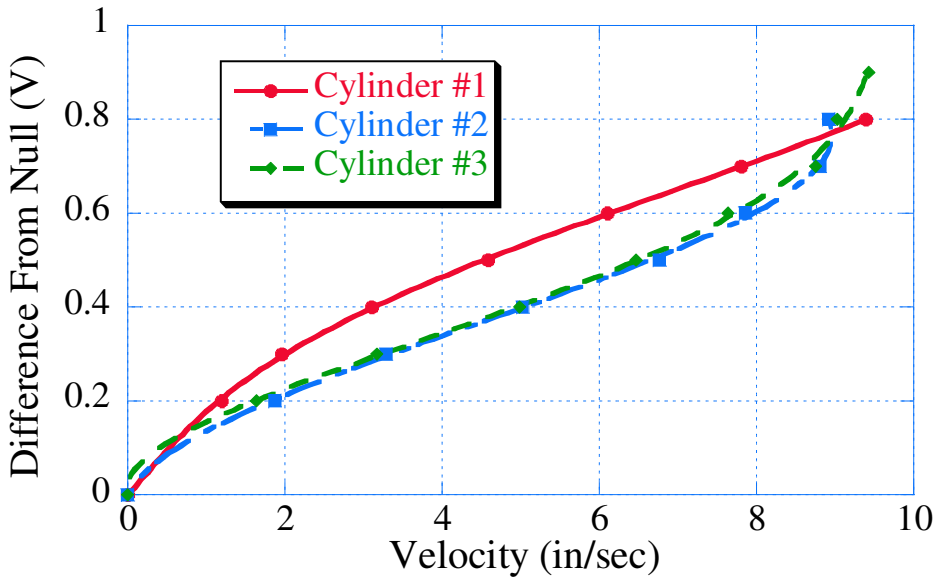

Figure 21: Hyper-Active Seat Cylinder Inverse Voltage/Velocity Relationship for Positive Velocities

experimental data collected from the cylinders as voltage less than the voltage associated with the null current was sent to the valve driver. Again, a fourth order polynomial equation was fit to the data. The equations for the voltages less than the voltages associated with the null current are:

$$Cylinder_1 = -5.4155x^4 - 36.185x^3 - 81.923x^2 - 65.284x - 15.287, R = 0.9986 \quad (28)$$

$$Cylinder_2 = 2.9187x^4 + 12.460x^3 + 15.8980x^2 + 11.2610x + 1.1144, R = 0.9985 \quad (29)$$

$$Cylinder_3 = 2.0414x^4 + 9.2241x^3 + 12.0650x^2 + 10.2930x + 1.0050, R = 0.9981. \quad (30)$$

Creating the functions mapping the inverse relationship between the valve driver voltage and cylinder velocity eliminated the dead band in each of the Hyper-Active seat cylinders. The dead band problem was still experienced in the excitation base cylinder. The same process of mapping the valve driver voltage verses the cylinder velocity was conducted. Figure 23 shows the nonlinear relationship between the voltage above and below the voltage associated with the null current, verses the excitation base cylinder velocity.

A fourth order polynomial function was fit to the two sections of the data; one for voltages greater than the voltage associated with the null current, and one for voltages less

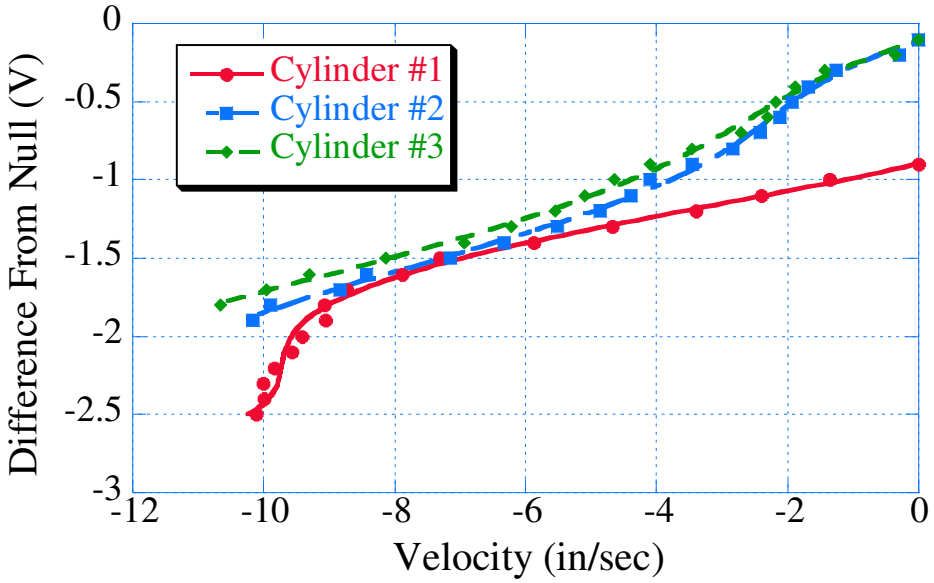

Figure 22: Hyper-Active Seat Cylinder Inverse Voltage/Velocity Relationship for Negative Velocities

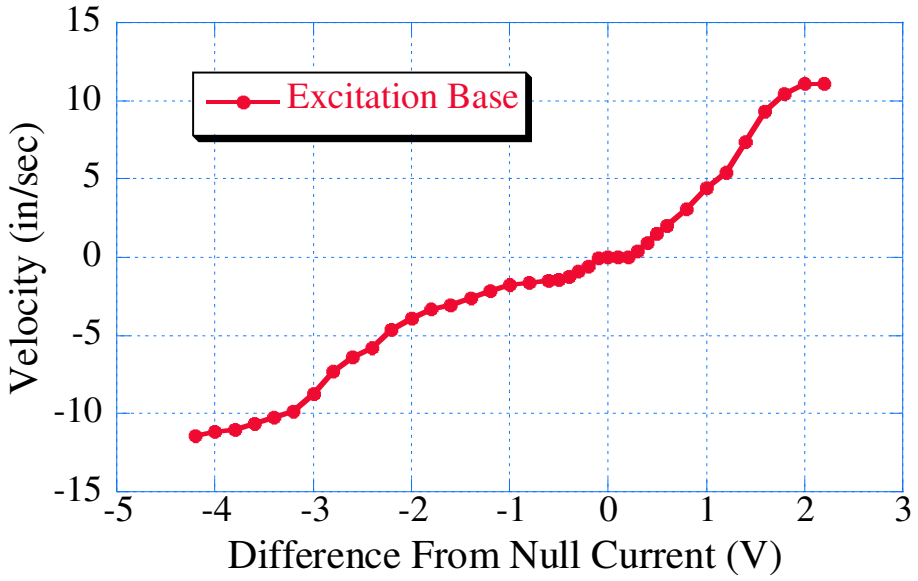

Figure 23: Excitation Base Difference From Null Current Verses Cylinder Velocity

than the voltage associated with the null current. Figure 24 shows the inverse relationship between the voltage greater than the voltage associated with the null current verses the velocity of the excitation base cylinder. The equation for the fourth order polynomial fit is:

$$Excitation_{Pos} = 0.0002x^4 - 0.0033x^3 - 0.0016x^2 + 0.257x + 0.1262, R = 0.9958. \quad (31)$$

Figure 25 shows the inverse relationship between the valve driver voltage less than the voltage associated with the null current and the cylinder velocity. The fourth order equation which fit the data is:

$$Excitation_{Neg} = -0.0012x^4 - 0.0224x^3 - 0.097x^2 + 0.4025x + 0.0337, R = 0.9977. \quad (32)$$

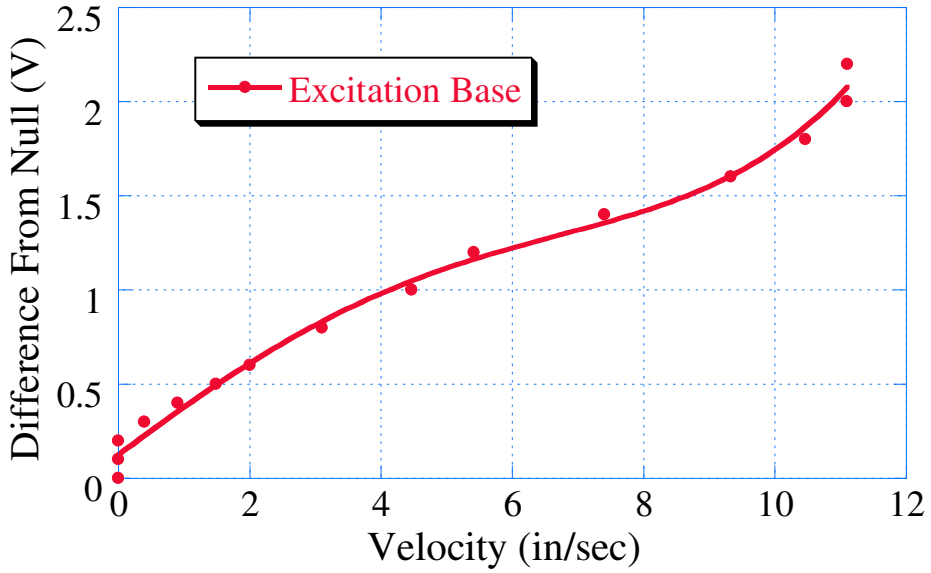

Figure 24: Excitation Base Cylinder Inverse Voltage/Velocity Relationship for Positive Velocities

The introduction of the fourth order polynomial functions into the control system eliminated the dead band in the cylinders. This allowed for the smooth operation of the cylinders, along with ensuring that the seat would move to the correct location.

2.5 Control System of the Hyper-Active Seat and Excitation Base

Two types of controllers were developed for the Hyper-Active seat. The first controller allows the use of the Hyper-Active seat as a parallel manipulator. In this mode, a position is given in the X, Y, θ space, and the seat moves to that position. The controller uses position feedback from the encoders to minimize the error between the desired position and the actual position. A Proportional-plus-Integral-plus-Derivative (PID) controller was

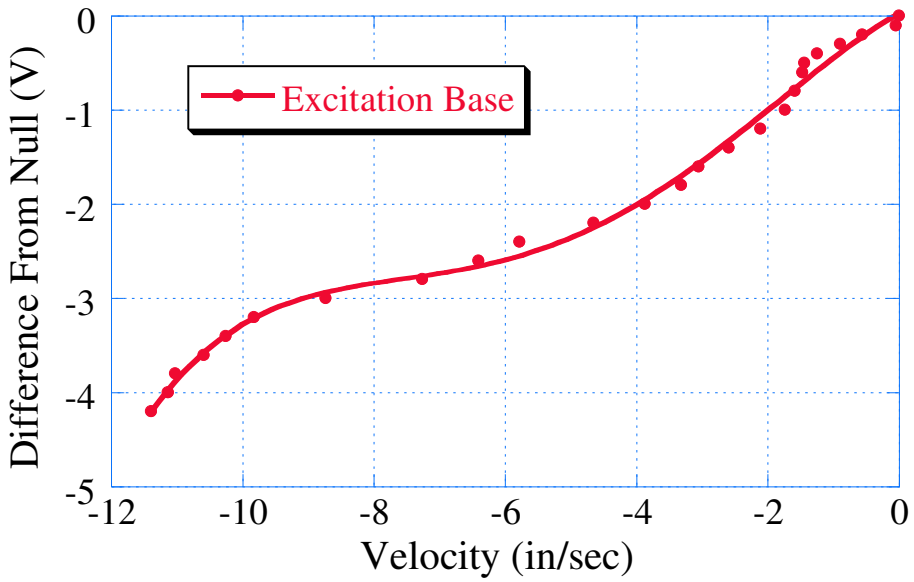

Figure 25: Excitation Base Cylinder Inverse Voltage/Velocity Relationship for Negative Velocities

designed to move the seat quickly with a small amount of steady state error. Section 3.4 shows the experimental results of the controller. This controller can also be used to position the Hyper-Active seat into the safety seat configuration designed in Section 4.5, in the time of a crash.

The second type of controller developed for the Hyper-Active seat is the vibration cancellation controller. This controller uses the feedback from the accelerometer on the base of the Hyper-Active seat to sense the vibration. The acceleration signal is then integrated to get the corresponding velocity. The velocity is then fed through the jacobian to get the velocity change in each of the leg lengths. Therefore, the seat attempts to move in the opposite way the excitation base moves, thereby canceling the vibrations.

A position feedback controller was also developed for the excitation base. The position of the base is measured using the string potentiometer. A Proportional-plus-Integral (PI) controller was developed to move the excitation base from one position to another quickly with little steady state error. This controller allows the controlled creation of vibrations for the Hyper-Active seat.

2.5.1 Hyper-Active Seat Position Control

The control of the Hyper-Active seat is a challenging task. Each leg length must be controlled separately, however, all three legs must move together to bring the seat to the desired configuration. Figure 26 shows the Simulink diagram of the Hyper-Active seat controller. The command for the seat is entered into the "Hyper-Active Seat Desired Input" block. The "Hyper-Active Seat Feedback" block contains the forward kinematics, as well as, the leg length calculations. The desired position is then compared with the current position, and the error is sent through the "Jacobian" block. The jacobian transfers the error in the coordinates to an error in the leg lengths. This signal is then sent to the "Hyper-Active Seat Controller" block where it is operated on by a PID controller. The signal is then sent to the "Signal Conditioning For Seat Hydraulics" block, where the desired velocity is converted into a desired voltage signal using the inverse voltage/velocity function discussed in Section 2.4.2. The voltage is then sent to the valve drivers, which control the leg lengths and position of the Hyper-Active seat.

2.5.2 Hyper-Active Seat Vibration Suppression Control

The vibration suppression controller is very similar to the position controller. The controller was designed using the "skyhook" control principle mentioned in Section 1.2.4. One novel difference in the controller design used in this research is that the seat bottom velocity was substituted into the equation instead of the seat top velocity. The Hyper-Active seat is a rigid mechanism, therefore when sensing vibrations, the seat bottom and seat top velocities are the same. This way, the vibration of the seat may be sensed slightly faster than the traditional "skyhook" method.

The acceleration of the seat bottom is measured with an accelerometer. This acceleration is then integrated to obtain the velocity of the seat bottom. To avoid a drift problem while integrating the acceleration, the change in acceleration was assumed zero if it was very close to zero. The seat bottom velocity is then compared to the desired seat top velocity, which is set to zero in most cases. Since the jacobian relationship is based on velocity, the position feedback controller gains need to be altered to velocity feedback controller gains. Figure 27

shows the Simulink diagram of the control system. One can see that the velocity of the seat base is feedback instead of the position of the seat. The seat is controlled in the opposite direction of the seat base, and the vibration is cancelled.

2.5.3 Excitation Base Position Control

The excitation base is controlled very similarly to the position control of the Hyper-Active seat. Figure 28 shows the Simulink diagram of the excitation base position controller. The position of the base is sensed using the string potentiometer, and that reading is compared with the desired position. The error signal is sent directly to a PI controller where it is operated on and then sent to the inverse voltage/velocity function. From there, the signal is sent to the valve driver to control the position of the excitation base. The base is capable of creating disturbances in the vertical direction from 0 to 7 Hz and in the pitch angle direction from 0 to 4 Hz. These results are shown in Section 3.6.

2.6 Division of Labor

The design and building of the Hyper-Active seat was a joint venture mainly between Dr. Kris Kozak and myself. Dr. Kris Kozak was mainly responsible for:

- Designing the 3R<u>P</u>R configuration of the Hyper-Active seat
- Ordering the Hyper-Active seat components
- Machining the Hyper-Active seat bottom and top plates

I was mainly responsible for:

- Theoretically and experimentally finding the workspace of the Hyper-Active seat
- Calculating the Hyper-Active seat forces
- Developing the software, using Simulink, for the Hyper-Active seat
- Ordering the correct data acquisition computer boards used for the Hyper-Active seat
- Developing the control system for the excitation base

- Developing the Hyper-Active seat vibration suppression Controller

Dr. Kris Kozak and myself shared equal responsibility for:

- Developing the design specifications for the Hyper-Active seat
- Calculating the jacobian of the Hyper-Active seat
- Calculating the inverse kinematics of the Hyper-Active seat
- Calculating the forward kinematics of the Hyper-Active seat
- Assembling the Hyper-Active seat
- Experimentally verifying the Hyper-Active seat speed calculations
- Designing the Excitation Base
- Assembling the Excitation Base
- Mapping the Hyper-Active seat voltage/velocity cylinder relationship
- Developing the Hyper-Active seat position controller

2.7 Summary

The Hyper-Active seat was designed and built using a number of components that were donated by Deere and Company. A 3R<u>P</u>R seat configuration was selected because it contains no platform singularities within the workspace. It also gives the advantage of three independent degrees of freedom, X or horizontal, Y or vertical, and θ or pitch angle. This mechanism is the first three degree of freedom fully active seat capable of these motions. These three degrees of freedom make the Hyper-Active seat ideal for reducing vibrations on off-road vehicles.

The components of the Hyper-Active seat were discussed in detail along with a number of calculations relating to the seat. These calculations showed the ability of the seat to support an operator of any size, as well as, have enough workspace to cancel unwanted

vibrations. The calculations also showed that the seat reacted very quickly, but not fast enough for a highly effective safety seat.

An excitation base was designed and built to induce vibration into the Hyper-Active seat. The design allowed for the excitation of the seat in both the vertical and pitch angle directions. This base allows for controlled vibrations for the seat, so that controllers can be tuned and the performance of the Hyper-Active seat optimized.

The software and controller design of the seat was outlined. MATLAB was used to control the seat using Simulink and the Real-Time Workshop. This allowed for the rapid design of controllers and the ability to change controller designs with a minimal amount of programming. The position and vibration cancellation controllers were discussed, as well as, the excitation base controller. The Hyper-Active seat will allow for the advancement of many different position and vibration cancellation control systems.

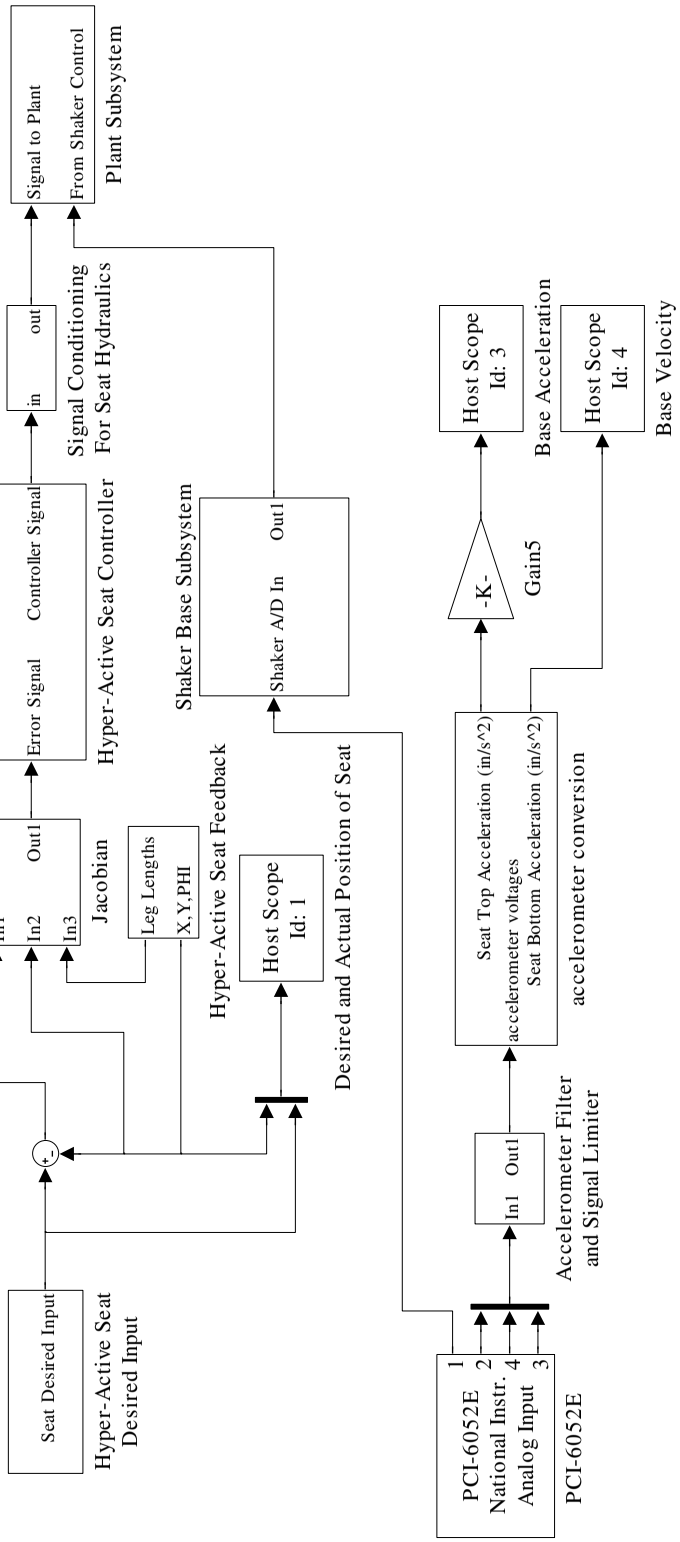

Figure 26: Simulink Diagram of the Hyper-Active Seat Position Controller

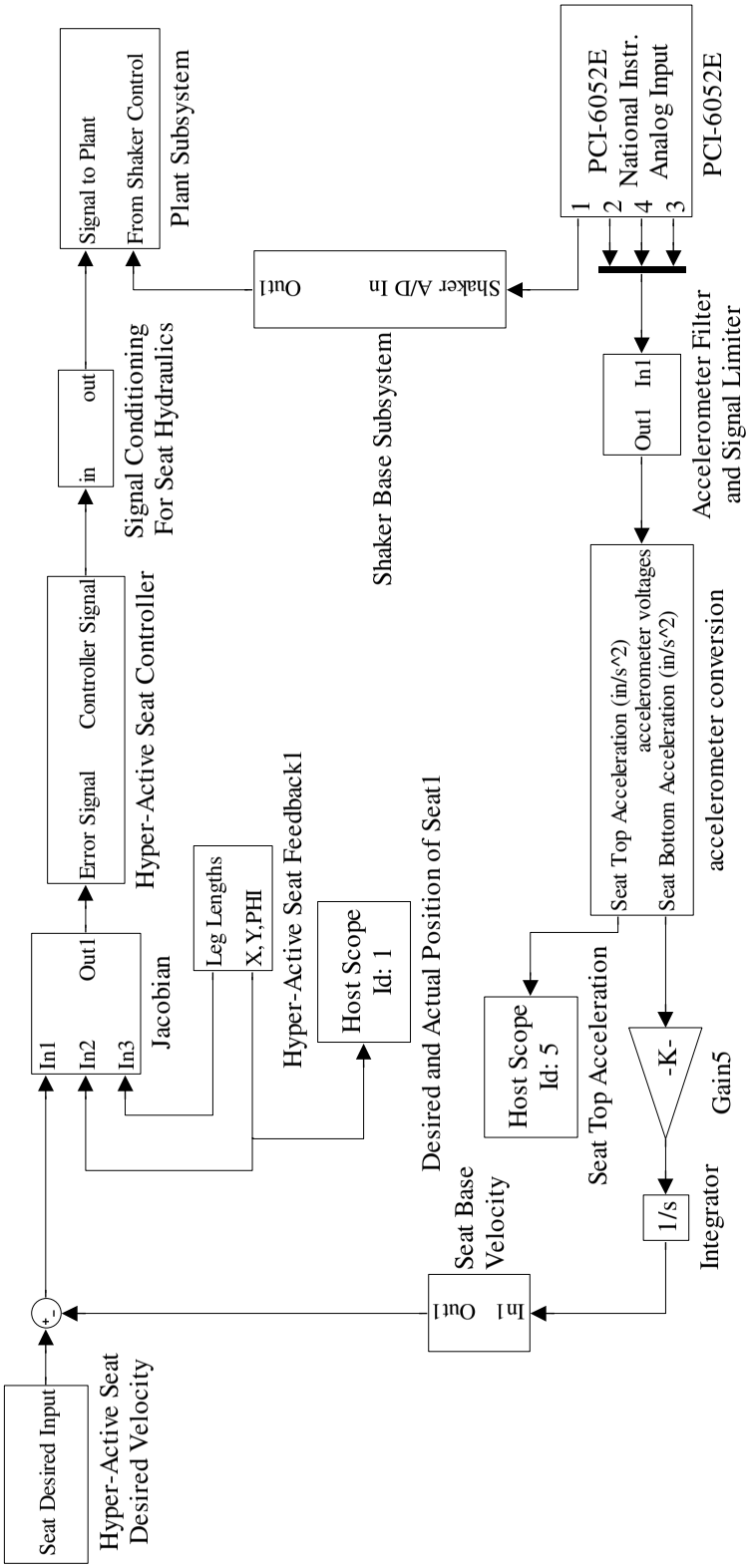

Figure 27: Simulink Diagram of the Hyper-Active Seat Velocity Controller

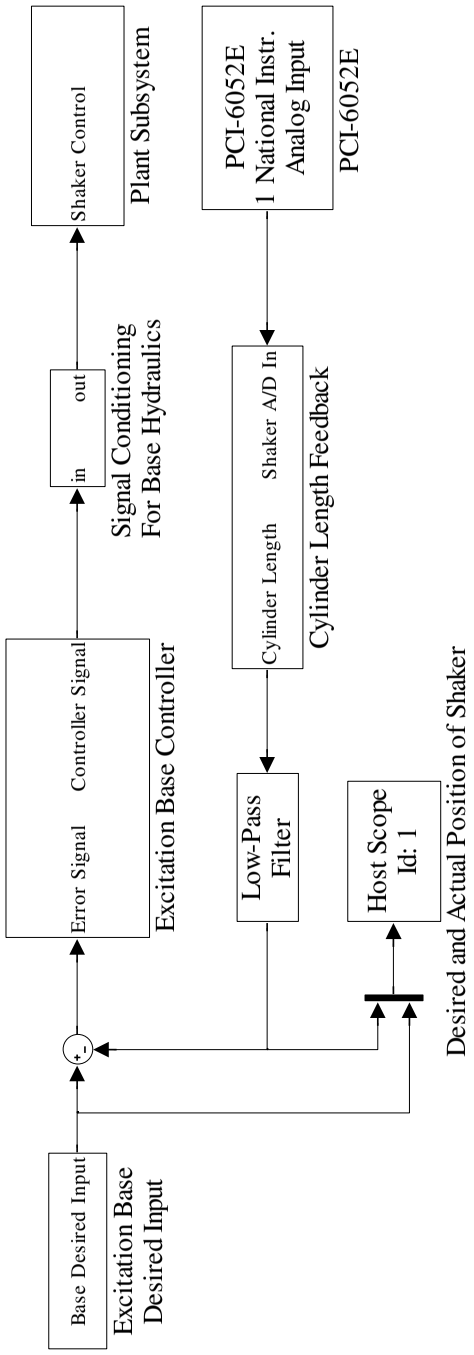

Figure 28: Simulink Diagram of the Excitation Base Position Controller

CHAPTER III

MODELING AND EXPERIMENTS

3.1 Hyper-Active Seat System Identification

To evaluate the potential of the Hyper-Active seat to suppress disturbances, and to create a model of the system, the step response and frequency response were explored. The open-loop step response of the seat characterizes the rise time of the seat, the damping ratio, as well as the residual vibration, and the open-loop frequency response of the seat indicates what bandwidth of frequencies the seat can suppress. The analysis of the data collected during the experiments led to the development of a simple model for each degree of freedom of the seat.

These experiments were conducted with the Hyper-Active seat unloaded and loaded to mimic an operator's weight. Knowledge of the seat's performance at two weights allows for the extrapolation of the data to other weights, assuming a somewhat linear relationship between weight and performance. The effective unloaded weight of the seat is 40 kg, and the effective loaded weight of the seat is 86 kg. The weights take into account the top steel plate of the seat, the mounting bracket of the cushion seat, and the cushion seat. In addition, the loaded seat has 40 kg's to simulate an occupant. The full weight of an occupant was not used because it is assumed some of the occupant weight will be supported by the floor and steering wheel.

3.1.1 Step Response

The open-loop step response of the Hyper-Active seat gives valuable information, to develop a model which can be used to determine what range of vehicle vibrations can be cancelled. To obtain the step response, a step command of 1 inch was sent to the seat in the vertical and horizontal directions, while a step command of 0.15 rad was sent to the seat in the pitch angle direction. The response of the seat is shown in Figures 29 - 34. To obtain the

step of 1 inch and 0.15 rad, the maximum possible voltage above and below the voltage associated with the null current was sent to the valve drivers for 0.050 sec. Analysis of the step response data indicated the damped natural frequency and damping ratio for each of the three directions. These values are tabulated in Table 9. Analysis of the step response data revealed the addition of mass to the seat reduced the damped natural frequency and damping ratio.

Table 9: Experimental Data and Model Predictions

		Damped Natural Frequency	Damping Ratio	Roll-Off frequency	Model Roll-Off Frequency	Model Damping Ratio
Vertical	Unloaded	12.0 Hz	0.24	12.0 Hz	12.0 Hz	0.26
	Loaded	10.0 Hz	0.17	10.3 Hz	8.3 Hz	0.17
Horizontal	Unloaded	5.0 Hz	0.22	6.0 Hz	5.2 Hz	0.25
	Loaded	3.6 Hz	0.20	3.5 Hz	3.6 Hz	0.22
Pitch Angle	Unloaded	7.1 Hz	0.17	12.0 Hz	12.5 Hz	0.20
	Loaded	5.0 Hz	0.16	5.0 Hz	8.6 Hz	0.18

Figure 29 and Figure 30 show the unloaded and loaded system step response in the vertical direction. The non-linearities of the system are evident in the residual vibration, because the responses do not show a constant damped natural frequency, as evident after the first peak overshoot. The overshoot was expected to be similar to a second order system, however, due to the non-linearities and stiffness in the system, the overshoot is smaller.

The unloaded and loaded system step response in the horizontal direction is shown in Figures 31 and 32. The rise time and settling time are greater in the horizontal direction because the actuators cannot generate as much force horizontally due to the geometry. Section 2.1.5 showed that the difference in force between the vertical direction and the horizontal direction was about 900 lbf. This significant difference is reflected in the rise time and settling time.

Figures 33 and 34 show the unloaded and loaded system step response in the pitch angle direction. The step responses are unlike that of the vertical and horizontal directions because it is rotation and not translation. The Hyper-Active seat is very rigid in the pitch angle direction, which causes the step response to have a minimal amount of overshoot.

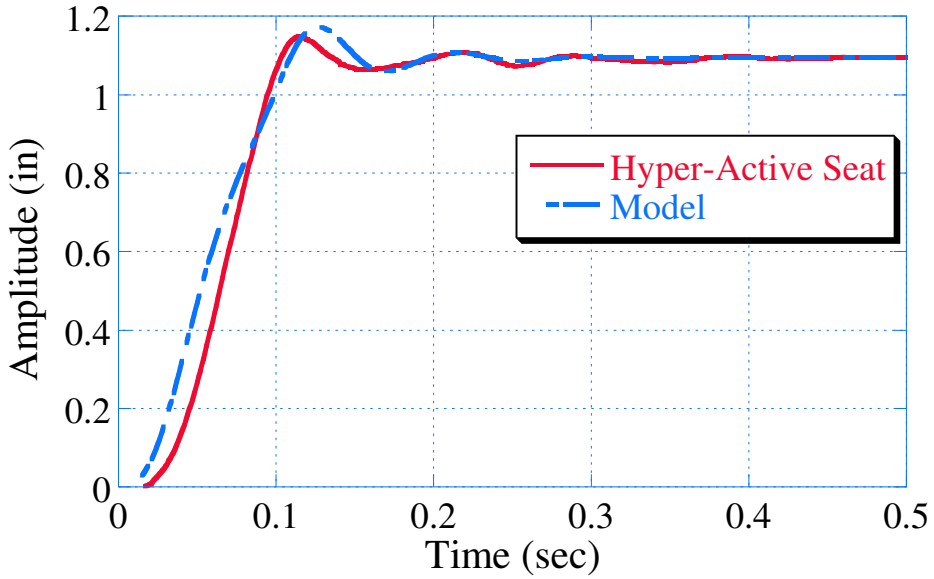

Figure 29: Vertical Unloaded Step Response

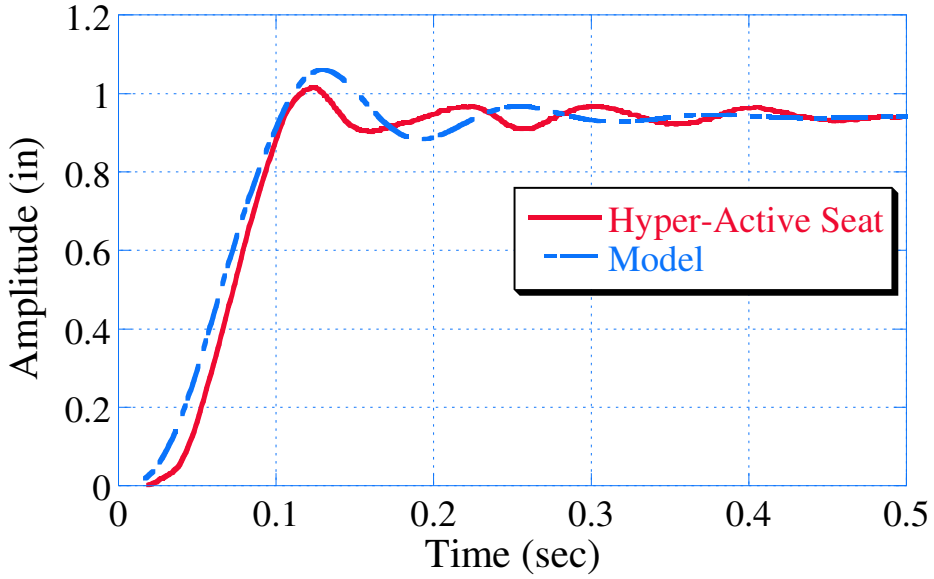

Figure 30: Vertical Loaded Step Response

3.1.2 Frequency Response

Frequency response data was collected along the three degrees of freedom: vertical, horizontal, and pitch angle. The frequency response was collected in all three directions by sending a voltage sine wave of known frequency and amplitude into the inverse kinematics of the Hyper-Active seat. The inverse kinematics transferred the desired X, Y, and θ directions

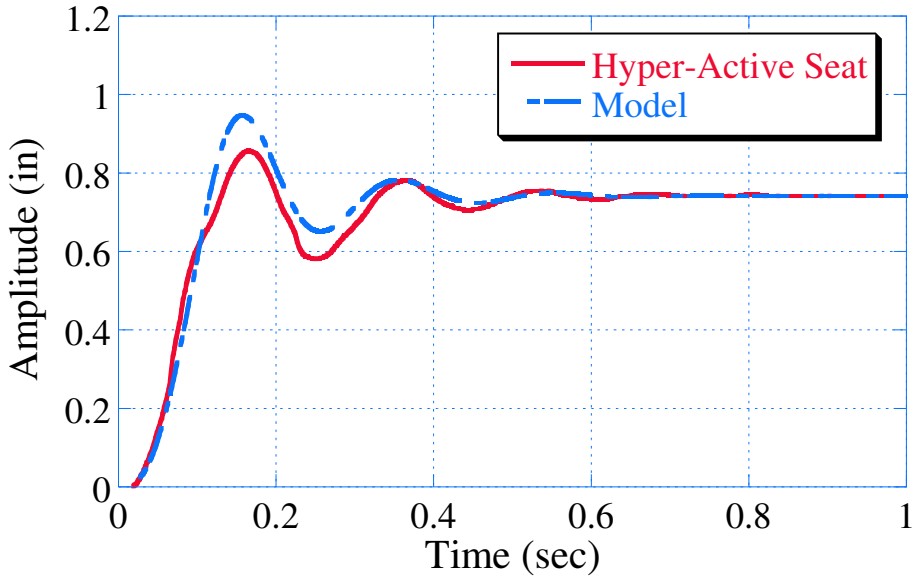

Figure 31: Horizontal Unloaded Step Response

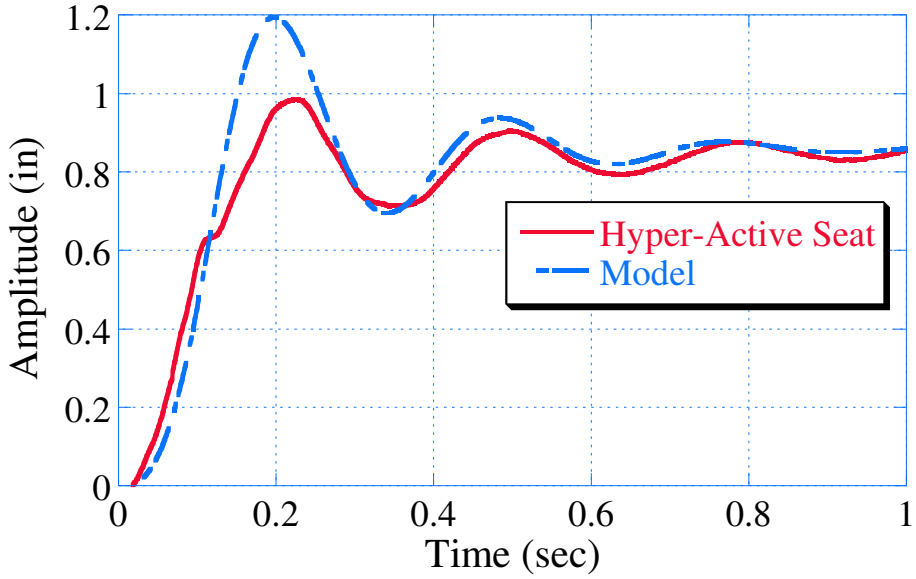

Figure 32: Horizontal Loaded Step Response

into leg lengths. The magnitude and phase shift of the system was recorded by comparing the actual X, Y, and θ position to the desired voltage sine waves. The frequency response gives a clear understanding of the roll-off frequency of the seat in each of the three directions as shown in Table 9. Knowledge of the roll-off frequency indicates the bandwidth the of potential vibration suppression of the Hyper-Active seat.

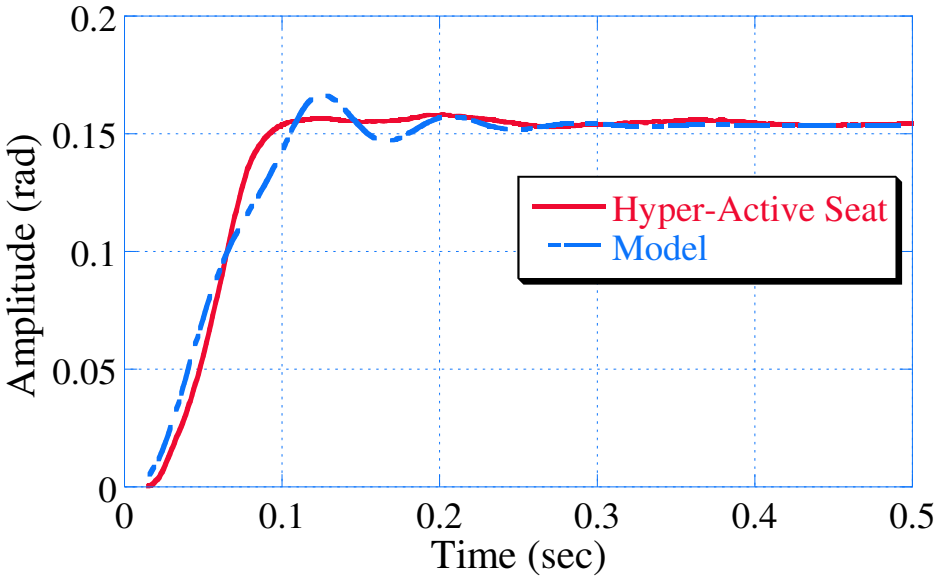

Figure 33: Pitch Angle Unloaded Step Response

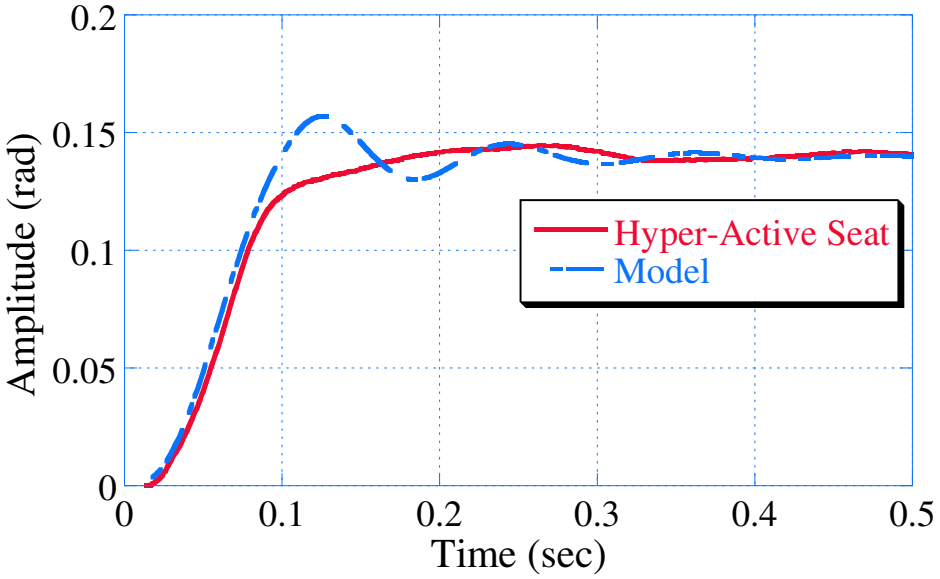

Figure 34: Pitch Angle Loaded Step Response

Figure 35 and Figure 36 show the frequency response of the unloaded and loaded Hyper-Active seat in the vertical direction, while Figures 37 and 38 show the frequency response of the (unloaded and loaded) Hyper-Active seat in the horizontal direction. The Hyper-Active seat has a much lower roll-off frequency in the horizontal direction compared to the vertical direction, due to the geometry of the seat. The stiffness of the system in the horizontal

direction is lower due to increased rotation of the revolute joints shown in Figure 8.

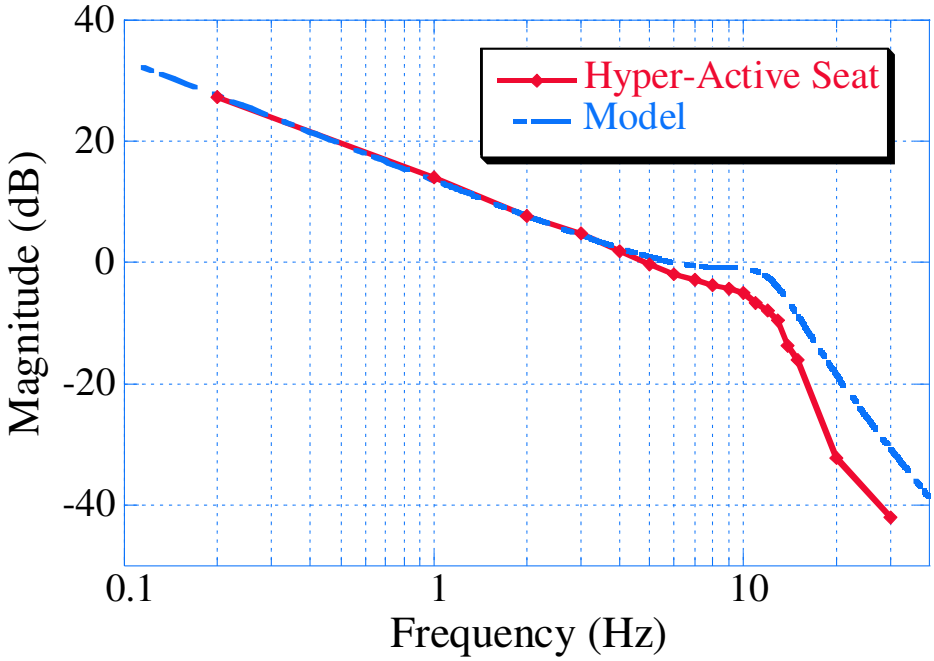

Figure 35: Vertical Unloaded Frequency Response

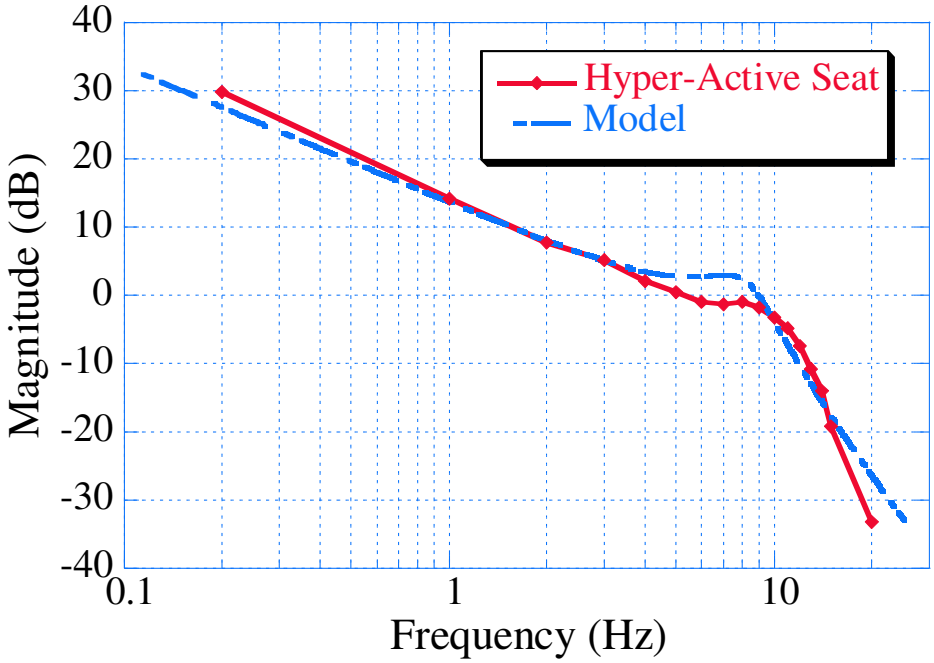

Figure 36: Vertical Loaded Frequency Response

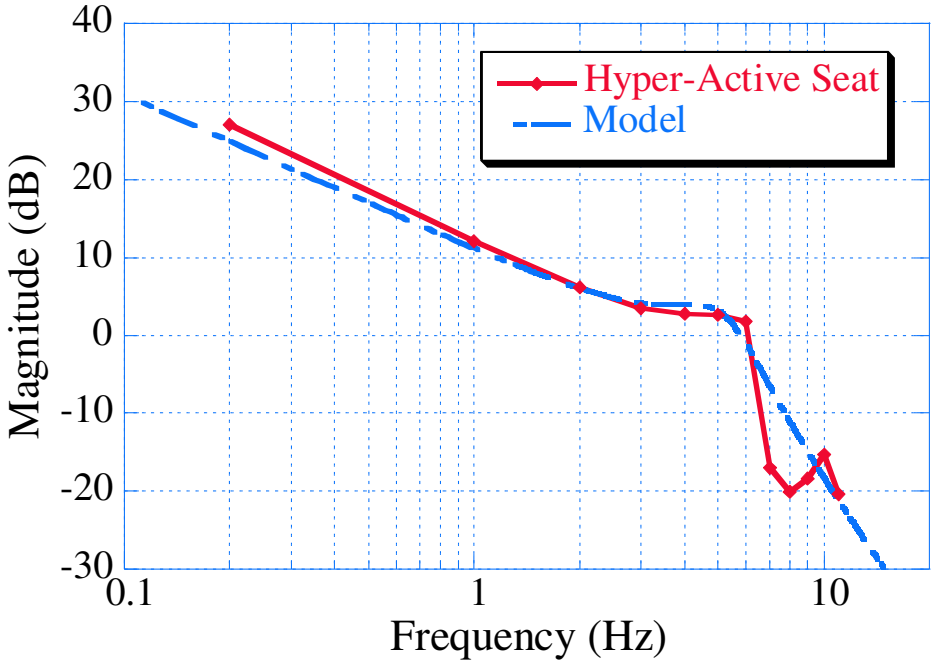

Figure 37: Horizontal Unloaded Frequency Response

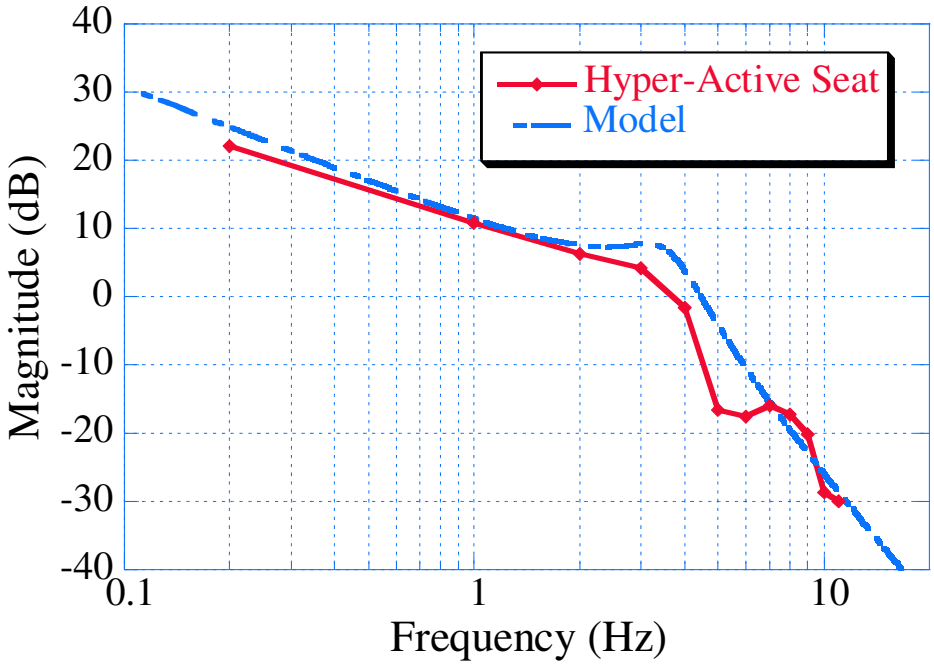

Figure 38: Horizontal Loaded Frequency Response

Figures 39 and 40 show the frequency response of the unloaded and loaded Hyper-Active seat pitch angle. The roll-off frequency of the pitch angle was lower than the vertical

direction, due to the geometry and motion of the seat. The stiffness of the seat is lower because of the increased rotation of the revolute joints. Also, the pitch angle is a rotation and not a translation, so the inertia properties relative to the available forces are different.

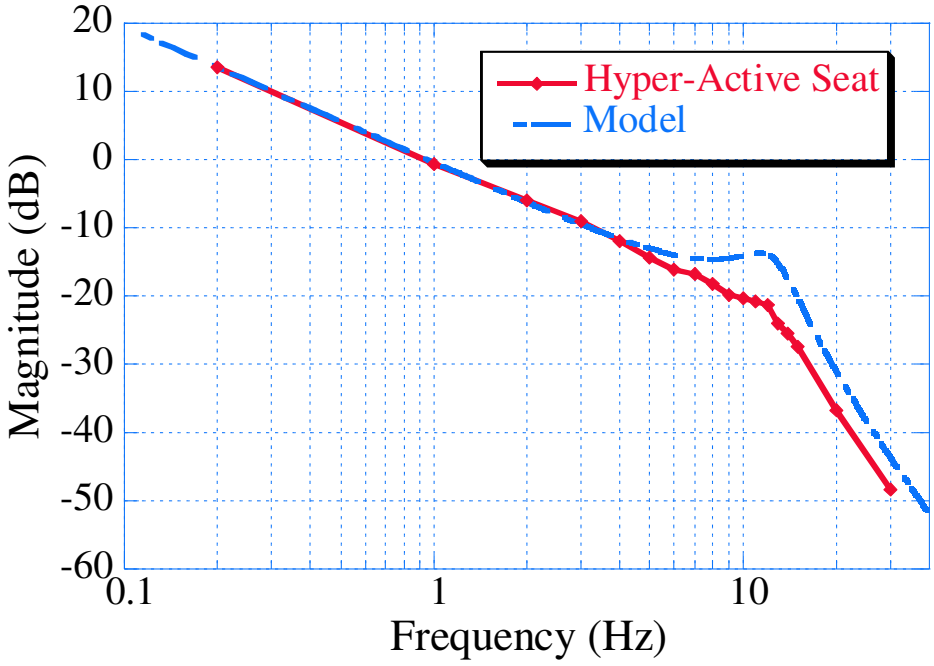

Figure 39: Pitch Angle Unloaded Frequency Response

3.2 Modeling of the Hyper-Active Seat

A model of the Hyper-Active seat was developed to assist in controller development. A simple model of the seat was developed from the data for each of the three degrees of freedom and not the whole seat due to coupling between the actuators. Each direction was modeled as third order system, of the form:

$$Gp(s) = \frac{c\frac{k}{m}}{s\left(s^2 + \frac{b}{m}s + \frac{k}{m}\right)}, \tag{33}$$

where c, b, and k were determined by fitting the unloaded step and frequency responses using the optimization toolbox in MATLAB. The weight of the seat, m, for the unloaded and loaded seat is a known quantity. A third-order model was selected due to the Hyper-Active seats mechanical dynamics, namely inertia, being modeled as second-order, and the hydraulics of the seat being modeled as a simple integrator. An integrator was chosen for

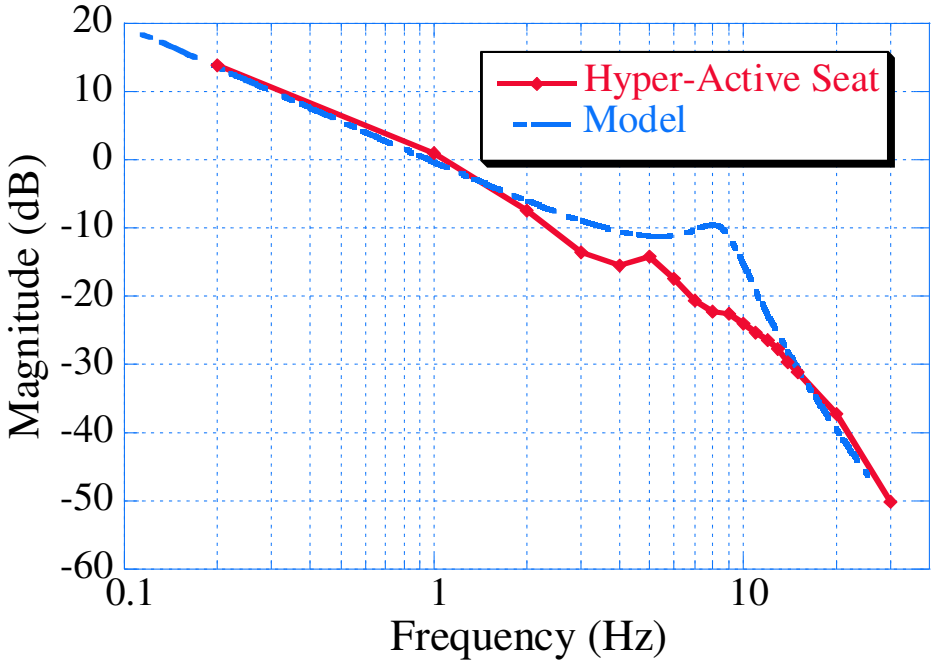

Figure 40: Pitch Angle Loaded Frequency Response

the hydraulics due to the evidence of a zero at the origin as seen in Figures 35-40. Physically, this arises because the distance the seat moves is the integral of the distance the hydraulic valve is open. The model of the seat was only fit for low frequencies and not valid for frequencies above the roll-off frequency. This was done since the low frequencies are more harmful to the operator and it is the most important dynamic region for the purpose of this research.

Once c, b, and k were determined for the unloaded seat, they were then calculated for the loaded case. The damping constant was increased by 30% due to the loading of the seat. This is justified because loading the seat increases the physical damping effects. Table 9 compares the roll-off frequencies and damping ratios predicted by the model versus the experimental data. The models predicted a decrease in roll-off frequency and damping ratio which correlates to the experimental data.

A comparison of the models and the experimental results can be seen in Figures 29-40. Note that the pitch angle response of Figures 34 and 40 fit well for higher roll-off frequency, but does not take into account the lower frequency present. The model breaks down due

to the rigidity of the seat. To increase the accuracy of the model a fifth-order model was tried, however this model did not capture the rise time of the step response.

3.3 Hyper-Active Seat Move into a Safety Seat

The speed of the Hyper-Active seat was recorded to compare the experimental results with the theoretical results discussed in Section 2.1.6. To move the Hyper-Active seat into a safety seat, the front of the seat must be quickly elevated. The front cylinder of the Hyper-Active seat was extended, keeping the other cylinders fixed. The length of the cylinder was recorded, and the slope, which corresponds to the velocity, was recorded. The cylinder had a maximum velocity of 13.05 in/sec. This is slightly slower than the 15.25 in/sec calculated theoretically. This would mean that the cylinder did not have a flow rate of 7 gpm. This could be due to the holes in the cylinder and manifold (discussed in Section 2.2.2) actually reducing the flow to 6 gpm instead of 7 gpm.

To calculate the time required to elevate the front of the Hyper-Active seat 10 deg, the experimental speed is entered into (87) in Section B.3.2. The result shows that the Hyper-Active seat will take 97 ms to move its position into a safety seat. This is close to the theoretical calculation of 84 ms. As mentioned before, the move time of the Hyper-Active seat could be increased by placing a high speed actuator in the front of the seat to quickly reposition the Hyper-Active seat into the safety seat configuration during a front-end collision.

3.4 Hyper-Active Seat Position Controller

A controller was developed in Section 2.5.1 to control the position of the Hyper-Active seat. Figure 41 shows the response of the Hyper-Active seat in the vertical direction when a 1 Hz sine wave command, centered about the center of the workspace, is sent to the seat. The small disturbance at the beginning of the data reflects the seat moving to the center of the workspace. Figure 42 shows the response of the seat in the horizontal direction to the same sine wave. Finally, Figure 43 show the position control of the Hyper-Active seat in the pitch angle direction to the sine wave. The magnitude of the seat movement tracks

very well with the desired input, however there is a phase shift between the desired and actual position. This can be expected from a simple PID controller. A solution to this problem would be to add a lead compensator, which would add a positive phase shift at the appropriate frequencies. This would minimized the phase shift and cause the Hyper-Active seat to more closely track the desired signal.

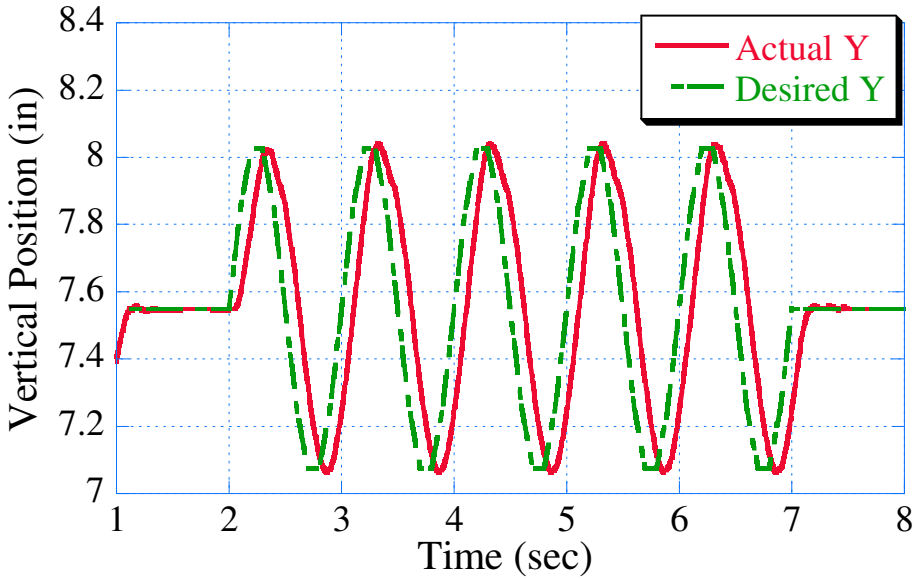

Figure 41: Vertical Hyper-Active Seat Position Controlled Response

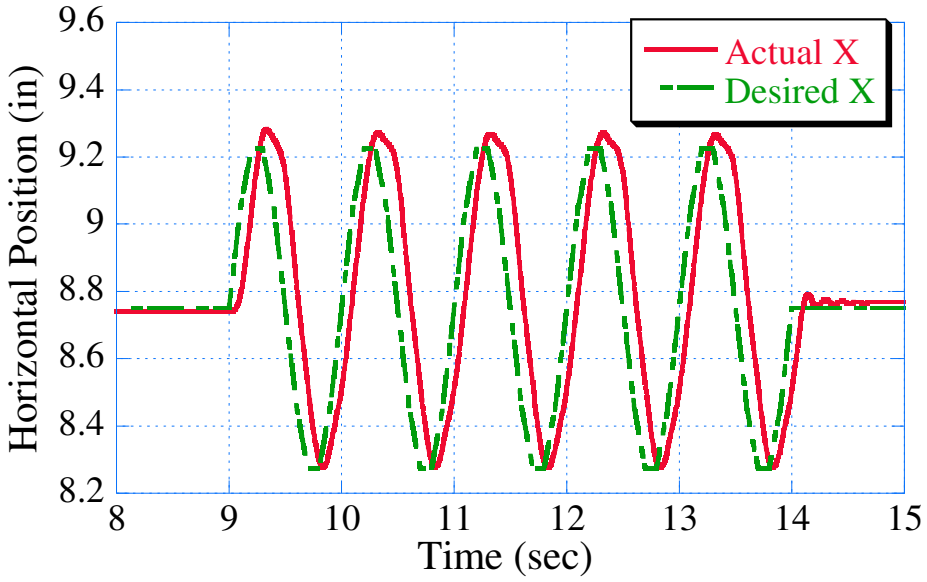

Figure 42: Horizontal Hyper-Active Seat Position Controlled Response

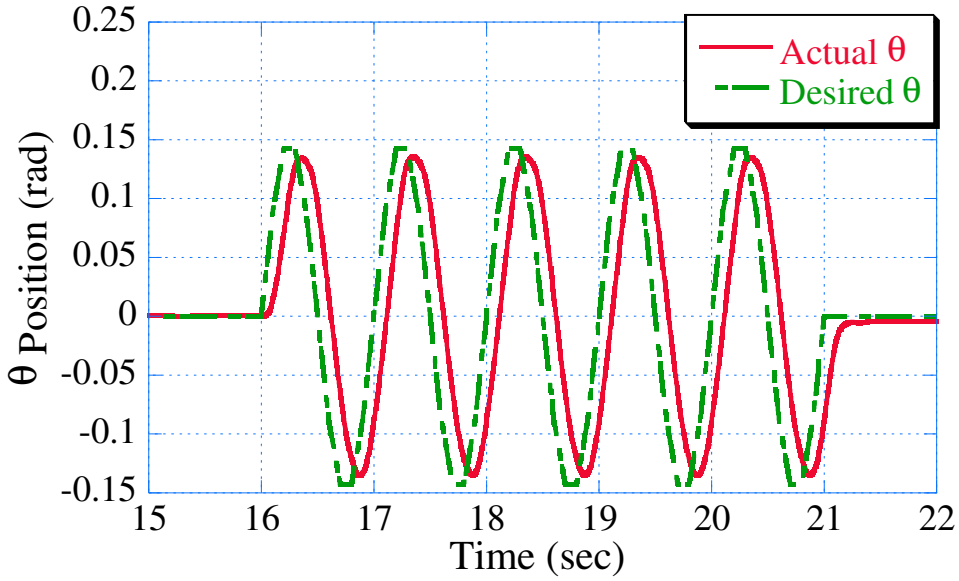

Figure 43: Pitch Angle Hyper-Active Seat Position Controlled Response

3.5 Hyper-Active Seat Vibration Cancellation Controller

To evaluate the capability of the Hyper-Active seat to reduce the harmful vibrations, a series of tests were performed. These tests investigated the reduction in displacement and acceleration of an uncontrolled Hyper-Active seat, verses a controlled seat. The vibration cancellation controller developed in Section 2.5.2 was tested for different inputs. These experiments concentrate on the vibration cancellation in the vertical direction. The Hyper-Active seat and excitation base were configured so that most of the vibrations were input in the vertical direction, similar to the configuration shown in Figure 17. Their was some pitching motion that was coupled with the vertical direction, however in this configuration, the pitching motion was minimized. The Hyper-Active seat was sent a one period sine wave disturbance at different frequencies. This correlates to a vehicle hitting a bump at different velocities. This input gives a realistic representation of off-road vehicle vibration.

The experiments were conducted twice. Once with the vibration cancellation controller off, and once with the vibration cancellation controller on. To measure the effectiveness of the controller, two vital pieces of information were recorded. First, the peak-to-peak displacement of the seat top from the center of the workspace was recorded. This represents the overall displacement of the operator as the vehicle encounters a disturbance. Second,

the seat top acceleration was recorded. The acceleration of the occupant is important for tracking the acceleration reduction of the controller.

The Hyper-Active seat top displacement was recorded as a function of the disturbance frequency. Figure 44 shows the peak-to-peak displacement amplitude for the controlled and controlled Hyper-Active seat. The vibration cancellation controller decreases the displacement amplitude considerably. Figure 45 shows the percent decrease of the controlled displacement amplitude over the uncontrolled. The vibration cancellation controller generally decreases the displacement amplitude between 40 and 45%.

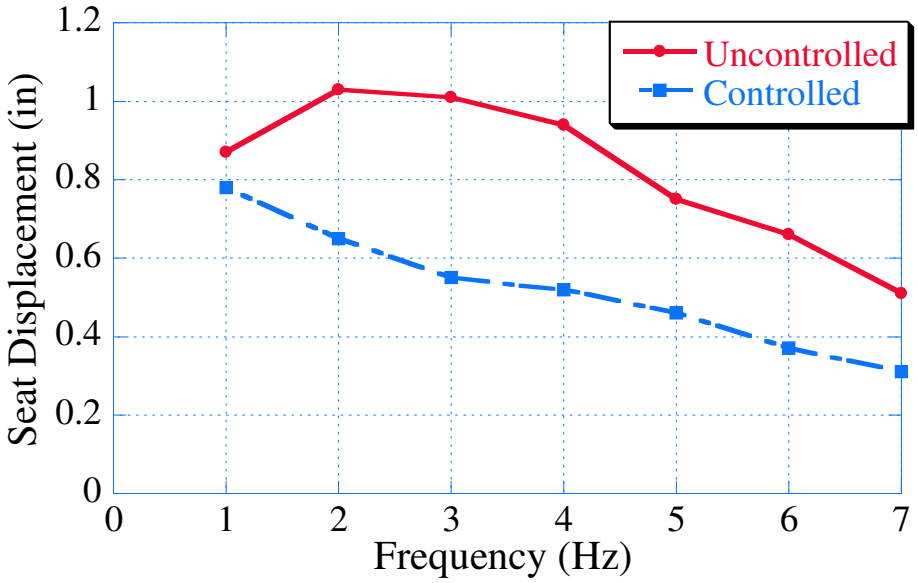

Figure 44: Peak-to-Peak Displacement of the Hyper-Active Seat Top

To determine the level in the reduction of the acceleration, the Root-Mean-Squared (RMS) average was taken over the duration of the disturbance. The formula for this average is:

$$RMS = \sqrt{\frac{\sum_{i=1}^{n} acc_i^2}{n}}, \tag{34}$$

where n is the number of time-steps of interest, and acc_i is the corresponding acceleration level at each of the time-steps. The RMS average can give a better understanding of the overall acceleration reduction than simply studying the acceleration plot.

A positive sine wave was used as the disturbance, meaning a positive amplitude for the

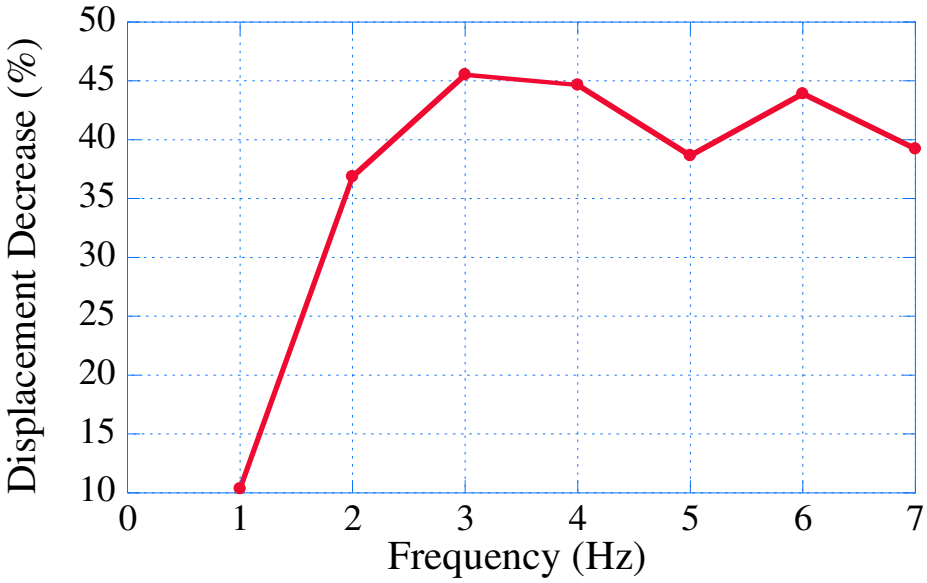

Figure 45: Percent Decrease of Peak-to-Peak Seat Top Displacement

first half of the sine wave, and then a negative amplitude for the remainder of the period. The amplitude was set to 0.4 in and the frequency of the disturbance was varied from 1 to 7 Hz. Figure 46 shows the change in displacement of the top of the seat for a 3 Hz bump. The uncontrolled response has a peak-to-peak amplitude of 1.01 in, while the controlled seat has an amplitude of 0.55 in. The controller decreased the seat displacement by 46%. The acceleration which corresponds to the 3 Hz sine wave is shown in Figure 47. One can see that the peak acceleration is greatly decreased. The uncontrolled seat has a RMS average acceleration of 37 in/sec^2, while the controlled seat has a RMS average acceleration of 24 in/sec^2. The addition of the vibration cancellation controller decreased the RMS average acceleration 35%.

The RMS average acceleration was recorded at each disturbance frequency to measure the performance of the vibration cancellation controller over a range of conditions. Figure 48 shows the RMS average acceleration of the controlled and uncontrolled seat. At 7 Hz, the vibration cancellation controller is no longer more affective than the uncontrolled seat from the perspective of RMS average acceleration reduction. Since this is the end of the range of harmful frequencies mentioned in Section 1.1.1, the controller has met the requirements. Figure 49 shows the decrease in RMS average acceleration when comparing the uncontrolled

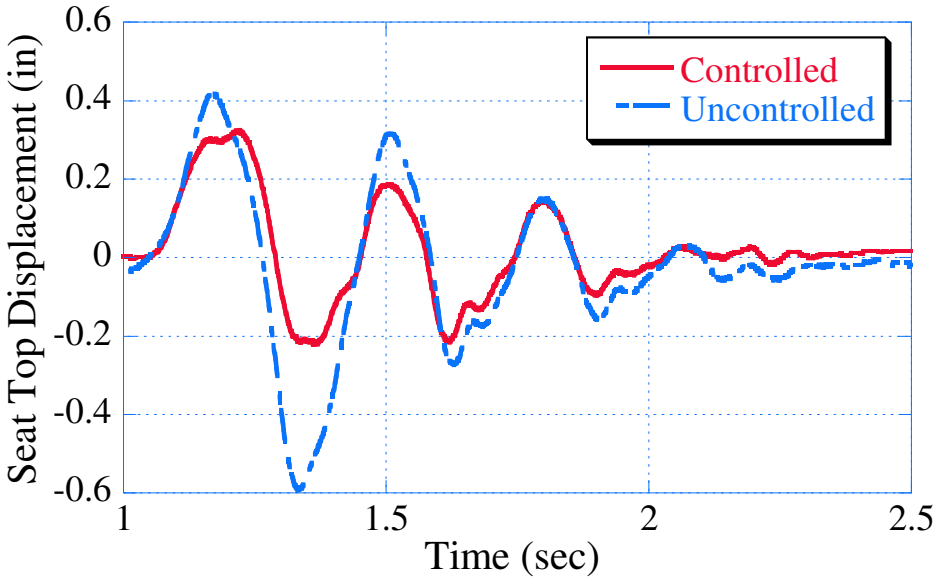

Figure 46: Hyper-Active Seat Top Displacement For a 3 Hz Input

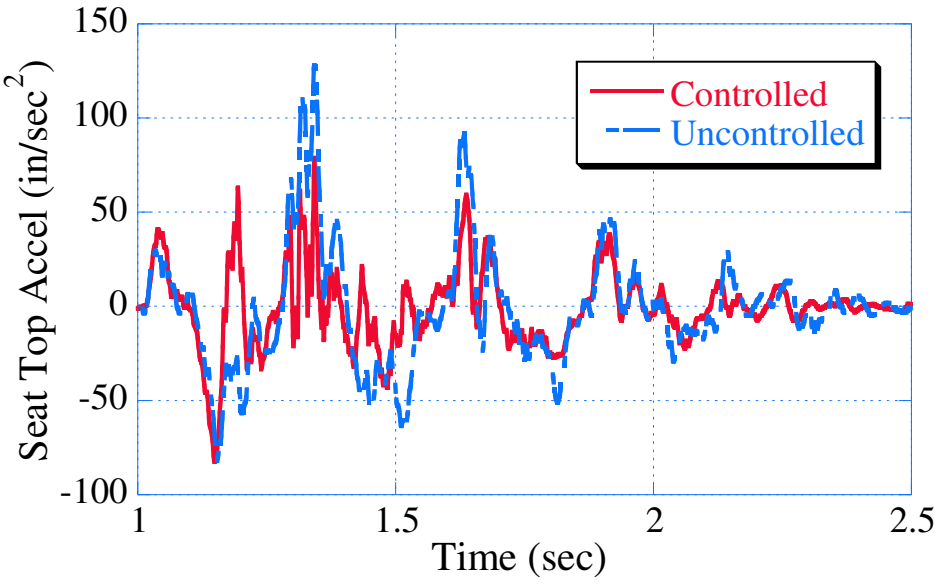

Figure 47: Hyper-Active Seat Top Acceleration For a 3 Hz Input

seat to the controlled seat. Again it is evident that the performance of the seat is good over the desired range.

3.6 Excitation Base Frequency Response

Frequency response data was taken with the Hyper-Active seat and excitation base in the vertical configuration (shown in Figure 17) and in the pitch angle configuration (shown in

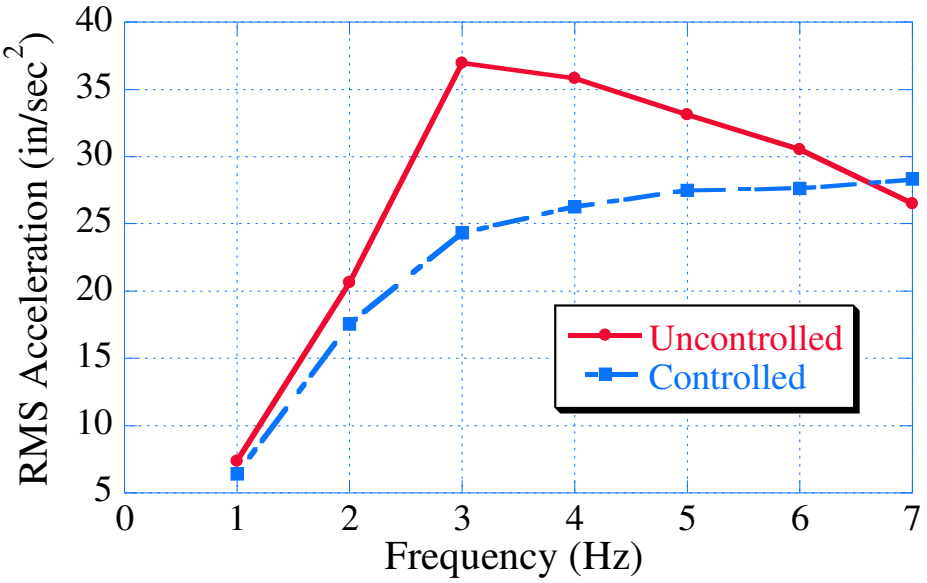

Figure 48: RMS Acceleration Average of the Hyper-Active Seat Top

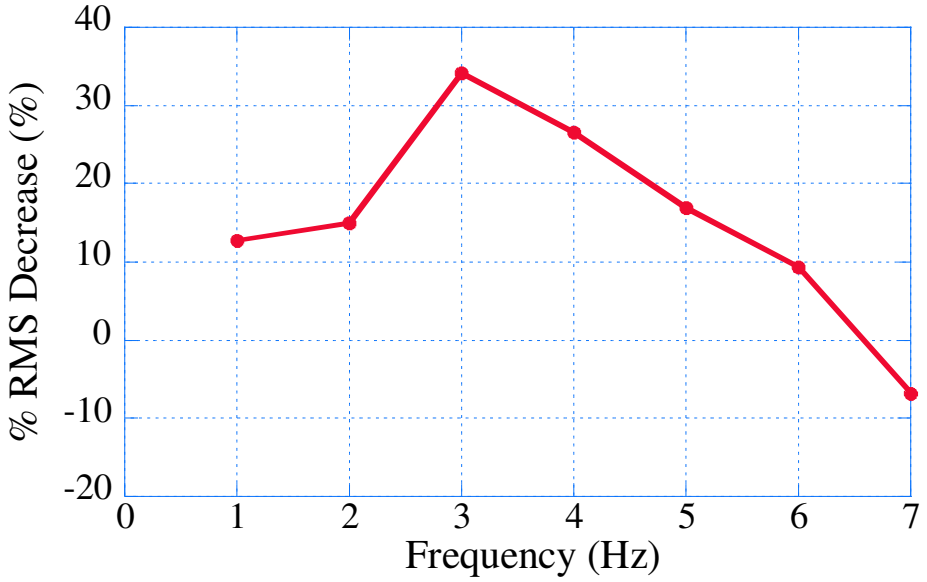

Figure 49: Percent Decrease of RMS Acceleration Average of the Hyper-Active Seat Top

Figure 18). The frequency response will show the roll-off frequency of the excitation base. To test the Hyper-Active seat vibration cancellation controller, it is important to know what frequency range the excitation base is capable of creating. The experiments were conducted with the Hyper-Active seat unloaded and loaded. Assuming a linear relationship between the weight on the seat and the frequency response, one can extrapolate the results to find

Table 10: Frequency Response of the Excitation Base

Direction	Weight	Roll-Off Frequency
Vertical	Unloaded	8 Hz
	Loaded	6 Hz
Pitch Angle	Unloaded	5 Hz
	Unloaded	2.5 Hz

the frequency response at other loads. The effective unloaded weight of the seat is 40 kg, and the effective loaded weight of the seat is 86 kg. This is the same loading used for the Hyper-Active seat system identification discussed in Section 3.1.

Figure 50 shows the unloaded frequency response of the excitation base in the vertical direction, while Figure 51 shows the loaded response. Table 10 shows the roll-off frequencies of the excitation base in the vertical and pitch angle directions. As expected, the bandwidth decreased with an increase in weight on the Hyper-Active seat. The data shows that the excitation base is capable of creating disturbances in the vertical direction for the harmful frequency range discussed in Section 1.1.1.

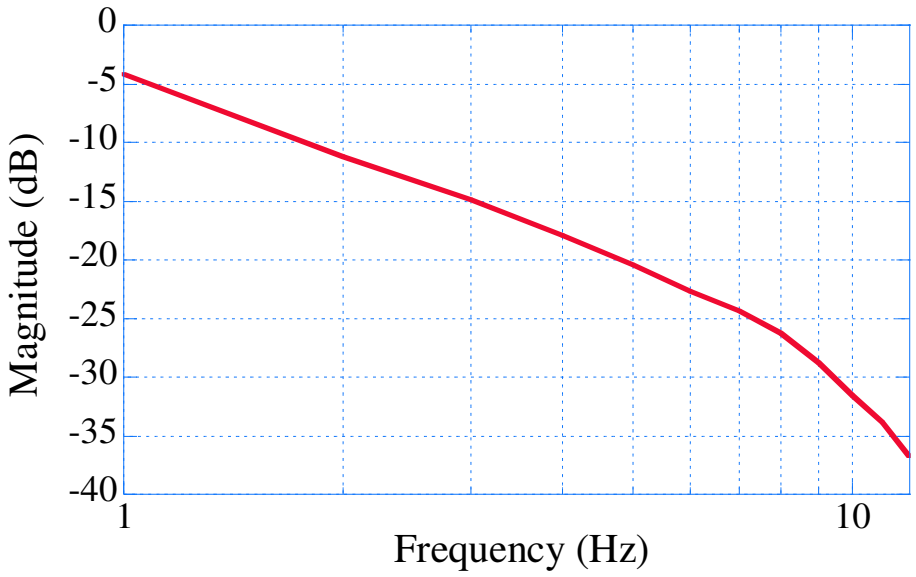

Figure 50: Excitation Base Vertical Unloaded Frequency Response

Figure 52 shows the unloaded pitch angle frequency response. The bandwidth in the pitch angle direction has decreased compared to the vertical direction. The decrease is due

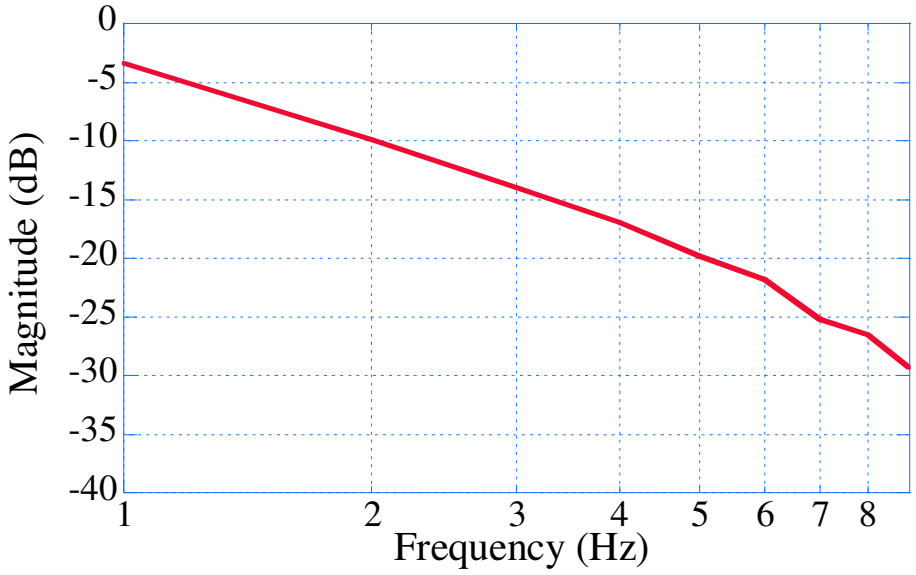

Figure 51: Excitation Base Vertical Loaded Frequency Response

to the inertia properties of the Hyper-Active seat. Figure 53 shows the loaded response. Again, the roll-off frequency has decrease due to the additional weight. The excitation base is only capable of creating pitch angle disturbances in the 0 to 4 Hz range, depending on the load on the seat.

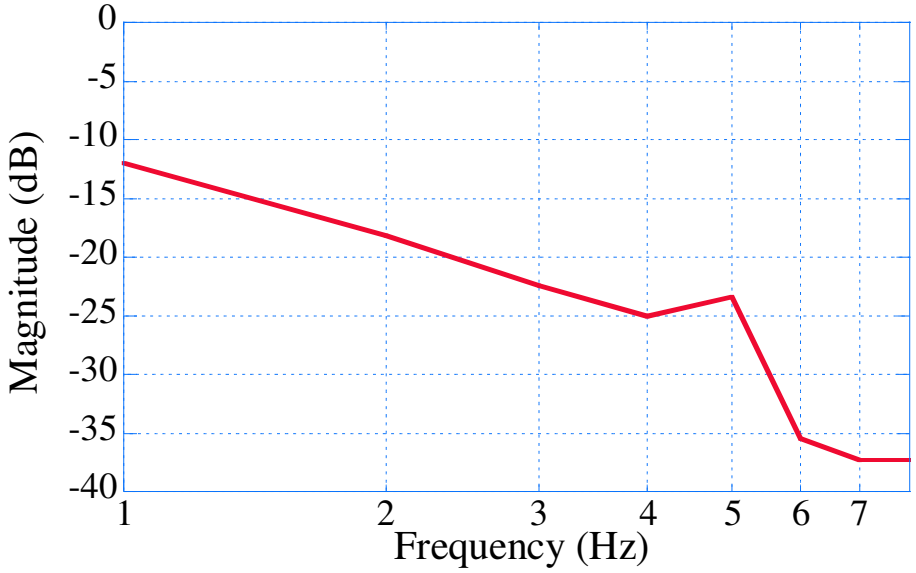

Figure 52: Excitation Base Pitch Angle Unloaded Frequency Response

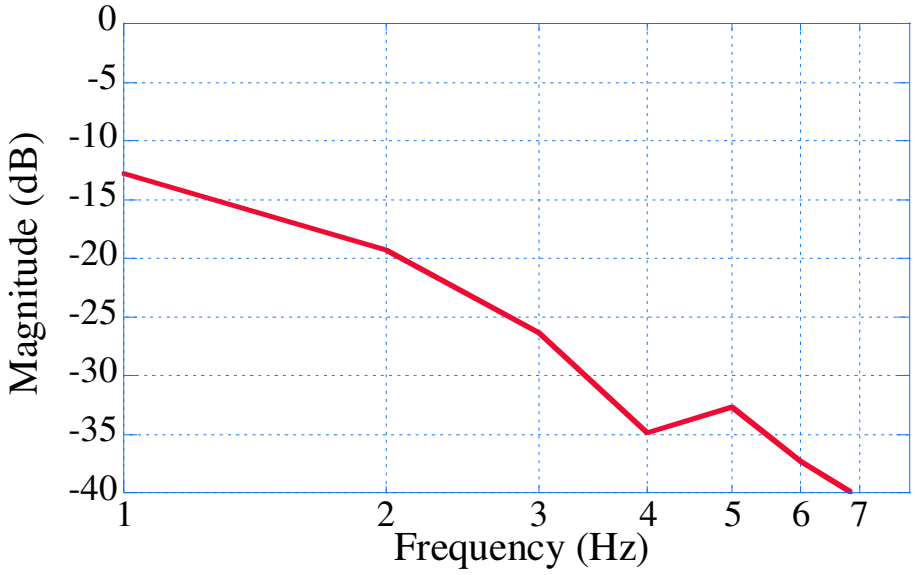

Figure 53: Excitation Base Pitch Angle Loaded Frequency Response

3.7 Summary

The performance of the Hyper-Active seat was evaluated using step and frequency response in multiple degrees of freedom. These experiments show that the Hyper-Active seat will be able to significantly reduce vibrations in the harmful frequency range. From these results a third-order model was developed for each of the three degrees of freedom which can be used to aid controller design. This model predicts the response of the vertical and horizontal directions, and predicted the correct trends for the pitch angle. From the analysis of the data, it can be concluded the Hyper-Active seat has the potential to suppress vibrations that are harmful to the operator.

The frequency response of the excitation base was discussed. The base is capable of creating disturbances in the vertical direction from 0 to 7 Hz and in the pitch angle direction from 0 to 4 Hz. The performance of the vibration cancellation controller was evaluated against an uncontrolled Hyper-Active seat. The controller showed excellent results in the 1 to 7 Hz range. The displacement of the amplitude was also decreased about 40% over the uncontrolled seat. The RMS average acceleration was reduced, thereby increasing the potential of the operator to work longer. The vibration cancellation controller met the specifications to reduce vibration in the harmful frequency range.

CHAPTER IV

SAFETY SEAT MOTION DESIGN

4.1 Fixed-Seat Model

A safety seat moves in some way to reduce injuries to the passenger during a crash. One way the seat reduces injuries is be reducing the relative velocity of the occupant. The relative velocity is one measure in which the severity of injuries can be predicted. Given that the Hyper-Active seat is equipped with powerful hydraulic actuators, it may be possible to add this important feature. There are a number of possible ways that a safety seat could move. One way is to elevate the front of the seat, thereby increasing the seat angle. Along with this motion, there is also the possibility of moving the seat in the X or Y direction. If the seat is going to move in the X or Y direction, will it take a straight path, or an curved path? Along with the questions of what path the seat will take and where the seat will move, there is the question of how long the seat will take to translate into the final position. To answer these questions, a model of a safety seat was created.

To initiate the investigation a fixed-seat model was created. A fixed-seat model is used to study the effect of various seat bottom angles. The coefficient of friction and changing the position of the occupant in the seat will also be studied with the fixed-seat model. The fixed-seat model will predict different trends which do not need a complicated model. The effect of changing the coefficient of kinetic friction, along with changing the position of the occupant will not change as the complexity of the model increases.

The degree of complexity of a seat and occupant model reported in the literature varies greatly. Liu and Wagner, used a very complicated model which looked in depth at the springs and foam used in the seat [28]. Although the seat and occupant can be modeled in detail as in Liu and Wagner, a simple seat and block mass such as that of Stein will suffice for the purpose of this study [46, 47, 48]. Figure 54 shows the occupant and seat bottom modeled as a block on a ramp. Since this is a simple model, several dynamic effects are

neglected, such as: compression of the seat, rotation of the occupant, effect of the occupants hands on the steering wheel or feet on the floor, effect of the vehicle impacting the occupant, and the effect of a seat belt or airbag. Also, the effects of the occupant flying through the air was neglected. These dynamics are neglected because the goal of this initial investigation is simple: determine the effect of the basic seat parameters such as seat bottom angle, coefficient of kinetic friction, and position of the occupant.

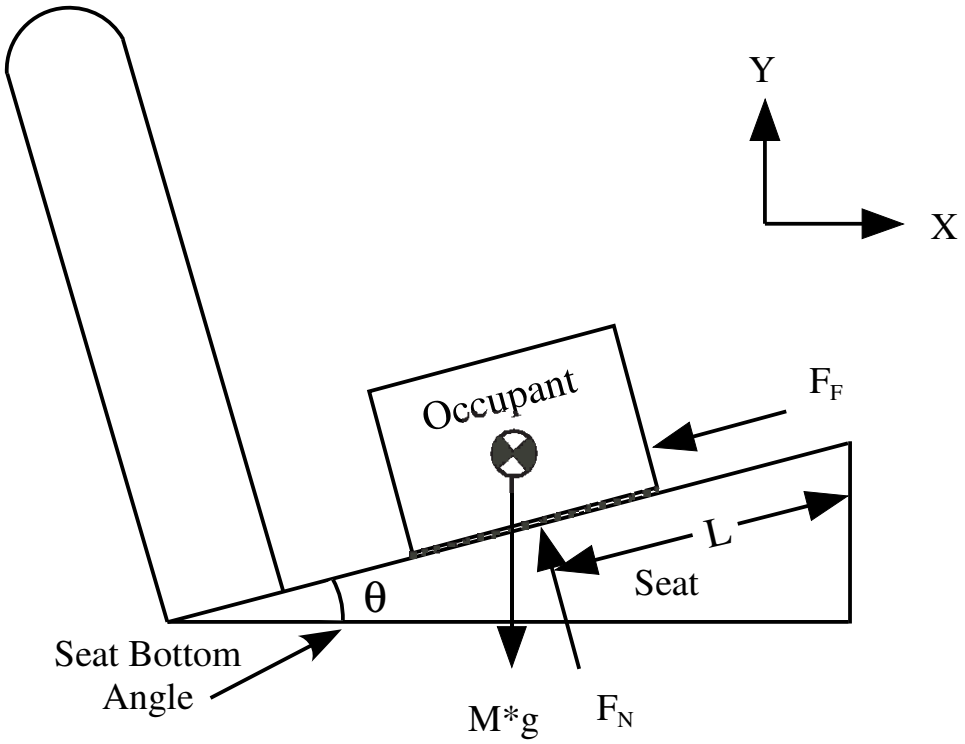

Figure 54: Fixed-Seat Model of Occupant and Seat as a Block and Ramp

The crash event, shown in Figure 55, is simulated here by accelerating the seat (modeled as a ramp) in the negative horizontal, X, direction. This has the same effect as modeling the seat as decelerating when the vehicle hits a fixed object. The relative acceleration of the occupant (the block) is then calculated with respect to the ramp. The total acceleration, A_T, is a combination of the relative acceleration and the acceleration of the crash-pulse:

$$A_T^X = A_R \cos(\theta) - A_P \tag{35}$$

$$A_T^Y = A_R \sin(\theta), \tag{36}$$

where A_P is the acceleration of the crash-pulse, A_T^X is the total acceleration in the X

direction, A_T^Y is the total acceleration in the Y direction, θ is the seat bottom angle, and A_R is the relative acceleration of the block with respect to the ramp.

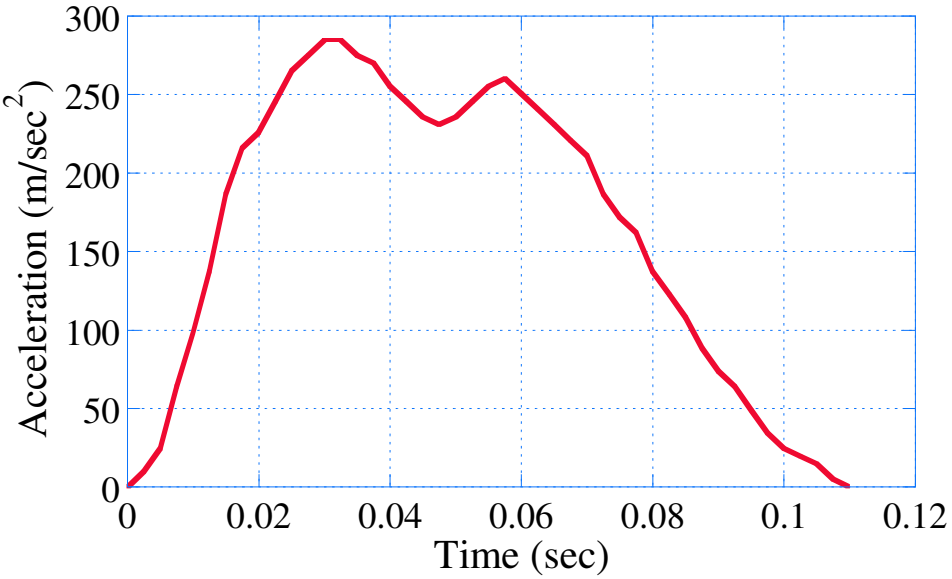

Figure 55: Crash Pulse Signature - 2000 Isuzu Rodeo

In order to solve (35) and (36), the forces on the block are summed in the X and Y directions:

$$MA_T^X = -F_F\cos(\theta) - F_N\sin(\theta) \tag{37}$$

$$MA_T^Y = -MF_G - F_F\sin(\theta) + F_N\cos(\theta), \tag{38}$$

where M is the mass of the block, F_F is the friction force, F_N is the normal force, and F_G is the force of gravity. Equations, (35) and (36) are substituted into (37) and (38) respectively to get:

$$M(A_R\cos(\theta) - A_P) = -F_F\cos(\theta) - F_N\sin(\theta) \tag{39}$$

$$MA_R\sin(\theta) = -MF_G - F_F\sin(\theta) + F_N\cos(\theta). \tag{40}$$

Another relevant equation is the law of coulomb friction, which relates the friction force to the normal force through the proportionality constant μ_K:

$$F_F \leq \mu_K F_N, \tag{41}$$

where μ_K is the coefficient of kinetic friction. Because the acceleration of the ramp caused by the crash-pulse is large, the effect of the static friction is ignored and it is assumed that

the block will begin sliding from the start of the crash-pulse. Therefore, the friction is modeled as:

$$F_F = \mu_K F_N. \tag{42}$$

Equations (39), (40), and (42) are solved to obtain the relative acceleration of the block with respect to the ramp, and the normal force:

$$A_R = -\mu_K F_G \cos(\theta) - \mu_K A_P \sin(\theta) - F_G \sin(\theta) + A_P \cos(\theta) \tag{43}$$

$$F_N = M(F_G \cos(\theta) + A_P \sin(\theta)). \tag{44}$$

Equation (43), which describes the relative acceleration of the block with respect to the ramp, is dependent on the seat bottom angle, gravity, the crash-pulse signature, and the coefficient of kinetic friction. Equation (44), which describes the normal force, is dependent on the seat bottom angle, the mass of occupant, gravity, and the crash-pulse signature. The position where the occupant is sitting relative to the front edge of the seat, L, as shown in Figure 54, is not taken into account in the above equations, but is accounted for later in the process. It is important to note that (43) and (44) can be used for any vehicle by simply utilizing the correct crash-pulse signature.

This dynamic model only applies when the occupant is in contact with the seat. It is assumed that during the crash, the occupant only looses contact with the seat when the front edge of the seat is reached. Using this assumption, the occupant will slide to the front edge of the seat at some point and the forces from the seat will no longer affect the occupant. This phenomena is not accounted for in (43) or (44), therefore the accumulation of relative velocity must be divided into two parts: the time when the block is in contact with the ramp, and the time after the block leaves the ramp. Figure 56 illustrates the two parts of the dynamic model.

Equations (43) and (44) explain the motion of the block for the first part of the simulation, from t_0 to t_1. For this part of the simulation, the block is sliding on the ramp. The relative velocity is found by integrating (43) and the X and Y relative velocity components are recorded, as well as the time. The second part of the simulation accounts for the remainder of the crash-pulse from t_1 to t_2, once the block reaches the front edge of the ramp

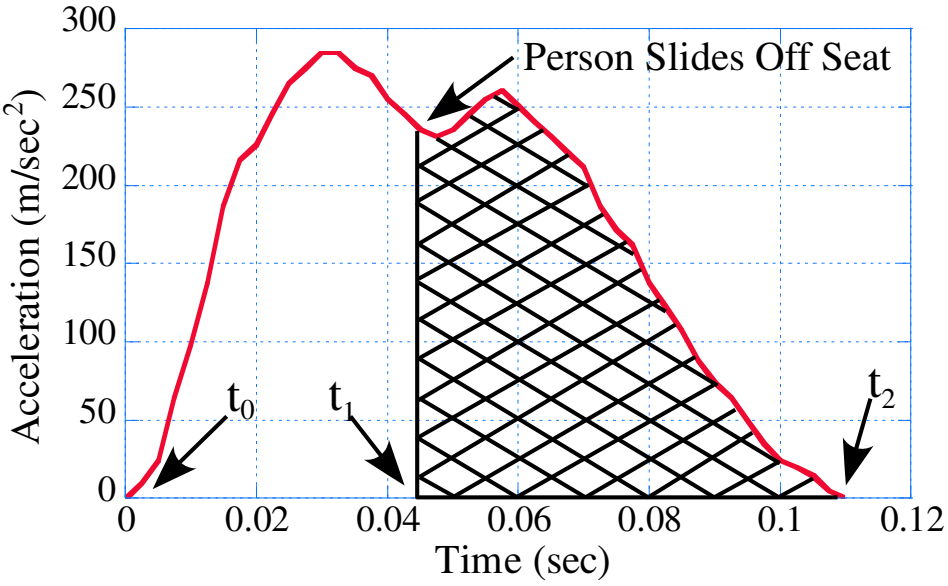

Figure 56: Two Segments of the Dynamic Model

and leaves the ramp. The second part of the crash-pulse is integrated to get the remaining increase in relative velocity, which is independent of seat frictional forces. This is then broken into X and Y relative velocity components and recorded. Once all the variables are recorded, the two segments of the model are added together to get the corresponding normal force.

4.2 Fixed-Seat Simulation Results

In order to determine the response of the occupant to a crash, data was collected over a large range of parameters. The ramp angle was varied from 0 to 45 degrees. At each degree, the kinetic friction coefficient was varied from 0.1 to 0.6. On the low end, a value of 0.1 would represent silk pants on a leather seat and, on the high end, a value of 0.6 would represent heavy jeans on a cloth seat. The ramp length was set to 0.464 m, which was taken from the average seat bottom length of 41 different vehicles [19]. This length assumes that the occupant is sitting all the way back in the seat when the collision occurs. To study the sliding distance, L, the starting position of the occupant is changed. The mass of the occupant was assumed to be 81.6 kg (180 lbs).

The relative velocity is broken into components to understand their individual contribution to the total relative velocity. Figures 57 and 58 show the X and Y relative velocity components of the occupant with respect to the seat at the end of the crash-pulse as a function of ramp angle and friction. As expected, the relative horizontal velocity component decreases as the ramp angle increases. Unfortunately, the relative vertical velocity component increases up to a point as the ramp angle increases. As the friction coefficient is increased, the maximum possible vertical relative velocity component decreases and so does the angle at which it occurs. When changing the position of a safety seat, it must be clear how much the relative velocity increases in the vertical direction to prevent the occupant from being driven into the roof and thereby increasing injuries. Both Figures 57 and 58 portray the significant effect of changing the coefficient of kinetic friction and the ramp angle. These results form the foundation of the claim that rapidly changing the position of a seat can decrease injuries during a crash.

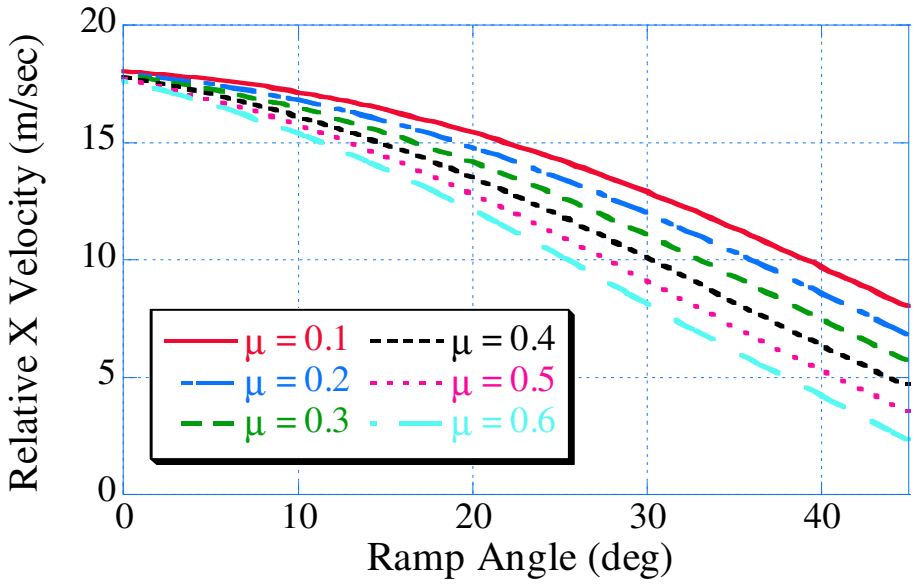

Figure 57: Horizontal Velocity of the Block Verses Ramp Angle

The total relative velocity, however, is dependent on both the X and Y relative velocity components. Figure 59 shows that as the ramp angle increases, the total relative velocity decreases, even though the relative velocity in the Y direction increases. Figure 60 shows that, correspondingly, the kinetic energy decreases as the ramp angle increases.

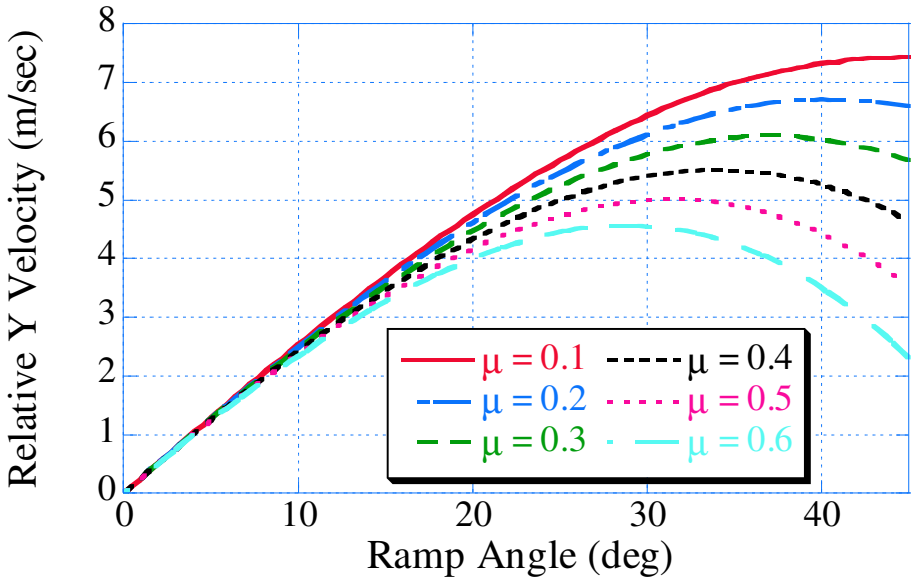

Figure 58: Vertical Velocity of the Block Verses Ramp Angle

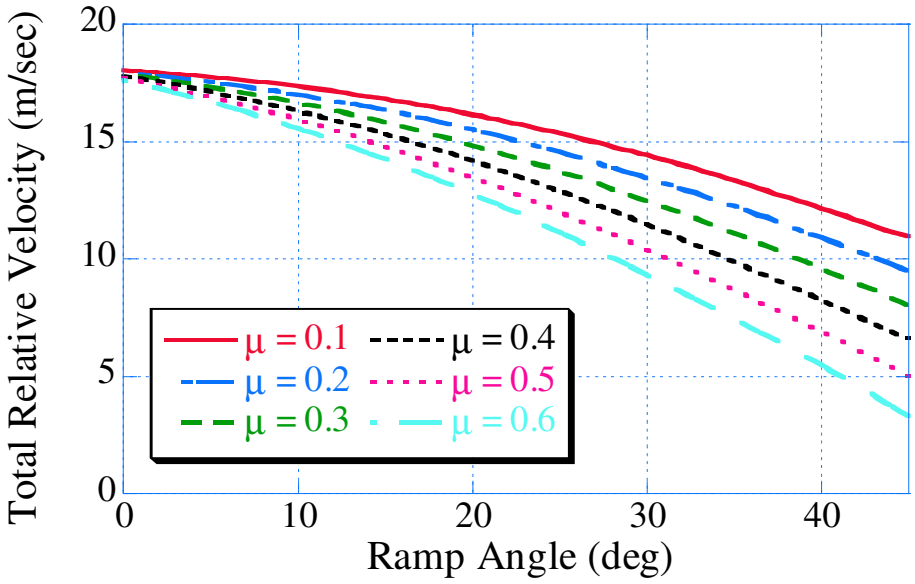

Figure 59: Total Relative Velocity of the Block Verses Ramp Angle

These results verify that increasing the seat angle will decrease the relative kinetic energy of the occupant and possibly lower the chances of injury in a front-end collision. Figures 59 and 60 show that an extremely large seat bottom angle will be the safest. However, current seats are far from this angle [19]. Figure 61 shows the percent change in kinetic energy as the ramp angle is varied from the industry average seat bottom angle of 15 degrees [19].

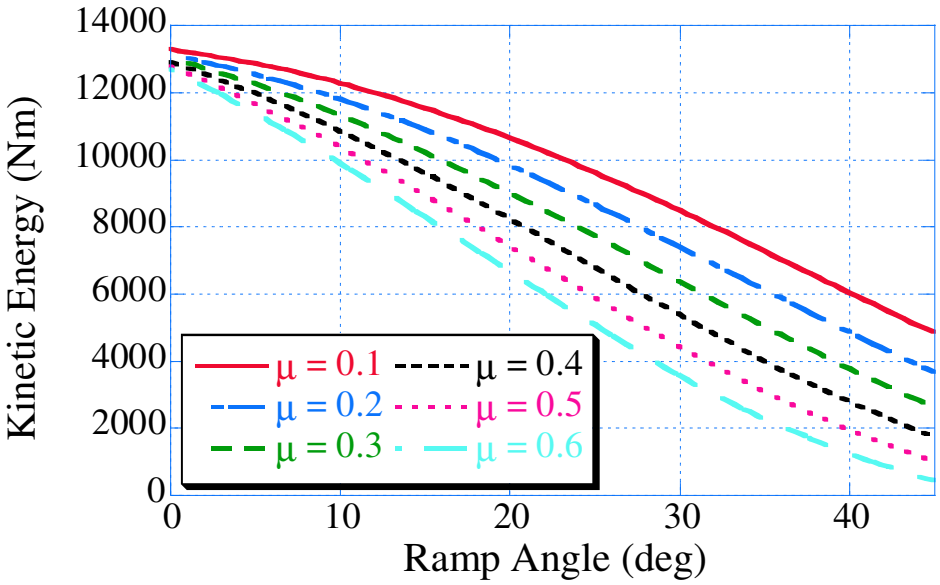

Figure 60: Relative Kinetic Energy of the Block Verses Ramp Angle

Figure 61 can be used as a guide to designing a safety seat.

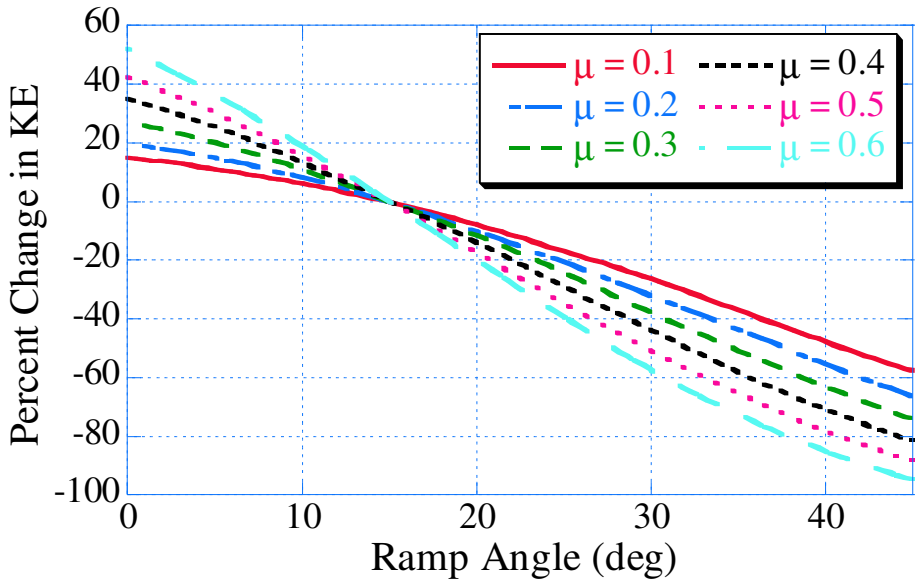

Figure 61: Percent Change in Relative Kinetic Energy of the Block Verses Ramp Angle

Singer, *et al.* designed a passive safety seat that would follow an optimal trajectory during a crash [45]. Their safety seat increased the seat bottom to an angle of 25 degrees. Comparing a 15 degree seat to a 25 degree seat, our results would predict a decrease in the kinetic energy of the block anywhere from 24 to 40 percent, based on coefficients of kinetic

friction between 0.3 and 0.6. Beauvais and Meade designed a safety seat that increased the angle from 15 degrees under normal conditions to 45 degrees in the time of an accident [6]. That corresponds to a 58 to 95 percent decrease in kinetic energy.

However, there are negative effects of severely increasing the ramp angle, (e.g. the increase in the vertical velocity shown in Figure 58). This leads to the possibility of sending the occupant into the roof of the car causing neck injuries. Furthermore, another adverse effect is a massive increase in normal force. Figure 62 shows the normal force increases as the ramp angle increases. The normal force has a nearly linear response to an increase in the ramp angle. Increasing the normal force beyond human limits has the advert affect of possible injuring the occupants back.

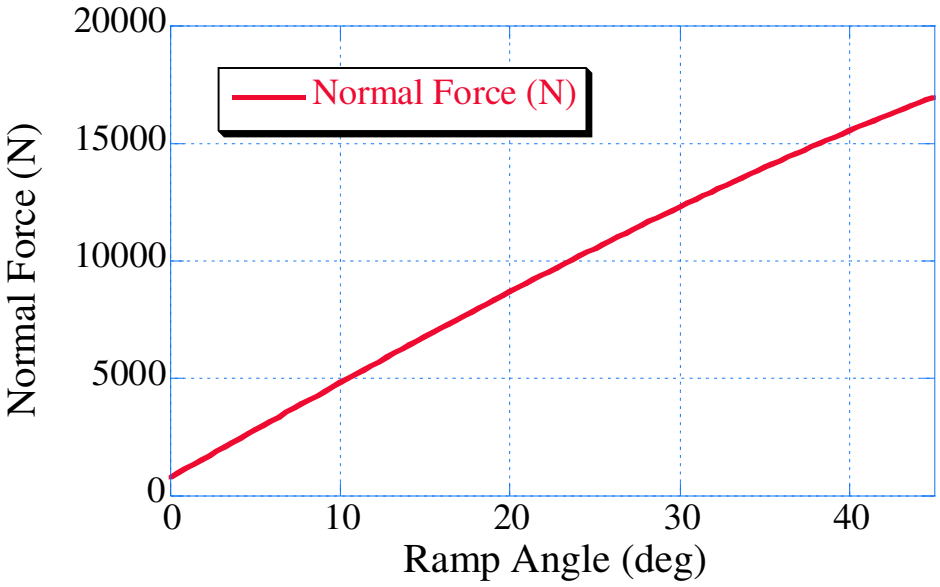

Figure 62: Normal Force between the Block and the Ramp Verses Ramp Angle

By increasing the ramp angle from 15 to 25 degrees, the normal force increases 55 percent. Some, such as Bullerdieck and Hasstedt, have proposed to increase the seat angle to 90 degrees, in which case the relative kinetic energy will be decreased to zero [22, 8]. However, by increasing the ramp angle from 15 to 90 degrees, the normal force increases from 6,800 to 23,200 N. This trade-off between decreasing the total relative velocity and increasing the normal force is clear. Both results must be understood to properly design a safety seat. Although decreasing the relative kinetic energy of the occupant will decrease the occupant's

chances of being injured, increasing the normal force too much might inadvertently injure the occupant.

The previous data was presented with a constant occupant sliding distance. During a collision, one cannot guarantee that the occupant is going to be sitting against the seat back. Some occupants sit closer to the steering wheel than others, and seats can vary in lengths [19]. In the fixed-seat simulation, this effectively changes the sliding distance of the block with respect to the ramp. Figure 63 shows what effect changing the sliding distance would have on the relative kinetic energy of the block. The longer the block slides on the ramp, the less kinetic energy the occupant has at the end of the crash-pulse. Figure 63 shows that sitting back in the seat and thus increasing the sliding distance required to reach the front edge of the seat has a large effect on decreasing the relative velocity of the occupant with respect to the seat.

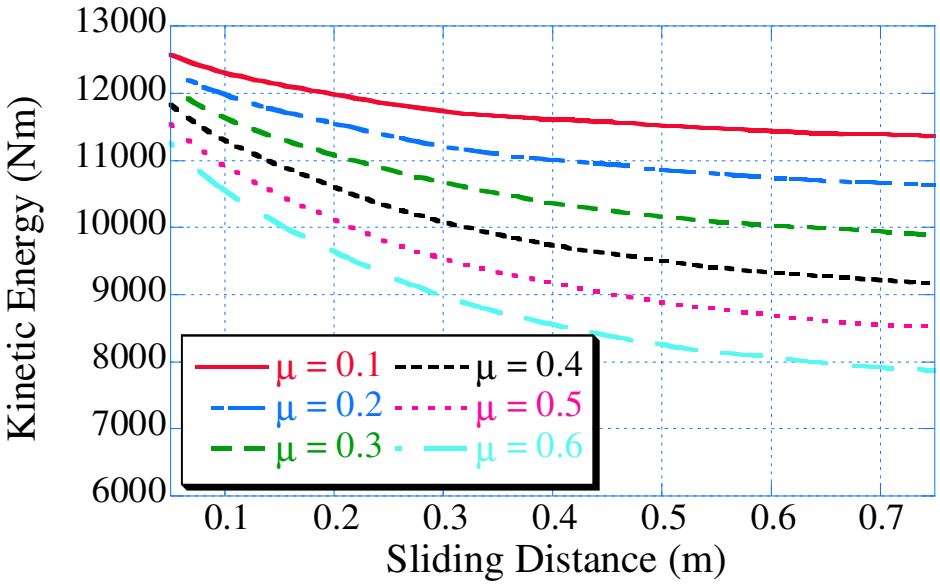

Figure 63: Relative Kinetic Energy of the Block Verses Sliding Distance

Many important trends can be discerned from this simple fix-seat model. It was shown that increasing the seat angle decreases the overall relative velocity, however it may increase the vertical velocity. Along with the vertical velocity, the normal force on the occupant is increased as the seat angle is increased. The coefficient of kinetic friction plays a big role in determining how much the relative velocity is decreased as the seat angle is increase.

Finally, increasing the sliding distance decreased the relative velocity of the occupant with respect to the seat. Understanding these fundamental trends can lead to the development of a better safety seat.

4.3 Moving-Seat Model

Now that some of the important trends are understood about fixed seats, the model can be expanded to analyze other motions of the seat. Along with rotating the seat through some angle, another important motion of the seat is to move the center of mass of the seat in the horizontal and vertical direction. Increasing the complexity of the model in this way will allow the determination of how moving the seat during a crash will affect the relative velocity.

A more complex model of the occupant and seat was derived to analyze the effect of the seat moving. Instead of having the seat fixed, the expanded model simulates the seat moving from a beginning position to a final position. In order to be more realistic, the simulation includes a delay to simulate the crash sensor response. Figure 64 shows the model that was used to derive the equations of motion.

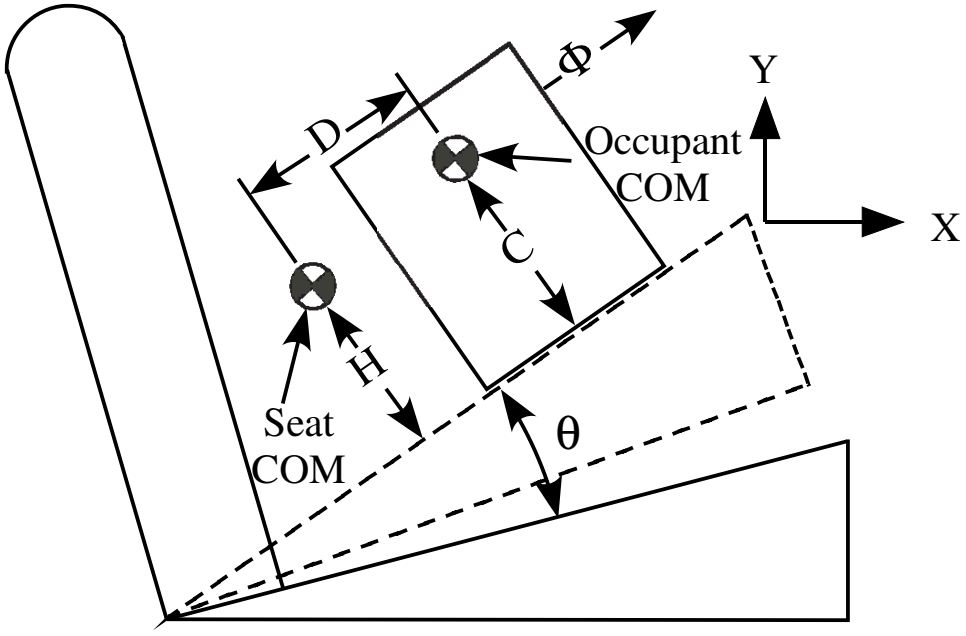

Figure 64: Moving-Seat Model of Person and Seat

The equations of motion were derived in a similar way to the fixed-seat model. The

relative acceleration of the occupant with respect to the seat for the moving-seat model is:

$$\begin{aligned} A_R = {} & A_P\cos(\theta) - \ddot{X}\cos(\theta) - \ddot{Y}\sin(\theta) + \ddot{\theta}HL + \ddot{\theta}C + \dot{\theta}^2\Phi + \dot{\theta}^2 D \\ & + \mu_K \mathrm{sgn}(\dot{\Phi})\ddot{X}\sin(\theta) - \mu_K \mathrm{sgn}(\dot{\Phi})\ddot{Y}\cos(\theta) - \mu_K \mathrm{sgn}(\dot{\Phi})A_P\sin(\theta) \\ & - \mu_K \mathrm{sgn}(\dot{\Phi})\ddot{\theta}\Phi - 2\mu_K \mathrm{sgn}(\dot{\Phi})\dot{\theta}\dot{\Phi} - \mu_K \mathrm{sgn}(\dot{\Phi})\ddot{\theta}D + \mu_K \mathrm{sgn}(\dot{\Phi})\dot{\theta}^2 C \\ & - \mu_K \mathrm{sgn}(\dot{\Phi})F_G\cos(\theta) + \mu_K \mathrm{sgn}(\dot{\Phi})\dot{\theta}^2 HL + F_G\sin(\theta), \end{aligned} \tag{45}$$

where X is the movement of the center of mass (COM) of the seat in the horizontal direction, Y is the movement of the COM of the seat in the vertical direction, D is the starting distance from the COM of the seat to the COM of the occupant, H is the negative distance from the COM of the seat to the seat bottom, C is the distance from the COM of the occupant to the seat bottom, and Φ is the distance the occupant travels relative to the seat. The relative velocity, $\dot{\Phi}$, is calculated when the relative distance, Φ, equals the seat distance. The normal force on the occupant is:

$$\begin{aligned} F_N = {} & M(\ddot{\theta}\Phi + 2\dot{\theta}\dot{\Phi} + \ddot{\theta}D + \ddot{Y}\cos(\theta) + A_P\sin(\theta) \\ & - \ddot{X}\sin(\theta) + F_G\cos(\theta) - \dot{\theta}^2 HL - \dot{\theta}^2 C). \end{aligned} \tag{46}$$

The other variables in (45) and (46) are the same as in the simple seat model. Information about the human body, such as weights and lengths of appendages were taken from anthropometry and human factor tables [42, 10, 56, 57]. The parameters used in the moving-seat simulation are shown in Table 11

In (45) and (46), many variables can be specified. The movement of the seat in the X, Y, and θ direction are known as a function of time. An S-curve was used when moving the seat in the X, Y, and θ direction. Since the duration is the same for the move in the X and Y direction, this translates to the seat moving in a straight line from the starting point to the ending point. Section 4.6 will discuss the effects of a curved path. Figure 65 shows an example of the seat moving from a starting angle of 15 degrees (0.262 rad) and ending at an angle of 20 degrees (0.349 rad). The figure also shows a 10 ms delay and it takes the seat a duration of 50 ms to complete the move. Therefore the total move time is 60 ms. The S-curve was used to change position because it is a realizable command the system can

Table 11: Parameters Used in the Moving-Seat Model

Parameter	Value
Sensor Delay (t_0)	0.01 sec
Duration of Configuration (d)	0.02 to 0.05 sec
Seat Start Angle (θ)	15 deg
Seat End Angle (θ)	15 to 35 deg
Seat Start Position (X)	0 m
Seat End Position (X)	-0.10 to 0.10 m
Seat Start Position (Y)	0 m
Seat End Position (Y)	-0.10 to 0.07 m
Kinetic Friction Coefficient (μ_K)	0.3
Mass of Occupant (M)	81.648 Kg
COM of Seat to Seat Bottom (H)	-0.087 m
COM of Seat to COM of Occupant (D)	-0.0236 m
COM of Occupant to Seat Bottom (C)	0.376 m

follow. If a step command was used, the system could not follow the command due to the mass of the occupant and seat, and the resulting response of the seat would be similar to an S-curve.

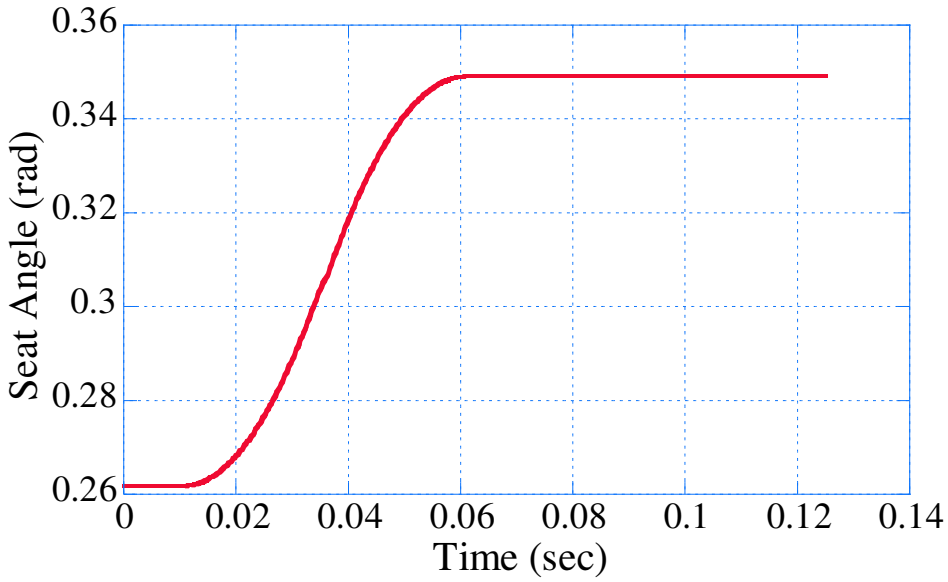

Figure 65: S-Curve Path Used to Change Position

Figures 66 and 67 show the corresponding angular velocity and angular acceleration of

the seat. The position, velocity, and acceleration of the S-curve profile are:

$$\theta = \left\{ \begin{array}{cc} a & t \leq t_0 \\ \frac{4(b-a)(\frac{1}{2}t^2 - t_0 t)}{d^2} + \frac{a(t_0+d)^2 - 2a(t_0+d)t_0 - at_0^2 + 2t_0^2 b}{d^2} & t_0 < t \leq t_0 + \frac{1}{2}d \\ \frac{4(b-a)(t_0+d)t - \frac{1}{2}t^2)}{d^2} + \frac{(2a(t_0+d)^2 - b(t_0+d)^2 - 2b(t_0+d)t_0 + t_0^2 b)}{d^2} & t_0 + \frac{1}{2}d < t \leq t_0 + d \\ b & t > t_0 + d \end{array} \right\} \quad (47)$$

$$\dot{\theta} = \left\{ \begin{array}{cc} 0 & t \leq t_0 \\ \frac{4(\mathrm{b-a})(-\mathrm{t_0+t})}{\mathrm{d}^2} & t_0 < t \leq t_0 + \frac{1}{2}d \\ \frac{4(-\mathrm{t+t_0+d})(\mathrm{b-a})}{\mathrm{d}^2} & t_0 + \frac{1}{2}d < t \leq t_0 + d \\ 0 & t > t_0 + d \end{array} \right\} \quad (48)$$

$$\ddot{\theta} = \left\{ \begin{array}{cc} 0 & t \leq t_0 \\ \frac{4(\mathrm{b-a})}{\mathrm{d}^2} & t_0 < t \leq t_0 + \frac{1}{2}d \\ \frac{-4(\mathrm{b-a})}{\mathrm{d}^2} & t_0 + \frac{1}{2}d < t \leq t_0 + d \\ 0 & t > t_0 + d \end{array} \right\}, \quad (49)$$

where a is the starting point of the move, b is the ending point of the move, t_0 is the delay, d is the duration of the move, and t is the time. Even though Figures 65 - 67 only show the change in angle, angular velocity, and angular acceleration, (47) - (49) are also used for changes in the X and Y directions.

4.4 Moving-Seat Simulation Results

The dynamic equations of motion were simulated for a wide range of seat trajectories and compared to the fixed-seat model. As and example, consider one case where the seat started at an angle of 15 degrees and transitioned to an angle of 25 degrees using an S-curve, while the horizontal and vertical position were held fixed. The sensor time delay was set to 10 ms and the transition time between 15 and 25 degrees was set to 50 ms. This simulation was then compared to the fixed-seat model with a ramp angle of 15 degrees. Both simulations used a μ_K of 0.3. The moving-seat simulation predicted a relative velocity of the block at the end of the crash of 14.5 m/sec as shown in Figure 68, while the fixed-seat simulation

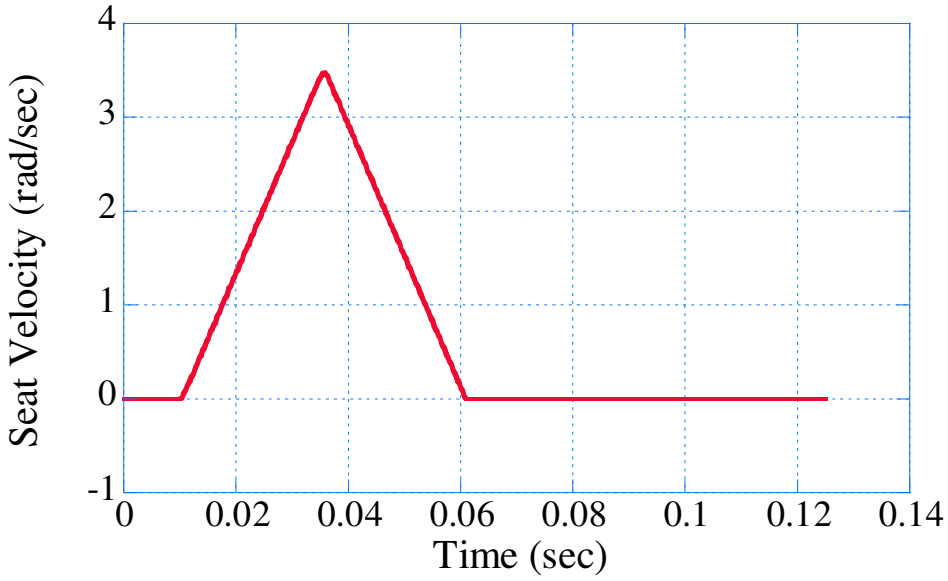

Figure 66: Path Used to Change Velocity

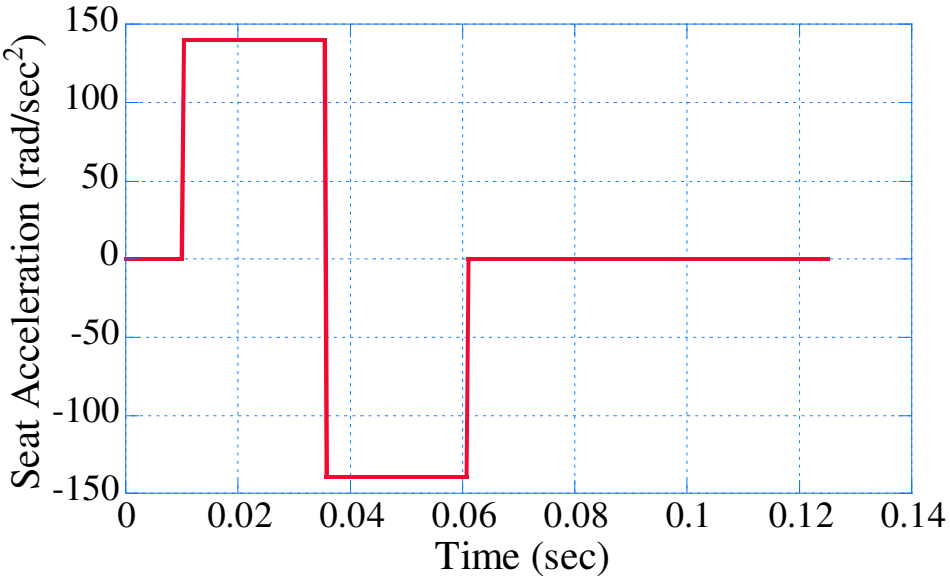

Figure 67: Path Used to Change Acceleration

predicted it would be 15.8 m/sec as shown in Figure 59. The relative velocity of the moving-seat model was 1.3 m/sec less compared to the fixed-seat model with an angle of 15 degrees.

The possible negative results of rapidly increasing the seat bottom angle in the time of a crash is an increase in the normal force on the occupant, as well as, an increase in the

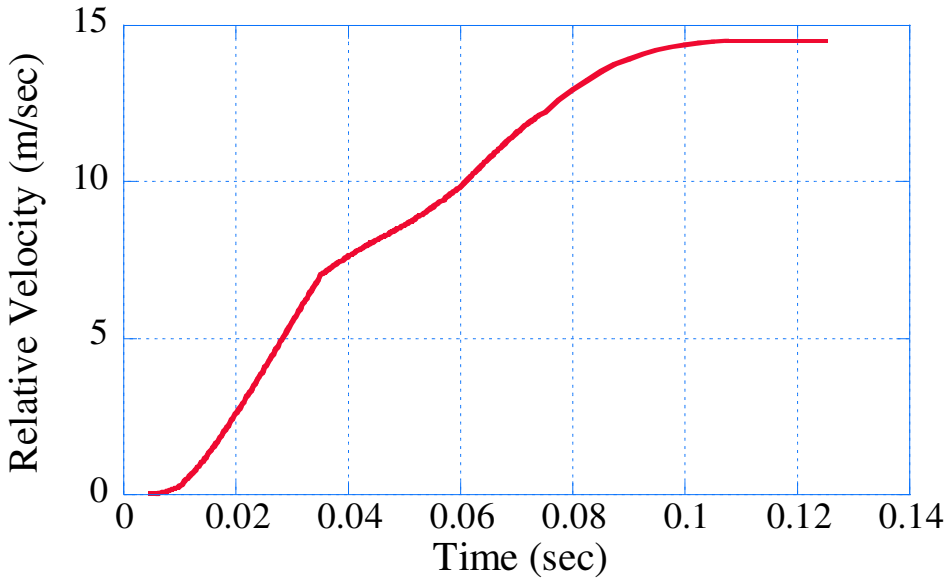

Figure 68: Relative Velocity of the Block with respect to the Ramp

occupant's vertical velocity. Figure 69 shows the normal force on the occupant verses time. The normal force reaches a maximum of about 16,600 N, which is considered just beyond the safe upper limit of the human spine. Studies show that accelerations of the human body above 20 g's, or approximately 16,000 N for the 81.6 kg occupant, may fracture the lumbar vertebrae [10]. Therefore, increasing the seat bottom angle from 15 to 25 degrees in 60 ms may result in injuries of that nature.

Increasing the seat angle from 15 to 25 degrees during the first 60 ms of a crash will decrease the relative velocity of the occupant more than the current industry standard seat fixed at 15 degrees [19]. This was only one example, and it is possible to move the seat in more complicated trajectories. To obtain even more improvement, the possible design space must be systematically and thoroughly explored. It is important to note that when S-curve position verses time profiles are used to specify the X and Y direction motion of the seat, the resulting seat path is a straight line.

4.5 Designing Safety Seats

The results of the moving-seat model have shown that the relative velocity of the occupant can be decreased, however, care must be taken not to increased normal force beyond a safe

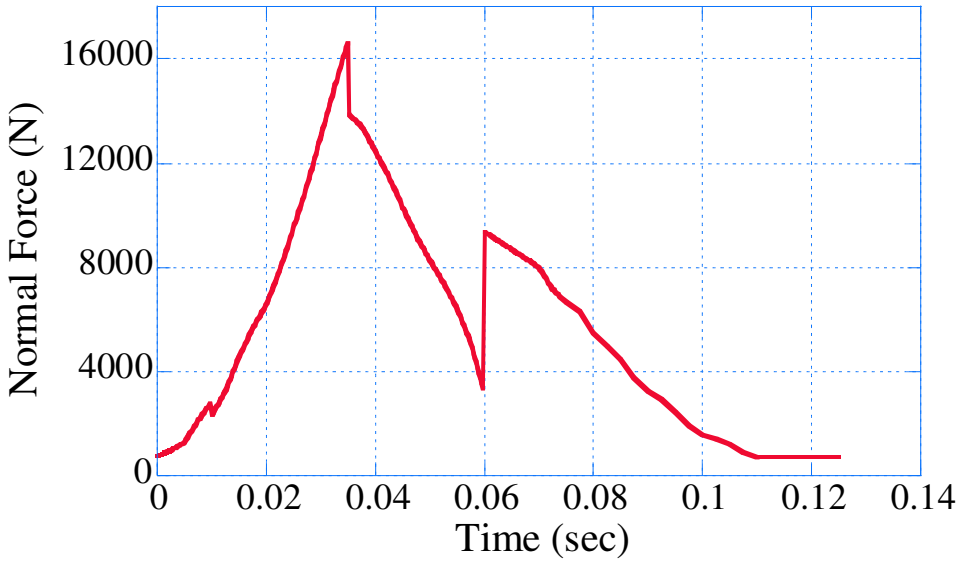

Figure 69: Normal Force on the Block with respect to Time

limit or excessively increase the relative velocity in the Y direction. In order to design a safety seat, different variables need to be optimized to give the minimum final relative velocity, while keeping the other factors within an acceptable range.

The four parameters that need to be optimized are:

1. Final X position of the seat
2. Final Y position of the seat
3. Final θ of the seat bottom
4. Duration of the move.

The parameters were optimized by searching a reasonable workspace. The center of mass of the seat started at zero in the X and Y directions. From there, the seat was moved to an ending location. The ending location varied between -0.10 m and 0.10 m in the X direction, and -0.10 m and 0.07 m in the Y direction. The bottom seat angle started at 15 degrees, and then ended somewhere between 15 degrees and 35 degrees. The duration was varied between 20 ms and 50 ms, while the delay due to the crash sensor was set to 10 ms.

As the parameters were varied, two important pieces of data collected were the final velocity of the occupant relative to the seat, and the maximum normal force. These values

were recorded, as well as the four motion parameters that were varied. Once the data was collected for the workspace, a searching algorithm was created. The user was able to input a limit on the maximum normal force and then was given the X, Y, θ, and duration design parameters for the minimum relative velocity.

The entire matrix of data was accessible via a GUI interface created in MATLAB. Figure 70 shows the viewer interface. The two plots show the relative velocity and corresponding normal force for the area surrounding the motion parameters selected. The black dot on both of the plots show the selected parameters. The four pull-down menus at the bottom of the window give the current selection of the X, Y, θ, and duration parameters. The screen in the bottom right displays the corresponding values for the relative velocity and normal force for the parameters selected. Finally, the checkbox in the bottom middle gives the user the option of freezing the axis so the normal force plot does not go above the acceptable level of a human. This data viewer window allows the user to spot trends and get a feel for how changing one of the parameters affects the overall relative velocity and normal force.

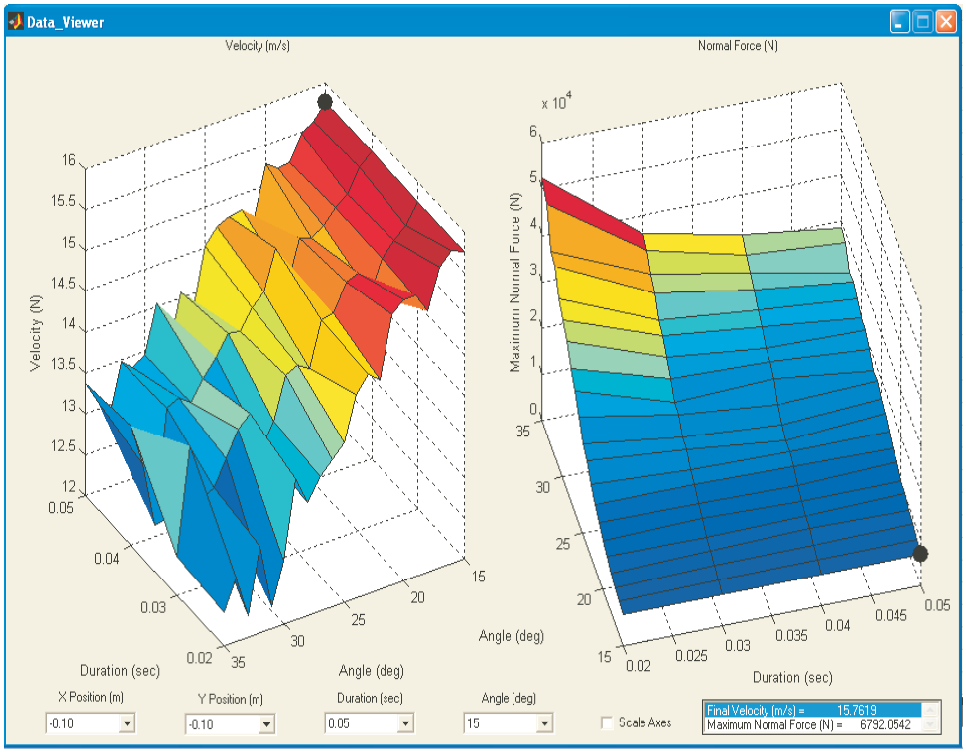

Figure 70: GUI Interface Used for Viewing Design Parameters

To better understand how the maximum normal force affects the relative velocity, another optimization program was written. This program allows the user to input the maximum normal force the occupant will be subjected to, and the program searches the data displayed in the data viewer window for the corresponding minimum relative velocity. The program then displays the minimum relative velocity, corresponding normal force, along with the four parameters, ending X and Y position, ending θ position, and the duration during which the seat moves. As mentioned earlier, the maximum acceptable normal force is 16,000 N. Figure 71 shows how the relative velocity changes as the maximum allowable normal force increases from 12,000 N to the upper limit of 16,000 N. As expected, the relative velocity of the occupant decreases as the maximum normal force limit on the occupant increases. As the maximum normal force limit is increased, the seat can move in a path which is more restraining on the occupant and the relative velocity of the occupant is decreased. The steps in the data are due to the fineness of the mesh which was used in collecting the data for the data viewer window.

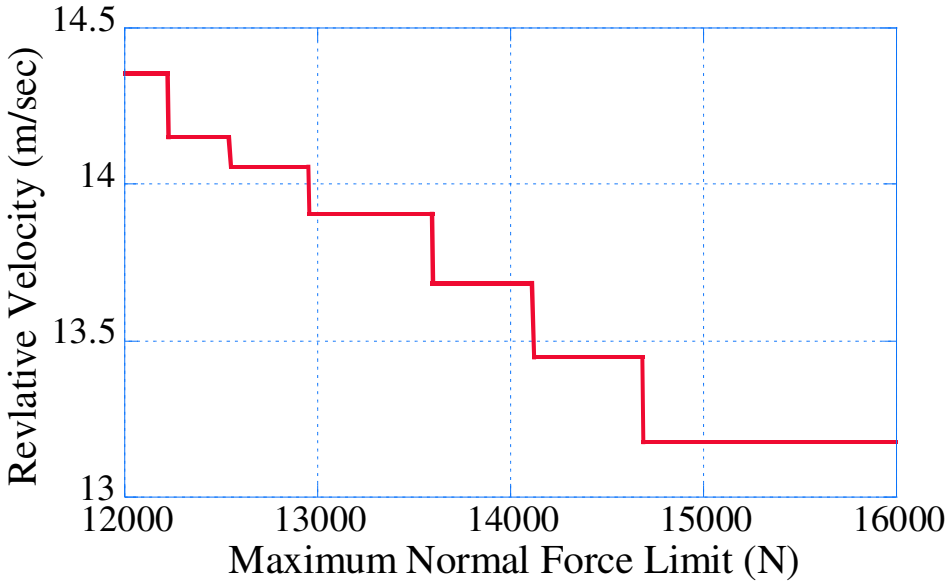

Figure 71: Relative Velocity Verses Maximum Normal Force

As was just shown, increasing the maximum normal force limit on the occupant decreases the relative velocity, but how does increasing the maximum normal force limit affect the optimal ending position of the seat. Figure 72 shows how the ending angle, θ_f, changes as

the maximum normal force limit is increased. Intuitively, one would expect that θ_f should increase as the maximum normal force limit is increased. Figure 72 shows the ending angle should increase from 23 degrees to 28 degrees, as the maximum normal force limit is increased from 12,000 N to 16,000 N. Again, the steps in the data are due to the mesh that was used for the data viewer window. If a finer mesh was used, one would expect that the data would poise a more linear relationship.

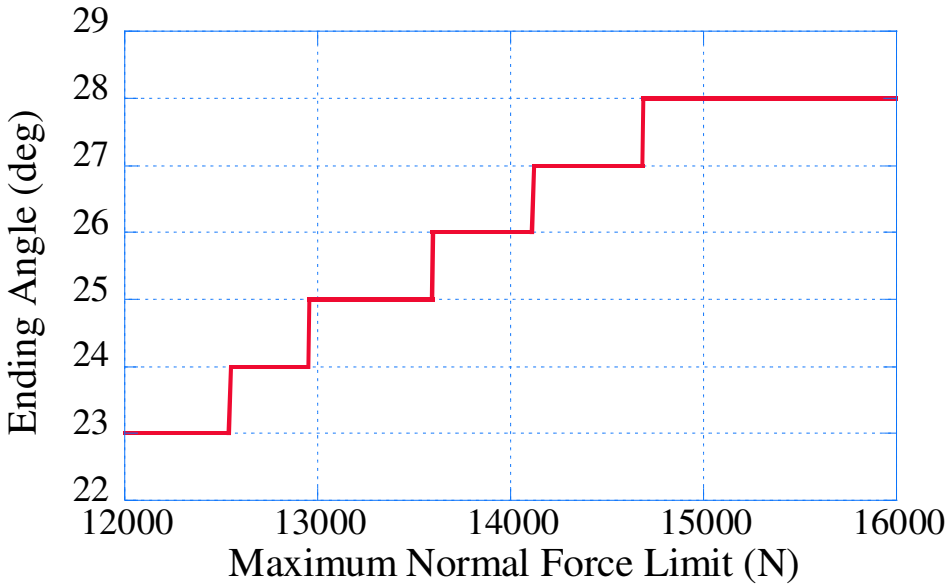

Figure 72: Optimal Ending Angle Verses Maximum Normal Force

One may expect the increase in the ending angle, however, intuition does not help predict the optimal ending position of the seat in the vertical and horizontal directions. Figure 73 shows that the ending position of the seat does not change as the limit on the maximum normal force is increased. The ending X_f position should be 0.03 m, and the ending Y_f position should be 0.01 m. Figure 74 shows how the duration of the move changes as the limit on the maximum normal force is increased. Generally, the duration should be decreased, which was expected. As the maximum normal force limit is increased, more force will be applied to the occupant, which in turn is caused by increasing the velocity of the move, which is directly related to the duration of the move.

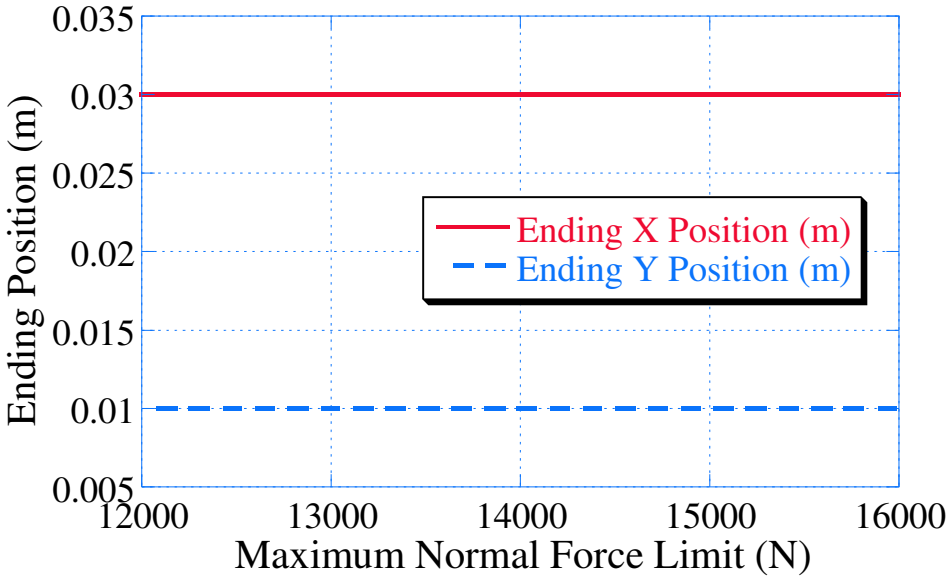

Figure 73: Optimal Ending Position Verses Maximum Normal Force

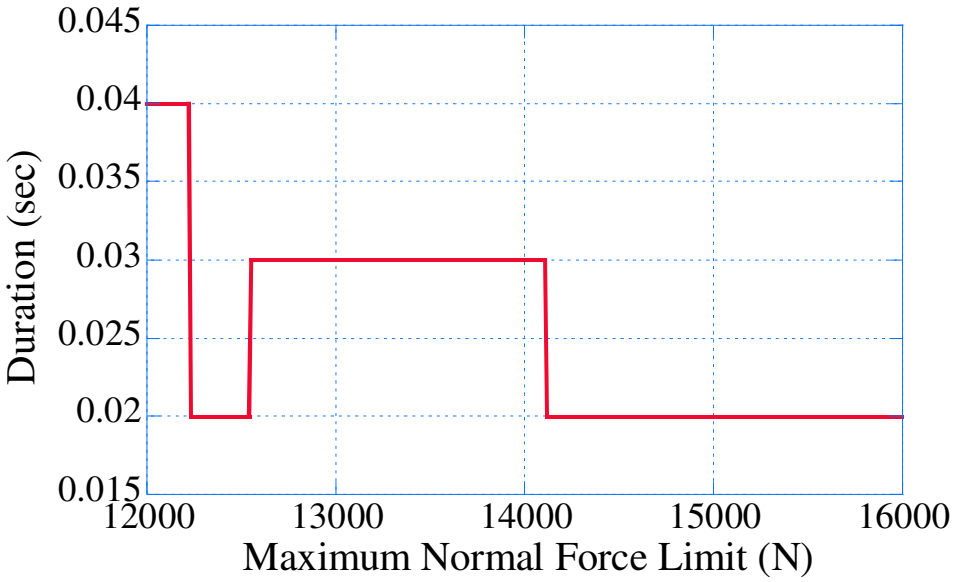

Figure 74: Optimal Duration of Move Verses Maximum Normal Force

4.6 Curved Path Move

As mentioned in Section 4.4, the safety seat travelled in a straight line when it moved to a new (X, Y) location. There are an infinite number of paths that a safety seat could take. This section examines an arced path. To create such a path, there are a few parameters which must be specified. The starting and ending points have already been defined, as well

as the duration and any delay in the sensor, however, one must provide details about the curvature of the arc, as well as a convex or concave direction.

First, the degrees of curvature in the arc needs to be specified. For example, a straight line would have zero degrees of arc. One should note that the arc has a limit of 90 degrees. To create an arc, the circle equation is used:

$$r^2 = (x-a)^2 + (y-b)^2, \tag{50}$$

where r is the radius of the circle and a and b are the coordinates of the center of the circle. The radius of the circle is found using the starting and ending point, as well as the arc length. Equation 50 is solved using the parameters defined for the center of the circle. The solution to (50) will consist of two points, one for a concave arc and another for a convex arc. Once the direction of the path is selected, the final path is found from:

$$X = r\cos(\omega(t-t_0)) + x_1 \tag{51}$$

$$Y = r\sin(\omega(t-t_0)) + y_1 \tag{52}$$

where r is the radius of the circle, ω is the frequency of the circle which is found using the duration, t_0 is the delay from the sensor, and x_1 and y_1 are the center point of the circle.

Once the path of the arc has been defined, the velocity and acceleration of the seat can be calculated through differentiation. The velocity and acceleration equations become:

$$\dot{X} = -r\omega\sin(\omega(t-t_0)) \tag{53}$$

$$\dot{Y} = r\omega\cos(\omega(t-t_0)) \tag{54}$$

$$\ddot{X} = -r\omega^2\cos(\omega(t-t_0)) \tag{55}$$

$$\ddot{Y} = -r\omega^2\sin(\omega(t-t_0)), \tag{56}$$

where the variables are the same as in (51) and (52). An example of an arced safety seat path is shown in Figure 75. A starting and ending point of (0,0) and (0.03,0.01) were selected, as well as a duration of 0.050 sec and a delay of 0.010 sec. Four different degrees per arc, 1, 30, 60, and 90 degrees all in a concave shape, were selected as the parameters. Figure 76 shows the different X and Y positions of the seat with respect to time.

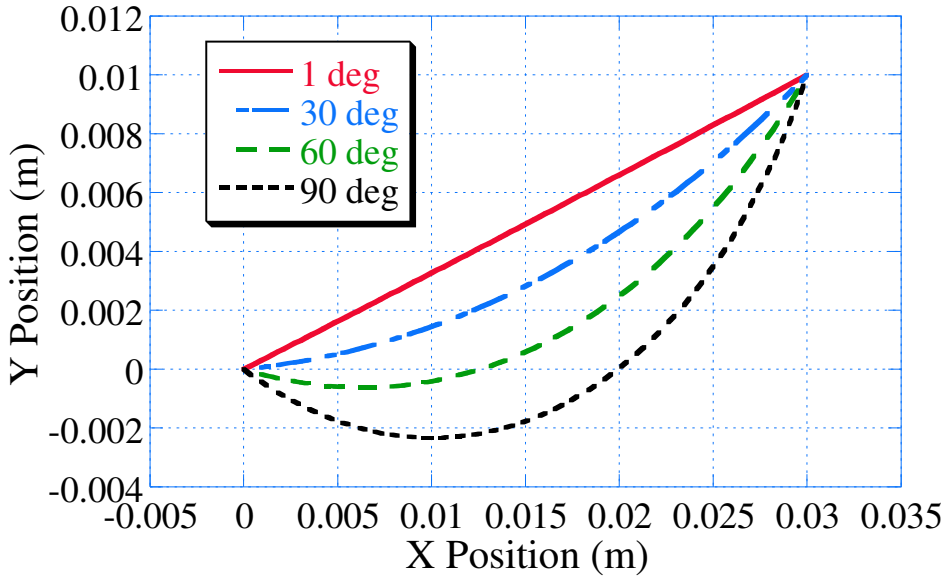

Figure 75: Curved Path of Safety Seat

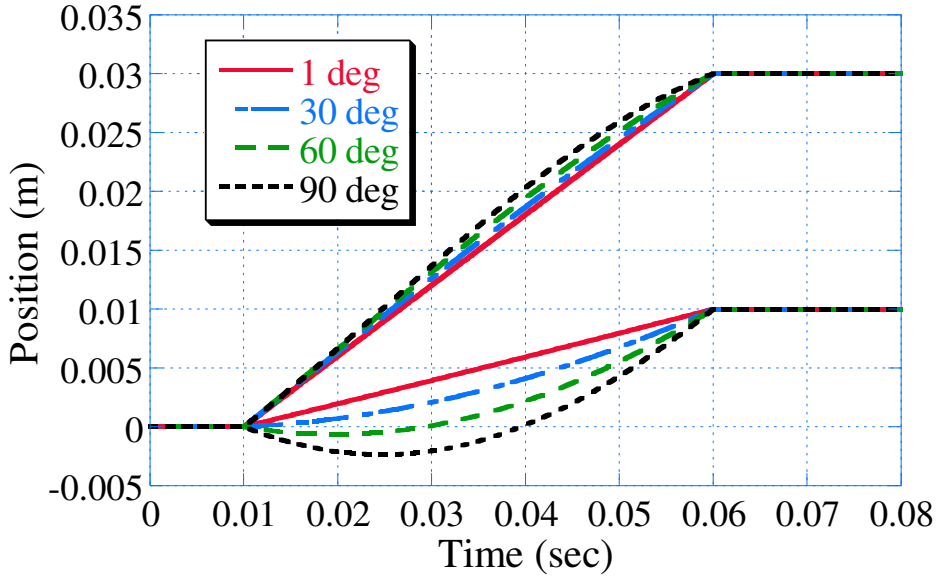

Figure 76: X and Y Path of a Safety Seat Verses Time

An arc path adds another two parameters, degrees in the circle along with the shape of the arc, to the four parameters discussed in Section 4.5. Six parameters would be very difficult to optimize and design the best safety seat. To see how the two new parameters affect the safety seat design, the X and Y position were fixed, as well as, the angle θ and the duration. Arced paths were constructed using a concave shape and varying the degrees in

the circle from zero degrees, a straight line, to 90 degrees. The two boundary seat positions were (0,0) and (0.05,0.05), along with a motion duration of 0.050 sec and an ending angle of 20 degrees. Figures 77 and 78 show how the ending relative velocity and maximum normal force change as the degrees in the arc are varied from zero to 90. These results show that the best design for a safety seat is to actually have a straight path and not to use an arced path.

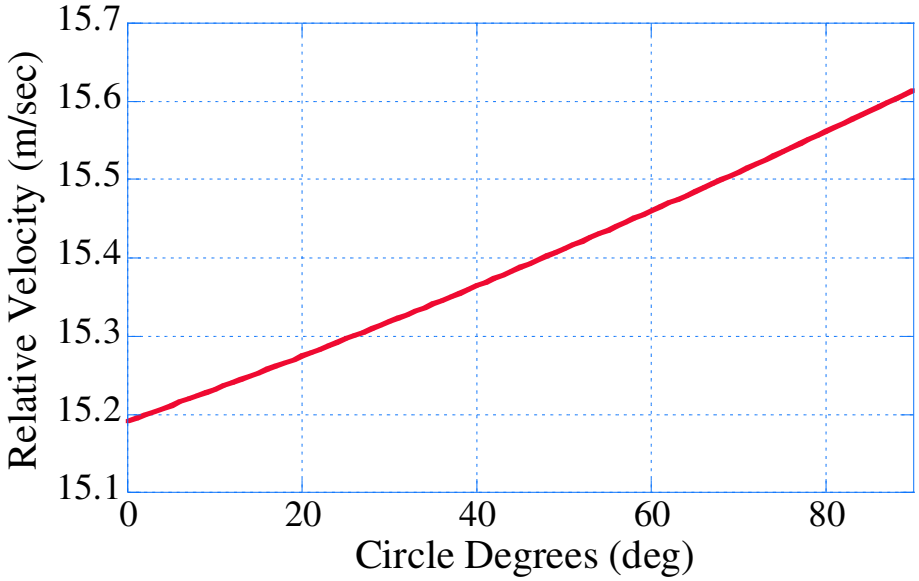

Figure 77: Relative Velocity of Safety Seat Verses Degrees in the Circle

Since the Hyper-Active seat is a fully active seat, it is possible to implement any desired path. Singer *et al.* patented a passive safety seat which uses an arced path [45]. This design was necessary because it was a passive safety seat. This research shows that a straight line is the optimal path; however, the safety seat needs to be an active seat to achieve this path.

4.7 Summary

A fixed-seat model shows that the seat bottom angle, coefficient of kinetic friction, and slide distance all have a significant impact on the kinetic energy of an occupant during a front-end collision. Increasing any of these variables will decrease the kinetic energy of the occupant relative to the seat. The results of a moving-seat model shows that the kinetic energy of the occupant can be reduced, by moving the seat during the crash. The moving-seat

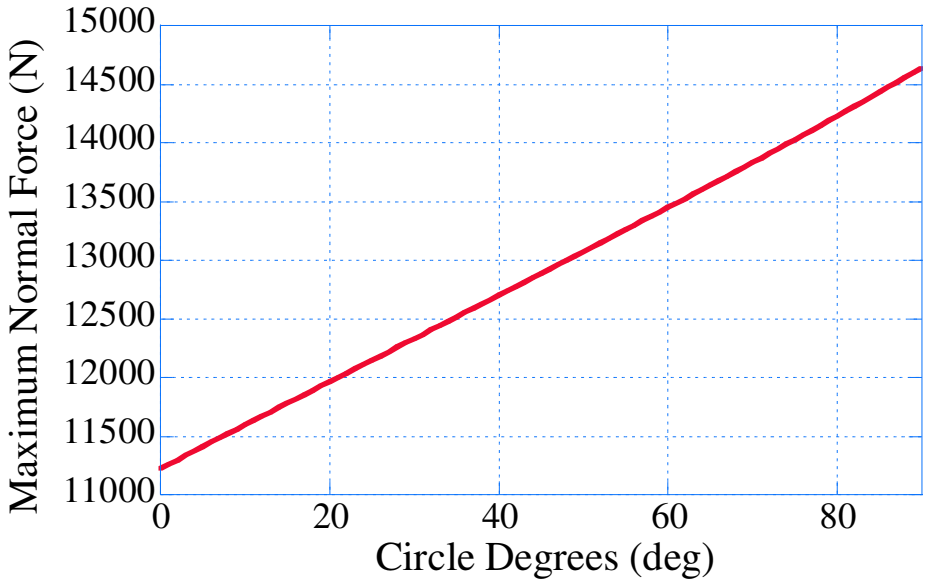

Figure 78: Maximum Normal Force Verses Degrees in the Circle

model was used to collect data about the relative velocity and maximum normal force of the occupant while varying four parameters; the X and Y end position, the ending angle θ, and the duration of the move. This data was put into a data viewer window so a safety seat designer could spot trends and design an optimal safety seat. The results show that as the limit on the maximum force is increased, the end seat angle θ increases, while the relative velocity and duration decreases. Figure 73 showed that the ending X and Y position should be fixed at 0.03 m and 0.01 m respectively. Finally an arced path was investigated to see the effect on the relative velocity and normal force on the occupant. Changing the degrees in the circle showed that the straight path was actual a better choice for the seat than an curved path. The data presented here clarifies the trade-off between minimum relative velocity and maximum normal force, and provides guidelines for designing an active safety seat that changes position during a crash.

CHAPTER V

CONCLUSION

5.1 Hyper-Active Seat Construction

A Hyper-Active seat was designed and built using a number of components that were donated by Deere and Company. A 3R$\underline{\text{P}}$R seat configuration was selected because it does not contain platform singularities within the workspace. It also gives the advantage of three independent degrees of freedom, X or horizontal, Y or vertical, and θ or pitch angle. This combination of degrees of freedom in an active seat has not been previously researched. These three degrees of freedom make the Hyper-Active seat ideal for reducing vibrations of off-road vehicles.

The components of the Hyper-Active seat were discussed in detail. A number of calculations showed the ability of the seat to support an operator of any size, as well as have enough workspace to cancel unwanted vibrations. The calculations also showed that the seat moved very quickly for some safety seat moves. However, certain changes could be made to increase the speed of the Hyper-Active seat, so it could be a more effective safety seat.

An excitation base was designed and built to induce vibration into the Hyper-Active seat. The design allowed for the excitation of the seat in both the vertical and pitch angle directions. This base allowed for controlled disturbances so that controllers can be tuned and the performance of the Hyper-Active seat optimized.

The software and controller design of the seat was outlined. MATLAB was used to control the seat using Simulink and the Real-Time Workshop. This allowed for the rapid design of controllers. The position and vibration cancellation controllers were discussed, as well as the excitation base controller. The Hyper-Active seat will allow for the design of many different position or vibration cancellation control systems for future research.

5.2 Hyper-Active Seat Performance

The current performance of the seat was evaluated using step and frequency response in multiple degrees of freedom. These experiments show that the Hyper-Active seat will be able to cancel vibrations in the harmful frequency range. From these results a third-order model was developed for each of the three degrees of freedom. This model predicts the response of the vertical and horizontal directions, and predicted the correct trends for the pitch angle. The model can be used in the development of a controller to suppress vibration.

The frequency response of the excitation base was discussed. The base is capable of creating disturbances in the vertical direction from 0 to 7 Hz and in the pitch angle direction from 0 to 4 Hz. The performance of the vibration cancellation controller was evaluated against an uncontrolled Hyper-Active seat. The controller showed excellent results in the 1 to 7 Hz range. The RMS Acceleration was reduced, thereby increasing the potential of the operator to work longer. The displacement of the amplitude was also decreased about 40% over the uncontrolled seat.

5.3 Safety Seat

Given the powerful actuators, the Hyper-Active seat can also be used as a safety seat. A fixed-seat model shows that the seat bottom angle, coefficient of kinetic friction, and slide distance all have a significant impact on the relative kinetic energy of an occupant during a front-end collision. Increasing any of these variables will decrease the kinetic energy of the occupant relative to the vehicle. The results of a moving-seat model showed that the kinetic energy of the occupant can be reduced. The moving-seat model was used to collect data about the relative velocity and maximum normal force of the occupant while varying four parameters; the X and Y end position, the ending angle θ, and the duration of the move. This data was put into a data viewer window so a safety seat designer can spot trends and design an optimal safety seat. The results showed that as the limit on the maximum force is increased, the end seat angle θ increases, while the relative velocity and duration decreases. The results also showed that the ending X and Y position should be fixed at 0.03 m and 0.01 m respectively. Finally analysis revealed that straight line motion

was optimal. The data presented clarifies the trade-off between minimum relative velocity and maximum normal force, and provides guidelines for designing an active safety seat that changes position during a crash.

5.4 Future Work

The research completed hear provides a foundation for continued research and development of the Hyper-Active seat. The design and building of the Hyper-Active seat open the door to many research possibilities. The system identification showed the potential of the seat. The model that was developed from the system identification experiments can be used to develop a more advanced controllers.

The Hyper-Active seat can be modified from a fully active seat to an active seat. This can lead to the Hyper-Active seat being used as a miniature active suspension. An active suspension controller can be tested which would optimize the performance of a vehicle under loaded and unloaded conditions.

Experiments could be conducted using the Hyper-Active seat as a safety seat. Chapter 4 laid the theoretical groundwork for optimal safety seat path. The Hyper-Active seat could be accelerated to resemble a seat under a frontal collision. These results could experimentally prove the effectiveness of an active safety seat.

APPENDIX A

CONTROLLING THE HYPER-ACTIVE SEAT

A.1 Controlling the Hyper-Active Seat Using MATLAB's xPC Target

The Hyper-Active seat is controlled using MATLAB's xPC Target and the Real-Time Workshop. In order to operate the seat, one must follow these simple instructions:

1. Boot-up host computer (See Figure 79).

Figure 79: xPC Host Computer

2. Boot-up target computer making sure xPC Target boot disk is in the 3.5 in floppy drive (See Figure 80).

3. Open MATLAB on host computer and type "Simulink" in the MATLAB command window (See Figure 81).

4. The Simulink library browser will open (See Figure 82).

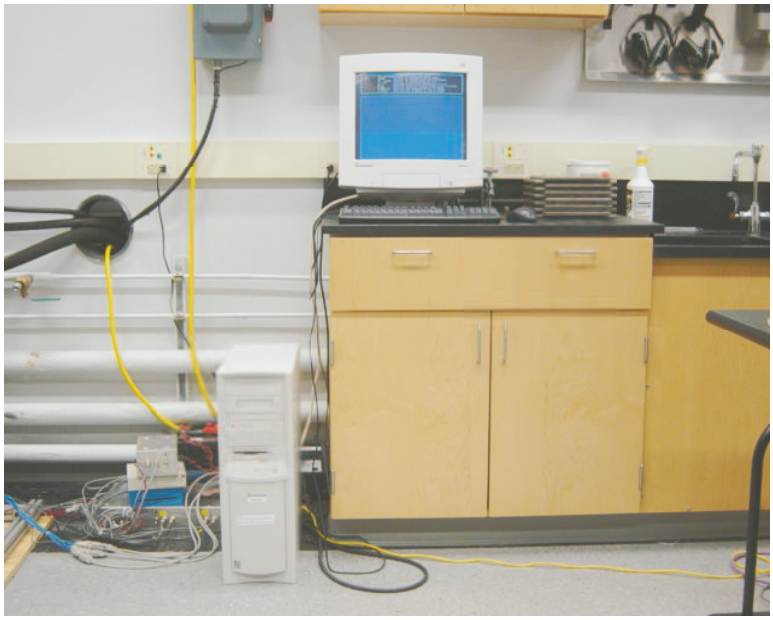

Figure 80: xPC Target Computer

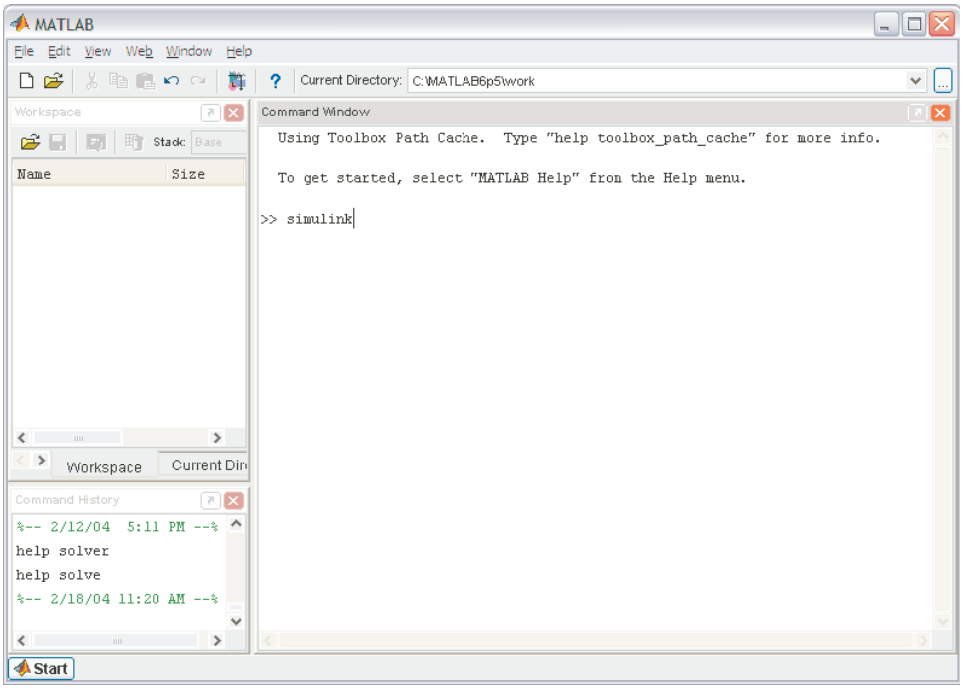

Figure 81: MATLAB Command Window

5. Click on the "create a new model" tab and a new model window should open up (See Figure 83).

6. Open the "Simulation Parameters" by clicking "Simulation" on the tool bar and then

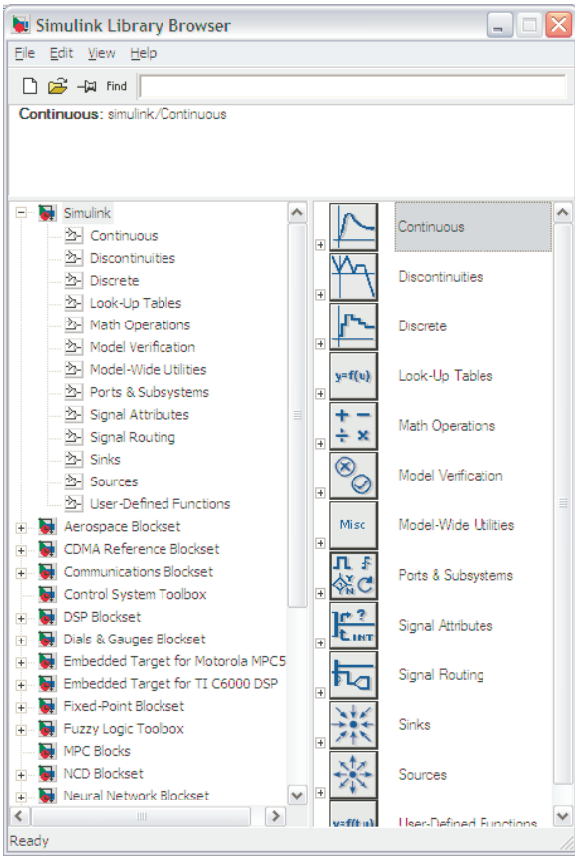

Figure 82: Simulink Library Browser

selecting "Simulation Parameters," or by pressing Ctrl + E (See Figure 84).

7. Click on the Solver tab.

8. In the "Solver options," change the "Type" to "Fixed-step" and "ode4 (Runge-Kutta)" (See Figure 84).

9. Click the "Real-Time Workshop" tab (See Figure 85).

10. Under the "configuration" section, change the "system target file" by clicking the "browse" button and then selecting "xpctarget.tlc" and clicking OK (See Figure 86).

11. Click OK.

12. Build a Simulink diagram.

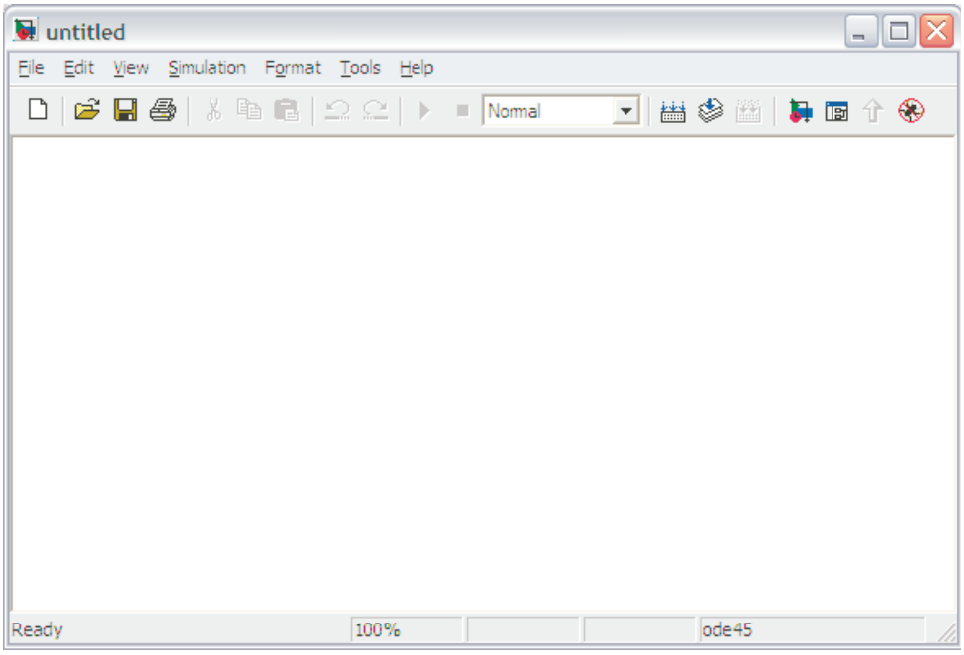

Figure 83: New Simulink Model Window

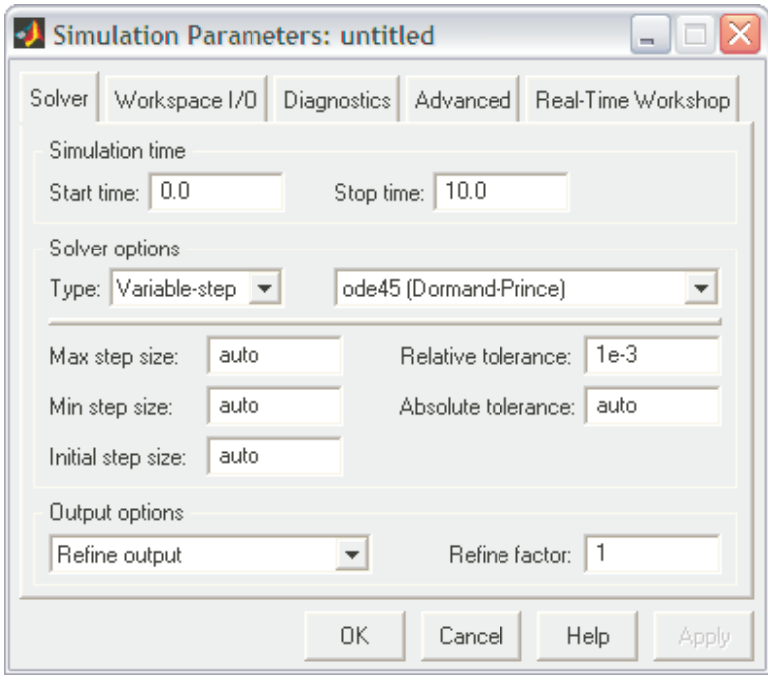

Figure 84: Simulation Parameters (Solver Tab)

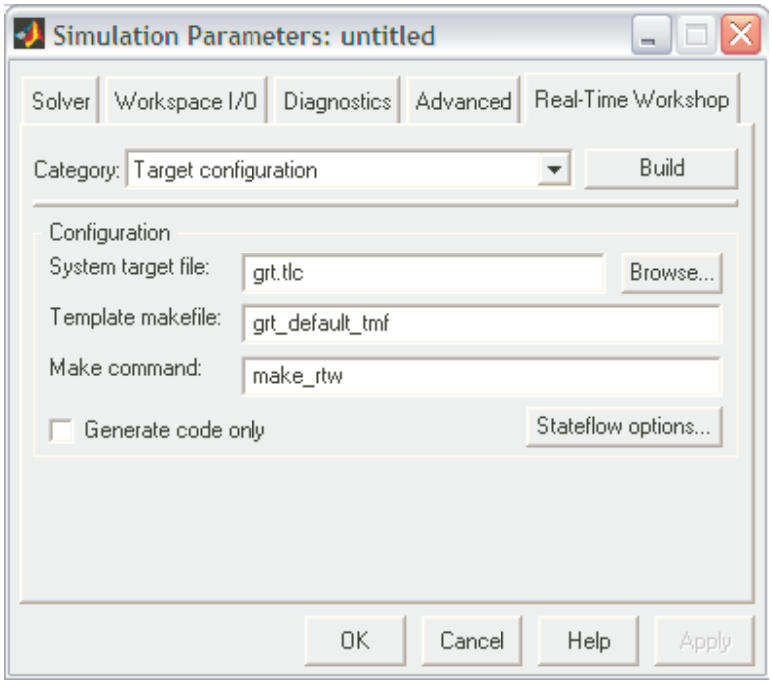

Figure 85: Simulation Parameters (Real-Time Workshop Tab)

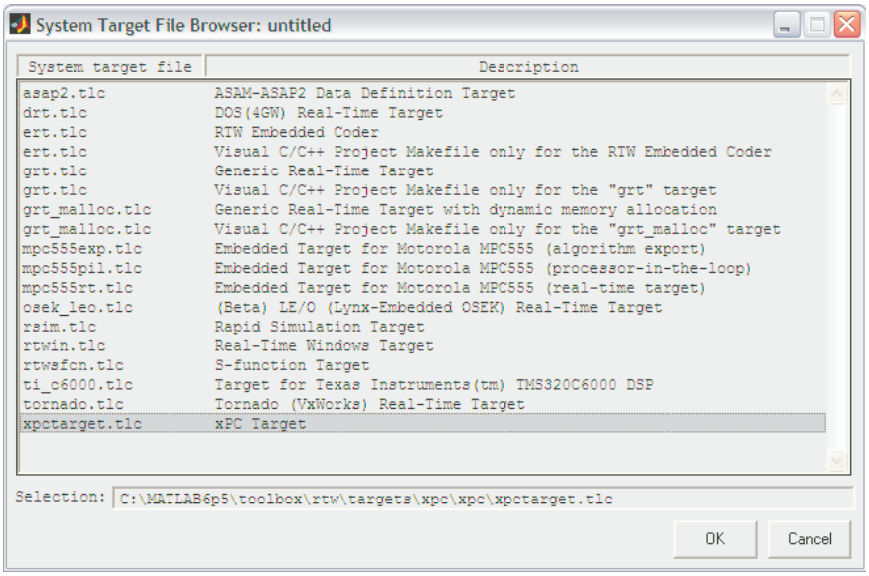

Figure 86: Simulation Parameters (Browse Menu)

APPENDIX B

CALCULATIONS

B.1 3RPR Workspace

The workspace of the 3RPR can be found using the law of cosines, along with other geometric properties.

B.1.1 Vertical Direction

Refer to Figure 87 for definitions of the variables.

$$Y_{Con} = \sqrt{(7.50in)^2 - (4.375in)^2} = 6.09in \tag{57}$$

$$Y_{Ext} = \sqrt{(10.00in)^2 - (4.375in)^2} = 8.99in \tag{58}$$

$$Y_{Travel} = 8.99in - 6.09in = 2.90in \tag{59}$$

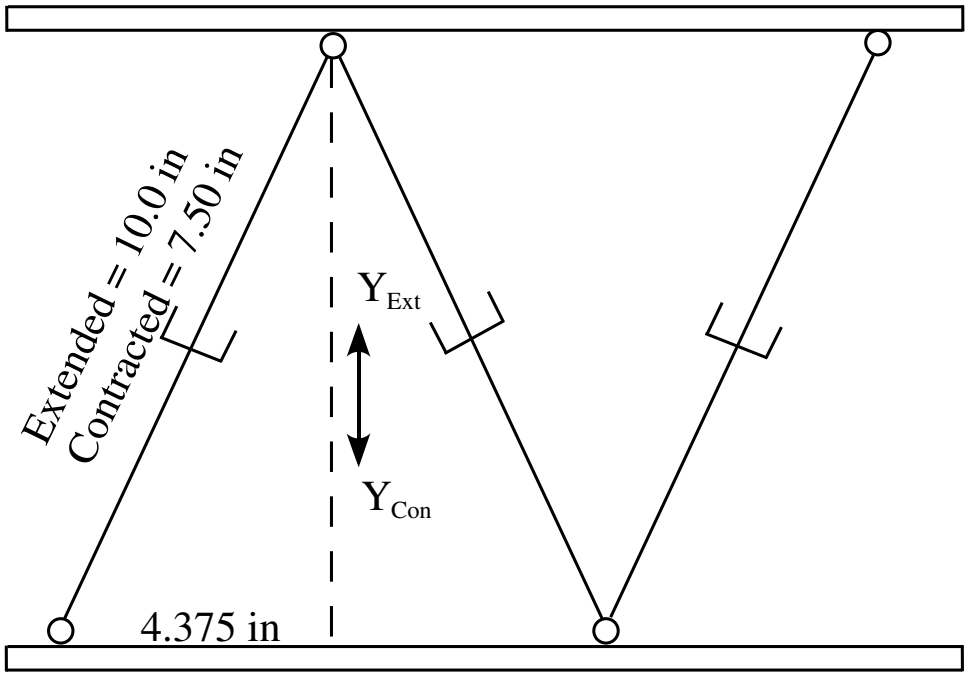

Figure 87: Hyper-Active Seat Sketch For Vertical Workspace Calculation

B.1.2 Horizontal Direction

Refer to Figure 88 for definitions of the variables.

$$X_{Ext} = \sqrt{(10.00in)^2 - (7.55in)^2} = 6.56in \tag{60}$$

$$X_{Con} = 8.75in + (8.75in - 6.56in) = 10.94in \tag{61}$$

$$X_{Travel} = 10.94in - 6.56in = 4.38in \tag{62}$$

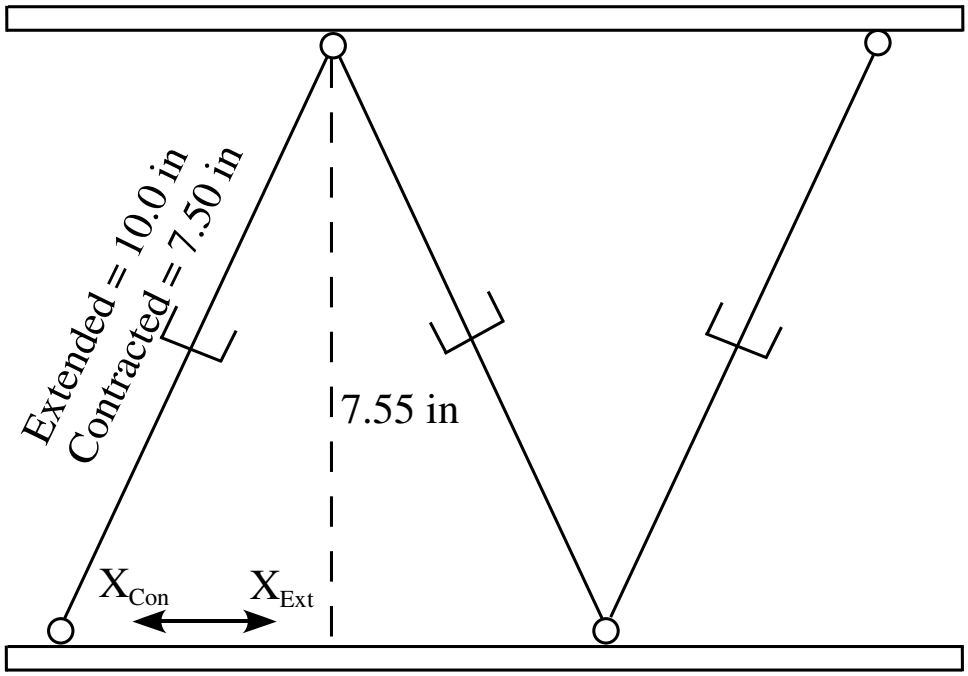

Figure 88: Hyper-Active Seat Sketch For Horizontal Workspace Calculation

B.1.3 Pitch Angle Direction

Refer to Figure 89 for definitions of the variables.

$$A = 7.55in \tag{63}$$

$$\theta_1 = 1.57rad \tag{64}$$

$$B = \sqrt{(7.55in)^2 + (4.375in)^2} = 8.73in \tag{65}$$

$$\theta_2 = \arcsin\left(\frac{7.55in}{8.73in}\right) = 1.05rad \tag{66}$$

$$\theta_3 = \arccos\left(\frac{4.375in^2 - 10.00in^2 - 7.55in^2}{-2 * 10.00in * 7.55in}\right) = 0.42rad \tag{67}$$

$$\theta_4 = \pi - 1.57rad - 1.05rad - 0.42rad = 0.10rad \tag{68}$$

$$C = \sqrt{10.00in^2 + 8.73in^2 - 2 * 10.00in * 8.73in * \cos(0.10rad)} = 1.61in \tag{69}$$

$$\theta_5 = \arccos\left(\frac{7.55in^2 - 4.375in^2 - 10.00in^2}{-2 * 10.00in * 4.375in}\right) = 0.78rad \tag{70}$$

$$\theta_6 = \arccos\left(\frac{8.73in^2 - 1.61in^2 - 10.00in^2}{-2 * 10.00in * 61in}\right) = 0.61rad \tag{71}$$

$$D = \sqrt{4.375in^2 + 1.61in^2 - 2 * 4.375in * 1.61in * \cos(0.78rad + 0.61rad)} = 4.375in \tag{72}$$

$$\theta = \arccos\left(\frac{1.61in^2 - 4.375in^2 - 4.375in^2}{-2 * 4.375in * 4.375in}\right) = 0.37rad \tag{73}$$

$$\theta_{Travel} = 2 * 0.37rad = 0.74rad \tag{74}$$

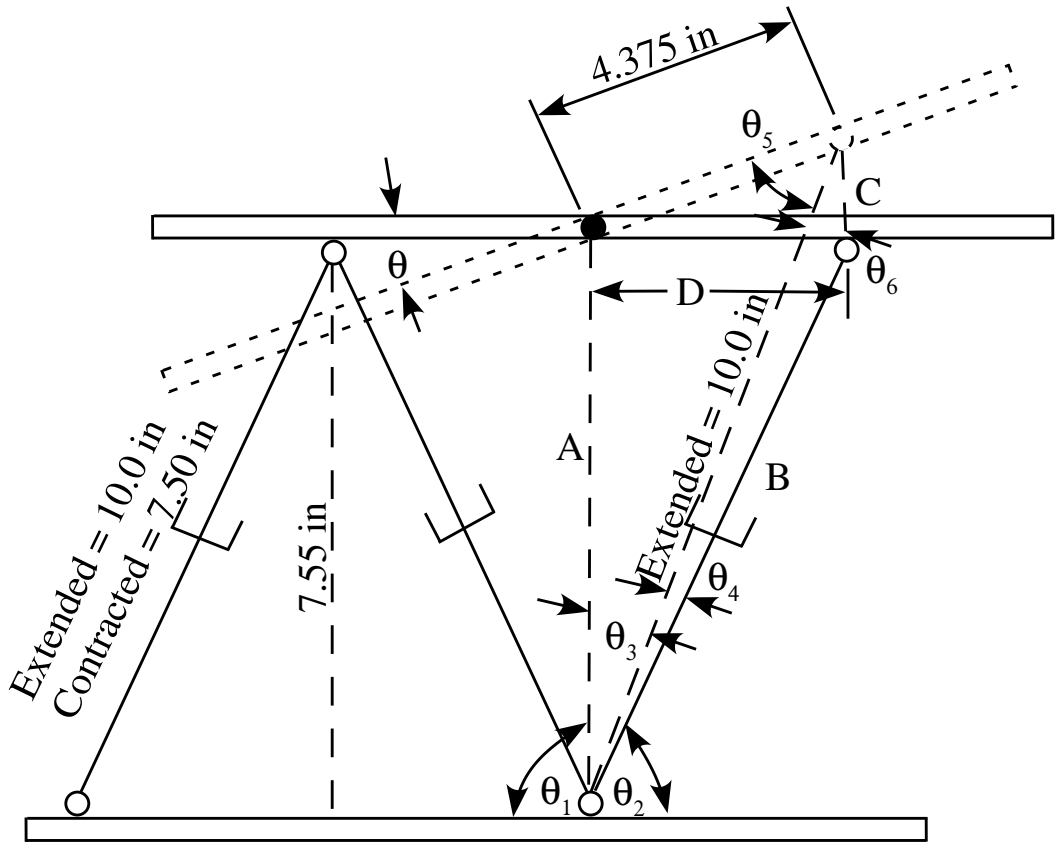

Figure 89: Hyper-Active Seat Sketch For Pitch Angle Workspace Calculation

B.2 Force

The force of a single piston can be calculated as follows:

$$F_{extension} = (500psi) * (\pi * 0.75in^2) = 883.6lbf \tag{75}$$

$$F_{contraction} = (500psi) * (\pi(0.75in^2 - 0.25in^2)) = 785.4lbf \tag{76}$$

Refer to Figure 13 for reference to the dimensions and Figure 14 for the directions being calculated. The pressure is set as 500 psi because this is the pressure the manifold supplies the cylinder (Section 2.2.2). The angle θ was calculated and can be used in all the force calculations:

$$\theta = \arctan\left(\frac{7.55in}{4.375in}\right) = 1.0456rad \tag{77}$$

B.2.1 Vertical

The vertical direction has all three cylinders extending in the up direction, and all three cylinders contracting in the down direction.

$$F_{up} = 3\,(883.6lbf * \sin 1.0456rad) = 2293.5lbf \tag{78}$$

$$F_{down} = 3\,(785.4lbf * \sin 1.0456rad) = 2038.6lbf \tag{79}$$

B.2.2 Horizontal

The horizontal direction has two cylinders extending and one cylinder contracting in the fore direction, while the opposite is true for the aft direction.

$$F_{fore} = 2\,(883.6lbf * \cos 1.0456rad) + (785.4lbf * \cos 1.0456rad) = 1279.8lbf \tag{80}$$

$$F_{aft} = 2\,(785.4lbf * \cos 1.0456rad) + (883.6lbf * \cos 1.0456rad) = 1230.6lbf \tag{81}$$

B.2.3 Pitch Angle

A torque is calculated in the pitch angle instead of a force. In the positive pitch angle direction, one cylinder is extending while the other two are contracting. The opposite is true for the negative pitch angle direction.

$$F_{positive} = 4.375in\,(\sin 1.0456rad\,(2 * 785.4lbf + 883.6lbf)) = 9290.8inlbf \tag{82}$$

$$F_{negative} = 4.375in\,(\sin 1.0456rad\,(785.4lbf + 2 * 883.6lbf)) = 9662.5inlbf \tag{83}$$

B.3 Speed Calculation

B.3.1 Single Cylinder

Here is the velocity calculation for a single cylinder in extension:

$$Velocity = \frac{77 * 7gpm}{20 * (\pi 0.75in^2)} = 15.25in/\sec \tag{84}$$

B.3.2 Safety Seat

To calculate the speed of a 10 deg increase in seat angle, I am assuming that only one cylinder extends. Figure 90 defines the variables in the calculations:

$$L_3 = \sqrt{4.375in^2 + \left(\sqrt{7.5in^2 - 4.375in^2} + 8.75in \sin 10\deg\right)^2} = 8.77in \tag{85}$$

$$\Delta l_3 = 8.77in - 7.5in = 1.28in \tag{86}$$

$$Time = \frac{1.28in}{15.25in/\sec} = 83.9ms \tag{87}$$

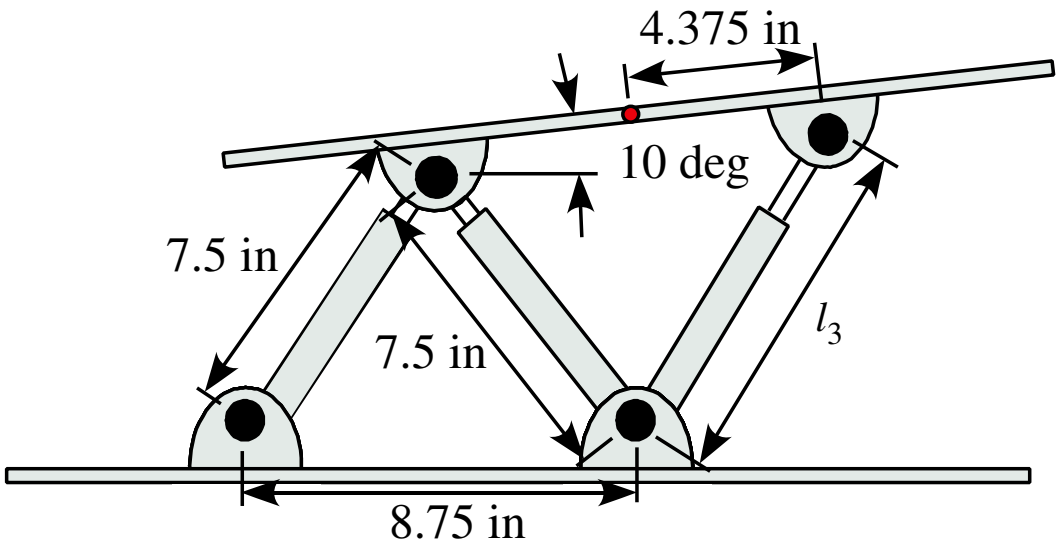

Figure 90: Hyper-Active Seat Sketch For Safety Seat Speed Calculation

REFERENCES

[1] "Captured german biophysics papers background for air force developments," *Air Technical Intelligence: Technical Data Digest*, vol. 14, no. 7, pp. 7–9, 1949.

[2] "Pre-safe headlines s-class revisions," *Automotive Engineering International*, pp. 56–57, December 2003.

[3] 2631-1, I., "Mechanical variation and shock - evaluation of human exposure to whole-body vibration. part i: General requirements," tech. rep., International Organization for Standardization, 1997.

[4] Ballo, I., "Power requirement of active vibration control systems," *Vehicle System Dynamics*, vol. 24, no. 9, pp. 683–694, 1995.

[5] Baumal, A. E., McPhee, J. J., and Calamai, P. H., "Application of genetic algorithms to the design optimization of an active vehicle suspension system," *Computer Methods in Applied Mechanics and Engineering*, vol. 163, no. 1-4, pp. 87–94, 1998.

[6] Beauvais, R. and Meade, A. J., "Vehicle safety device," Patent No. 5,022,707, October 6, 1988.

[7] Bohmler, K., "Restraining system for vehicle occupants," Patent No. 5,908,219, May 27, 1997.

[8] Bullerdieck, H. H., "Safety seat for vehicles," Patent No. 4,085,963, November 6, 1975.

[9] Calandra, D. A., Dirubbio, V., Vallone, J. R., and Vallone, I. S., "Safety vehicle seat system and trigger means for the same," Patent No. 3,858,930, July 11, 1972.

[10] Center, T. C. I. f. A. E. P. f. t. S. D., ed., *Handbook of human engineering data*. Medford: Tufts University, 2nd ed., 1952.

[11] Cheok, K. C., Hu, H. X., and Loh, N. K., "Discrete-time frequency-shaping parametric lq control with application to active seat suspension control," *IEEE Transactions on Industrial Electronics*, vol. 36, no. 3, pp. 383–390, 1989.

[12] Choi, S. B., Choi, J. H., Nam, M. H., Chieong, C. C., and Lee, H. G., "A semi-active suspension using er fluids for a commercial vehicle seat," *Journal of Intelligent Material Systems and Structures*, vol. 9, pp. 601–606, 1998.

[13] Choi, S.-B., Lee, B.-K., Nam, M.-H., and Cheong, C.-C., "Vibration control of a mr seat damper for commercial vehicles," *Smart Structures and Materials 2000: Smart Structures and Integrated Systems*, vol. 3985, pp. 491–496, 2000.

[14] Demic, M., "A contribution to optimization of vehicle seats," *Intl. J. of Vehicle Design*, vol. 12, no. 5/6, pp. 618–629, 1991.

[15] Deprez, K., Maertens, K., and Ramon, H., "Comfort improvement by passive and semi-active hydropneumatic suspension using global optimization technique," in *American Control Conference*, (Anchorage, AK, USA), pp. 1497–1501, 2002.

[16] Dufner, D. and Schick, T., "John deere active seat: A new level of seat performance," in *AgEng2002: Intl. Conf. on Agricultural Engineering*, (Budapest, Hungry), p. 7, 2002.

[17] Friedewald, K., "Design methods for adjusting the side airbag sensor and the car body," Tech. Rep. 98-S8-W-17, Volkswagen AG.

[18] Gaut, G. R., "Automotive safety device," Patent No. 3,452,834, November 21, 1969.

[19] Glass, W., "Technical report on the fmvss 213 crash pulse and test bench analysis," tech. rep., Department of the Navy Naval Air Warfare Center Aircraft Division, April 2002.

[20] Gniady, J. and Bauman, J., "Active seat isolation for construction and mining vehicles," in *SAE Tech. Paper Series*, pp. 1–6, 1991.

[21] Grimm, E. A., Huff, G. J., and Wilson, J. N., "An active seat suspension for off-road vehicles," in *Proceedings of the Symposium on Computers, Electronics, and Control*, vol. 3, (Calgary, Canada), pp. 1–8, 1974.

[22] Hasstedt, K. L., "Vehicle seat," Patent No. 4,634,169, May 28, 1985.

[23] Hurwitz, A., "Air cushion supports for vehicle seats," Patent No. 3,814,370, June 4, 1974.

[24] Junker, H. and Seewald, A., "A theoretical investigation of an active suspension system for wheeled tractors," Tech. Rep. AD-A148634, Inst. f. Kraftfahrwesen, TH Aaachen, BR Deutschland.

[25] Kawana, M. and Shimogo, T., "Active suspension of truck seat," *Journal of Shock and Vibration*, vol. 5, pp. 35–41, 1998.

[26] Kim, K. U., Hoag, D. L., and Hunt, D. R., "Ride simulation of passive, active, and semi-active seat suspensions for off-road vehicles," *Transactions of the ASAE*, pp. 56–64, 1984.

[27] Kullgren, A., Krafft, M., Nygren, A., and Tingvall, C., "Neck injuries in frontal impacts: Influence of crash pulse characteristics on injury risk," *Accident Analysis and Prevention*, vol. 32, pp. 197–205, 2000.

[28] Liu, X. and Wagner, J., "Design of a vibration isolation actuator for automotive seating systems - part i: Modeling and passive isolator performance," *Intl. J. of Vehicle Design*, vol. 29, no. 4, pp. 335–356, 2002.

[29] Liu, X. and Wagner, J., "Design of a vibration isolation actuator for automotive seating systems - part ii: Controller design and actuator performance," *Intl. J. of Vehicle Design*, vol. 29, no. 4, pp. 357–375, 2002.

[30] Marsili, A., Regni, L., Santoro, G., Servadio, P., and Vassalini, G., "Innovative systems to reduce vibrations on agricultural tractors: Comparative analysis of acceleration transmitted through the driving seat," *Biosystems Engineering*, vol. 81, no. 1, pp. 35–47, 2002.

[31] Mehta, C. R., Shyam, M., Singh, P., and Verma, R. N., "Ride vibration on tractor-implement system," *Applied Ergonomics*, vol. 31, pp. 323–328, 2000.

[32] Meyerson, S. L., Zuby, D. S., and Lund, A. K., "Repeatability of frontal offset crash tests," Tech. Rep. 98-S11-O-02, Insurance Institute for Highway Safety.

[33] Mikami, T., "Seat with user protecting means," Patent No. 5,556,160, October 4, 1994.

[34] Moseley, A. L. and McFarland, R. A., eds., *Human factors in highway transport safety*. Boston: Harvard School of Public Health, 1954.

[35] Nevala, K., Kangaspuoskari, M., and Leinonen, T., "Development of an active suspension mechanism for the seat vibration damping," in *Proceedings of the 4th IASTED Intl. Conf.: Robotics and Manufacturing*, (Honolulu, Hawaii, USA), pp. 337–339, 1996.

[36] Oshinoya, Y., Ooka, K., and Ishibashi, K., "Experimental study on active suspension of truck seat using sliding mode control," *Proceedings of the School of Engineering of Tokai University, Series E*, vol. 24, pp. 43–49, 1999.

[37] Pantelelis, N. G. and Kanarachos, A. E., "A simple and effective active seat suspension for agricultural vehicles," in *IFAC Control Applications and Ergonomics in Agriculture*, (Athens, Greece), pp. 301–306, 1998.

[38] Perisse, J. and Jezequel, L., "An original feedback control with a reversible electromechanical actuator used as an active isolation system for a seat suspension. part i: Theoretical study," *Vehicle System Dynamics*, vol. 34, no. 5, pp. 305–331, 2000.

[39] Prasad, N., Tewari, V. K., and Yadav, R., "Tractor ride vibration - a review," *Journal of Terramechanics*, vol. 32, no. 4, pp. 205–219, 1995.

[40] Rehn, B., Bergdahl, I. A., Ahlgren, C., From, C., Jarvholm, B., Lundstrom, R., Nilsson, T., and Sundelin, G., "Musculoskeletal symptoms among drivers of all-terrain vehicles," *Journal of Sound and Vibration*, vol. 253, no. 1, pp. 21–29, 2002.

[41] Ryba, D., "Semi-active suspension for a seat with a controlled electromagnetic damper," *Periodica Polytechnica: Transportation Engineering*, vol. 21, no. 3, pp. 247–265, 1992.

[42] Salvendy, G., ed., *Handbook of human factors and ergonomics*. New York: J. Wiley, 2nd ed., 1997.

[43] Schwarze, S., Notbohm, G., Dupuis, H., and Hartung, E., "Dose-response relationships between whole-body vibration and lumbar disk disease - a field study of 388 drivers of different vehicles," *Journal of Sound and Vibration*, vol. 215, no. 4, pp. 613–628, 1998.

[44] Simon, L. B., "Automatic vehicle occupant restraint," Patent No. 3,591,232, April 1, 1969.

[45] Singer, N. C., Gordon, S. J., Zirps, C. T., and Russo, M. A., "Safety seat," Patent No. 5,636,424, January 13, 1994.

[46] Stein, G. J., "Results of investigation of an electropneumatic active vibration control system for a driver's seat," *Proceedings of the Institution of Mechanical Engineers, Part D (Journal of Automotive Engineering)*, vol. 209, no. 3 Part D, pp. 227–234, 1995.

[47] Stein, G. J., "An electro-pneumatic active vibration control system for the driver's seat of agricultural tractors," *Archives of Acoustics*, vol. 21, no. 3, pp. 345–353, 1996.

[48] Stein, G. J., "New results on an electropneumatic active seat suspension system," *Proceedings of the Institution of Mechanical Engineers, Part D (Journal of Automotive Engineering)*, vol. 214, no. Part D, pp. 533–544, 2000.

[49] Stein, G. J. and Ballo, I., "Active vibration control system for the driver's seat for off-road vehicles," *Vehicle System Dynamics*, vol. 20, pp. 57–78, 1991.

[50] Stein, G. J., Ballo, I., and Gajarsky, M., "Active vibration control system for the driver's seat," in *25th ISATA Silver Jubilee Intl. Sym. on Automotive Tech. and Automation*, (Florence, Italy), pp. 183–190, 1992.

[51] Stikeleather, L. F. and Suggs, C. W., "The development of an active seat suspension system for off-road vehicles," *Transactions of the ASAE*, vol. 13, no. 1, pp. 99–106, 1970.

[52] Suggs, C. W., Stikeleather, L. F., and Abrams, C. F., J., "Field tests of an active-seat suspension for off-road vehicles," in *Transactions of the ASAE: Education and Research Division*, (Lafayette, Ind., USA), pp. 608–611, 1969.

[53] Sullivan, L. K. and Willke, D. T., "Dynamic evaluation of child restraints using various frontal crash pulses," technical report, National Highway Traffic Safety Administration Vehicle Research and Test Center, December 2001.

[54] Totani, H., "Safety system for an occupant of an automotive vehicle," Patent No. 5,449,214, October 27, 1993.

[55] Totani, H., "Safety system for occupant of an automotive vehicle," Patent No. 5,490,706, March 22, 1995.

[56] Weimer, J., *Handbook of ergonomic and human factors tables.* Englewood Cliffs: Prentice Hall, 1993.

[57] Woodson, W. E., Tillman, B., and Tillman, P., *Human factors design handbook : information and guidelines for the design of systems, facilities, equipment, and products for human use.* New York: McGraw-Hill, 2nd ed., 1992.

[58] Wooley, R. L., "Structures for lifting outboard side of seat of motor vehicle during side impact collision," Patent No. 5,149,165, May 6, 1991.

[59] Young, R. E. and Suggs, C. W., "An active seat suspension system for isolation of roll and pitch in off-road vehicles," in *1973 Annual Meeting of the American Society of Agricultural Engineers*, (Lexington, Kentucky, USA), p. 18, 1973.

[60] Young, R. E. and Suggs, C. W., "Seat suspension system for isolation of roll and pitch in off-road vehicles," *Transactions of the ASAE: Power and Machinery Division*, pp. 876–880, 1973.

[61] Yunzhao, L., "Safety seat equipped in automobile," Patent No. 5,167,421, July 5, 1991.

[62] Zhang, Y. and Alleyne, A., "A simple novel approach to active vibration isolation with electro-hydraulic actuation," *ASME-Journal of Dynamic Systems, Measurement, and Control*, vol. 125, pp. 125–128, 2003.